

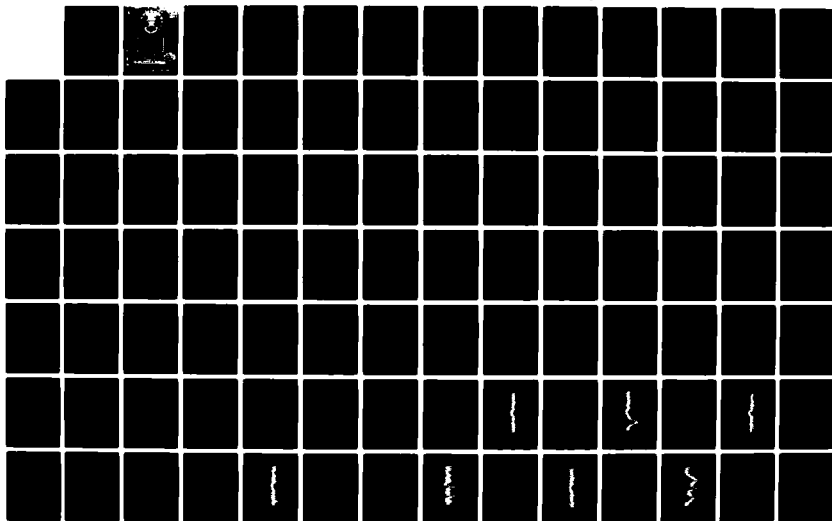
AD-A124 903

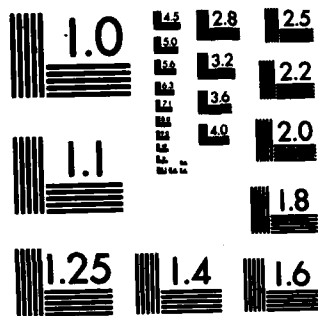
THE PERFORMANCE OF A PN SPREAD SPECTRUM RECEIVER  
PRECEDED BY AN ADAPTIVE... (U) AIR FORCE INST OF TECH  
WRIGHT-PATTERSON AFB OH SCHOOL OF ENGI... M M SHEPARD  
DEC 82 AFIT/GE/EE/82-62 F/G 17/4

1/2

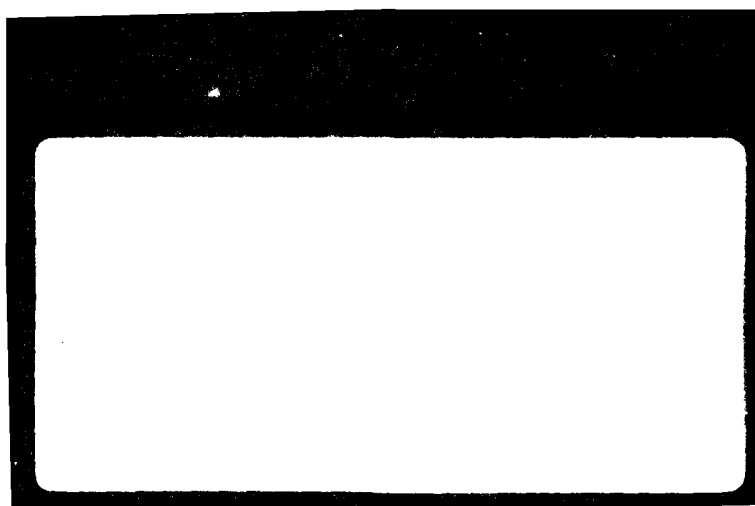
UNCLASSIFIED

NL





MICROCOPY RESOLUTION TEST CHART  
NATIONAL BUREAU OF STANDARDS-1963-A



AFIT/GE/EE/82-62

THE PERFORMANCE OF A PN  
SPREAD SPECTRUM RECEIVER PRECEDED  
BY AN ADAPTIVE  
INTERFERENCE SUPPRESSION FILTER  
THESIS

AFIT/GE/EE/82-62

Michael M. Shepard

2dLt

USAF



THE PERFORMANCE OF A PN  
SPREAD SPECTRUM RECEIVER PRECEDED  
BY AN ADAPTIVE  
INTERFERENCE SUPPRESSION FILTER

THESIS

Presented to the Faculty of the School of Engineering  
of the Air Force Institute of Technology  
Air Training Command  
in Partial Fulfillment of the  
Requirements for the Degree of  
Master of Science

by

Michael M. Shepard, B.S.

2dLt

USAF

Graduate Electrical Engineering

December 1982



Accession For	
NTIS GRA&I	<input checked="" type="checkbox"/>
DTIC TAB	<input type="checkbox"/>
Unannounced	<input type="checkbox"/>
Justification	
Distribution/	
Availability Codes	
Avail and/or	Special
Dist	
A	

## Preface

In January 1982, Capt. Gary Pennett proposed a thesis topic on adaptive interference suppression techniques for spread spectrum communications which sparked my interest. I began reading as much literature on the underlying theory as possible to gain a basic grasp of the topic. By February, I made the commitment to take on this research effort as my Masters level thesis work.

Lawrence L. Gutman, AFWAL/AAAI-2 volunteered to be my thesis advisor which greatly helped the already over burdened AFIT professors. Mr. Gutman and I spent many hours together in the months that followed studying this problem. His immense knowledge in this field provided most of the guidance by suggesting many possible approaches to solving the problem. I provided the legwork required to make the approaches happen. After having spent two months getting the computer simulation hosted on the base computer, and after having made many mistakes and false starts, we eventually organized the many efforts into the thesis that follows.

I wish to thank my sponsors, Capt. Thomas Harper and Mrs. Denise Jacobs of the Information Transmission Branch at the Avionics Lab, AFWAL/AAAI, for their outstanding support in seeing me through this research effort. Mrs. Jacobs provided much help in getting the computer simulation hosted on the base computer. Also I wish to thank their branch chief

Preface (cont.)

Mr. Charles Gauder for his overall support in allowing this thesis effort to be conducted in his branch.

Special thanks goes to Texas Instruments, and especially Dr. James Toplicar, for their providing me with the tools necessary to carry out this research. They allowed me the use, with Mr. Nick Kopchick's approval, of a computer simulation of the AIS filter implemented in a spread spectrum communications system, and information contained in a proposal on the AIS filter. Also, I carried out many lengthy phone conversations and actual visits, either here at Wright-Patterson AFB or at Texas Instruments, with Dr. Toplicar for additional guidance on this thesis effort.

I wish to also thank Maj. Kenneth Castor and Capt. Roger Colvin for the time they devoted to reading my draft and discussing this thesis and its goals.

Finally, but most importantly, I am grateful to our Lord and Saviour for His love and patience not only during this research effort but during this entire academic program, and beyond.

Michael M. Shepard

## Contents

	Page
Preface . . . . .	ii
List of Figures . . . . .	vi
List of Tables . . . . .	ix
List of Symbols . . . . .	x
Abstract . . . . .	xiii
I. Introduction . . . . .	1
Background . . . . .	1
Problem Statement. . . . .	5
Scope . . . . .	5
Assumptions . . . . .	6
Approach and Sequence of Presentation . . . . .	6
II. Spread Spectrum System Principles . . . . .	9
Spread Spectrum System Model . . . . .	11
Characteristics of PN Sequences . . . . .	13
Spread Spectrum System Performance . . . . .	18
III. SAW - Adaptive Interference Suppression Techniques . . . . .	30
Alternative Technologies . . . . .	30
SAW - Programmable Transversal Filter Technology . . . . .	32
SAW Device Theory . . . . .	33
Programmable Transversal Filters Utilizing Adaptive Interference Suppression Techniques . . . . .	41
Implementation of the Applebaum Algorithm in the Frequency Domain . . . . .	50
A Consideration of the Algorithm Adaption Time . . . . .	51
IV. Analysis of Adaptive Interference Suppression . . . . .	53
Pre-detection SNR Improvement . . . . .	54
Post-detection SNR Improvement . . . . .	80
Algorithm Convergence Rate . . . . .	92
V. Conclusions and Recommendations . . . . .	103



Contents (cont.)

Conclusions . . . . .	.103
Recommendations . . . . .	.106
Bibliography . . . . .	.108
Appendix A: A Survey of Adaptive Algorithms . . . . .	.111
Appendix B: Description of System Simulation Flowdiagrams . . . . .	.124
Vita . . . . .	.137

## List of Figures

Figure		Page
1	Direct Sequence Spread Spectrum Communications Model . . . . .	12
2	Data Modulation/Demodulation of a PN Sequence. .	14
3	Autocorrelation Function and Power Spectral Density of a PN Sequence . . . . .	16
4	Power Spectral Density of Interfering Signal . .	21
5	Spectra of Desired Signal and Interference . . .	22
6	Power Spectral Density of $n''(t)$ . . . . .	25
7	Typical SAW Device . . . . .	35
8	PTF Biphase Detector Array . . . . .	38
9	PTF Frequency Translation . . . . .	40
10	Tap Weight Control Range . . . . .	42
11	Configuration Utilizing Access to Individual Tap Outputs for Simultaneous Tap Weight Adjustment . . . . .	43
12	Configuration Utilizing a Single PTF Without Access to Individual Tap Outputs . . . . .	44
13	Configuration Utilizing Two PTF's: One for Interference Monitoring and One for Adaptive Interference Suppression . . . . .	45
14	Full Scale Adaptive Transversal Filter Block Diagram . . . . .	46
15	Implementation of Adaptive Algorithms in the Time or Frequency Domain . . . . .	48
16	PTF Device Model . . . . .	56
17	Pre-adaption Signal Plus Jammer Plus Noise Spectrum for Case 1 . . . . .	61
18	Adapted Filter Response for Case 1 . . . . .	62

# List of Figures (cont.)

Figure		Page
19	Post-adaption Signal Plus Jammer Plus Noise Spectrum for Case 1 . . . . .	63
20	Pre-adaption Signal Plus Jammer Plus Noise Spectrum for Case 2 . . . . .	65
21	Adapted Filter Response for Case 2 . . . . .	66
22	Adapted Filter Response for Case 6 . . . . .	67
23	Adapted Filter Response for Case 7 . . . . .	68
24	Pre-adaption Signal Plus Jammer Plus Noise Spectrum for Case 13 . . . . .	71
25	Adapted Filter Response for Case 13 . . . . .	72
26	Adapted Filter Response for Case 15 . . . . .	73
27	Post-adaption Signal Plus Jammer Plus Noise Spectrum for Case 15 . . . . .	74
28	Pre-adaption Signal Plus Jammer Plus Noise Spectrum for Case 17 . . . . .	76
29	Adapted Filter Response for Case 17 . . . . .	77
30	Post-adaption Signal Plus Jammer Plus Noise Spectrum for Case 17 . . . . .	78
31	Adapted Filter Response for Case 18 . . . . .	79
32	Adapted Filter Response for Case 21 . . . . .	81
33	Pre-adaption Correlation Response for Case 1 . .	87
34	Post-adaption Correlation Response for Case 1. .	89
35	Pre-adaption Correlation Response for Case 2 . .	90
36	Post-adaption Correlation Response for Case 2. .	91
37	Pre-adaption Correlation Response for Case 13. .	93
38	Post-adaption Correlation Response for Case 13 . . . . .	94
39	Pre-adaption Correlation Response for Case 18. .	95

List of Figures (cont.)

Figure		Page
40	Post-adaption Correlation Response for Case 18 . . . . .	96
41	Algorithm Convergence Rate for Cases 2 and 7 . .	97
42	Algorithm Convergence Rate for Cases 6 and 8 . .	98
43	Algorithm Convergence Rate for Cases 13, 15, and 16 . . . . .	99
44	Algorithm Convergence Rate for Cases 17, 18, and 19 . . . . .	.100
45	Adaptive Transversal Filter . . . . .	.113
46	Steepest Descent Adaptive Algorithm . . . . .	.118
47	Flowchart for Module MAIN . . . . .	.127
48	Flowchart for Subroutine PTF . . . . .	.132
49	Flowchart for Subroutine SPS . . . . .	.134

### List of Tables

Table		Page
I	Summary of Computer Simulation Parameters for the 22 Cases Analyzed . . . . .	55
II	Pre-detection SJR Before and After Filter Adaption and Improvement Factor . . . . .	60
III	Normalized Post-detection SJNR Before and After Filter Adaption and Improvement Factor . . . . .	86
IV	Description of Primary COMSIM Subroutines . . . .	125
V	User Entered Input Parameters and Their Nominal Nominal Values . . . . .	126

### List of Symbols

AIS	Adaptive Interference Suppression
$B_{\text{DATA}}$	Bandwidth of Data, $d(t)$
$B_{\text{RF}}$	Bandwidth of Transmitted Signal, $s(t)$
BLGN	Band Limited Gaussian Noise
BPSK	Binary Phase Shift Keyed
CCD	Charge Coupled Device
COMSIM	Communications Simulator
CW	Continuous Wave
$d(t)$	Digital Data Sequence
$d_j$	Estimate of the Desired Signal
DEL	Sampling Time Interval
DS	Direct Sequence
$c$	Sufficient Statistic
E/T	Signal Power
Erfc	Complimentary Error Function
FET	Field Effect Transistor
FH	Frequency Hop
FIR	Finite Impulse Response
GaAs	Gallium Arsenide
$h(t_n)$	Filter Tap Weights
I	In-Phase
IDT	Interdigital Transducer
IF	Improvement Factor
JSR	Jammer-to-Signal Ratio
$\text{LiNbO}_3$	Lithium Niobate

List of Symbols (con't.)

LMS	Least Mean Square
LPI	Low Probability of Intercept
MSE	Mean Square Error
MSK	Minimum Shift Keyed
MSW	Magnetostatic Wave Device
P	Cross Correlation of $d_j$ and $x$
P(E)	Probability of Error
PG	Processing Gain
PN	Pseudonoise
PN(t)	PN Code Sequence
PR	Pseudorandom
PSD	Power Spectral Density
PTF	Programmable Transversal Filter
Q	Quadrature
QPSK	Quadrature Phase Shift Keyed
R	Autocorrelation of $X$
R(t)	Received SS Signal
RF'	Radio Frequency
$R_{PN}(\tau)$	Autocorrelation of PN Sequence
S(t)	Transmitted SS Signal
SAW	Surface Acoustic Wave
Si	Silicon
SJNR	Signal-to-Jammer Plus BLGN Ratio
SJR	Signal-to-Jammer Ratio
SNR	Signal-to-Noise Ratio

List of Symbols (con't.)

$S_{PN}(\omega)$	PSD of PN Sequence
SS	Spread Spectrum
T	Message Bit Time Duration
$T_c$	PN Code Chip Time Duration
TH	Time Hop
TI	Texas Instruments
W	Tap Weight Vector
WGN	White Gaussian Noise
X	Filter Input Signal Vector
Y	Filter Output Signal
$\alpha$	Algorithm Loop Gain
$\alpha_n$	Intertap Delay Error
$\gamma_n$	Tap Weight Generation Error
$\nabla_k$	Gradient of MSE
$\Delta\phi$	Phase Error Between I and Q Channels
$\delta_n$	Summing Delay Error
$\delta(t)$	Kronecker Delta Function
$\epsilon$	Error Signal
$\lambda$	Filter Intertap Spacing
$\tau$	Time Shift of Autocorrelation



### Abstract

The performance of a spread spectrum receiver preceded by an adaptive interference suppression (AIS) filter is determined for various CW jamming signals. An analysis and simulation of an AIS filter, covering the band from 200-300 MHz, implemented with a SAW device is presented. The simulation includes modeling of the SAW device, filter tap weights, Applebaum and power inversion adaptive control algorithms, and filter fabrication and circuitry errors. Both desired and interfering signals are generated in the simulator, passed through the AIS filter, and demodulated by a simulated matched filter. System performance was determined by measuring the improvement in pre-detection signal-to-jammer ratio (SJR) and post-detection signal-to-jammer plus noise ratio (SJNR) provided by the AIS filter, and by computing the AIS filter convergence rate. To validate the AIS filter performance, the following additional simulation data was acquired both before and after filter adaption: the filter frequency response, the receiver correlation response, and the pre-detection signal plus jammer plus noise spectrum. In all 22 cases analyzed, the jammer power is 30 dB, the signal power is 0 dB, and the filter is allowed to adapt for 35 iterations. The AIS filter provided improvement in all cases analyzed except the case where the CW jammer is located at the center frequency of the signal. Typical improvement of pre-

Abstract (cont.)

detection SJR ranged from 20-49 dB. The Applebaum algorithm provided greater improvement in SJR and in SJNR than the power inversion algorithm. Both the Applebaum and power inversion algorithms implemented in the frequency domain converged faster than their respective time domain implementations. However, the time domain implementation of the adaptive algorithms provided greater improvement in SJR and in SJNR than the frequency domain implementation. Filter fabrication and circuitry errors caused the null depths of the adapted filter responses to be degraded relative to their respective responses without errors.

**THE PERFORMANCE OF A PN SPREAD SPECTRUM RECEIVER  
PRECEDED BY AN ADAPTIVE INTERFERENCE SUPPRESSION FILTER**

**I. Introduction**

**Background**

The purpose of any communication system is to transmit information or data with an acceptable probability of error or signal-to-noise ratio. In an ideal environment, a channel bandwidth approximately equal to the data rate is sufficient to transmit the information. In a noisy, crowded, or hostile environment, four classes of techniques exist which can be applied to achieve partially secure antijam communications:

- Brute-Force Techniques
- Spatial Discrimination Techniques
- Spread Spectrum Techniques
- Interference Suppression Techniques

Brute-force techniques include increasing the peak transmitted power or increasing the average power by extending the transmitter duty cycle or the bit period (Ref.22:2-1). However, these techniques increase the probability of interception of the signal by enemy receivers, increase the likelihood of self-interference, and are costly. Also, often the maximum transmitter power is limited by technology and by limited availability of prime power.

Spatial discrimination techniques include adaptive or null-steering antennas, low sidelobe antennas, and beam steering antennas for jammer suppression. However, these techniques have limitations due to the high cost of retrofitting aircraft platforms with advanced multi-element antennas, the high-gain antenna tracking and pointing problems, and the limited degrees of freedom inherent in an adaptive antenna.

Spread spectrum (SS) techniques include direct sequence (DS) or pseudonoise (PN), frequency hop (FH), time hop (TH), and any hybrid combination of these modulation schemes. SS communications systems are those systems in which the transmitted signal is spread over a wide frequency band. This band is much wider than the minimum bandwidth required to transmit the information being sent. Because an SS system distributes the transmitted energy over a wide bandwidth, the signal-to-noise ratio (SNR) at the receiver input is low. These systems are employed to reduce the probability of intercept and to increase the resistance to jamming or interference. Equivalently, SS systems are very useful for military communications because they make it difficult to detect the transmitted waveform, extract the message, or jam the intended receiver. The increased bandwidth required for SS operation creates two limitations. One is the limitation on transmission bandwidth set by the FCC. The other is that technology limits the speed of PN

codes (e.g. bandwidth).

Interference suppression techniques include active notch filters, weak signal enhancers, pulse suppression, frequency selective limiters, and frequency domain processors. These techniques are tunable and adaptive. However, they are limited by the maximum number of interfering signals which can be suppressed at one time, the cost of implementation, the tracking rate, and the bandwidth of the interfering signals. Given these limitations, an adaptive interference suppression (AIS) filter which is a programmable transversal filter (PTF) will be the tunable filter under study in this thesis.

As was described previously, SS techniques provide some antijam capability, however in a hostile scenario increased antijam protection may be needed. Additional immunity to jamming and interference can be realized by implementing the above described PTF in a SS system to perform filtering of the signal prior to detection.

There are many types of disturbances which can affect a communications system. White noise is always present. Further, many types of jammers may be employed by the enemy to degrade communication signals (Ref. 5:32). A continuous wave (CW) jammer is a single frequency sinusoidal jammer. A pulse jammer is a CW jammer that is turned on and off. A swept jammer is a CW jammer whose frequency is varied as a function of time. A partial band jammer is one that

continuously jams a band of frequency, and a barrage jammer is a partial band jammer that is turned on and off.

Much of the work in this thesis effort resulted from an on-going contract between the Air Force Avionics Laboratory and Texas Instruments. Texas Instruments (TI) is under contract to develop an adaptive interference suppression filter for possible implementation into the Integrated Communications, Navigation, and Identification Avionics program. Texas Instruments developed a computer simulation of an AIS-PTF device implemented in a SS system. Additionally, TI built an experimental surface acoustic wave (SAW) PTF device. The original version of TI's computer simulation was hosted on the Wright-Patterson Air Force base computer for both this thesis effort and a follow-on effort to be conducted by the Avionics Laboratory. Modifications to the simulation were made for this thesis effort. Namely, a white Gaussian noise (WGN) generator was added. Also, a statistical subroutine was added in order to assess performance improvement at the output of the correlator. Texas Instruments has investigated system performance only at the input to the correlation detector. Both pre-detection and post-detection system performance will be investigated in this thesis.

This thesis is not intended to be a review of the immense work done on surface wave phenomena and its application to SS devices since the initial inventions about

20 years ago. Rather, the work presented provides a working knowledge of SS system performance improvement utilizing a pre-detection surface wave device for the AIS function.

### Problem Statement

The improved performance of an SS receiver preceded by an AIS filter will be determined for various jamming signals. The basic philosophy is to suppress the interference with minimum degradation to the information which was transmitted. The performance improvement will be measured in terms of pre-detection signal-to-jammer ratio (SJR), and post-detection signal-to-jammer plus noise ratio (SJNR).

### Scope

This thesis will provide an analysis and simulation of an AIS filter implemented with a SAW device. The simulation includes modelling of the SAW device, tap weights, adaptive control algorithms, and filter fabrication and circuitry errors. Both desired and interfering signals will be generated in the simulator, passed through the AIS filter, and demodulated by a simulated matched filter. System performance improvement provided by the AIS filter will be determined.

## Assumptions

The following assumptions were made to narrow the problem to one that could be handled within the time allotted:

1. Simulation and analysis will utilize SS signals with emphasis on direct sequence PN biphas modulation.
2. Performance improvement will be investigated for one or more CW jammers. If time permits, the jammers will be pulsed or swept.
3. Synchronization of the PN code exists in the modem.
4. Because of certain hardware constraints imposed by the PTF, certain adaptive algorithms are more suitable than others for control of the filter tap weights. Factors that should be considered in choosing an algorithm include compatibility with the PTF, speed of convergence, computation time, and memory requirements (Ref.22:2-2). The Applebaum and the Power Inversion adaptive algorithms will be used to control the filter tap weights for the reasons stated above.

## Approach and Sequence of Presentation

The approach used in this thesis is to analyze the effect of processing operational threats through a DS modulated SS system which includes a pre-detection AIS filter.

Section II is a tutorial presentation of spread spectrum (SS) principles including a discussion of the performance of SS systems.

Section III discusses how improved SS system



performance can be realized by pre-detection adaptive interference suppression (AIS) techniques. Primary emphasis is directed toward the surface acoustic wave (SAW) device for application to the interference rejection problem. The underlying theory of SAW devices is presented followed by a detailed discussion of the SAW filter configuration chosen for study in this thesis.

Section IV presents an analysis of performance results due to the interference suppression filter. The SS system performance when utilizing a pre-detection filter is determined in terms of the signal-to-noise ratio (SNR) at both the input and output of the correlation detector. Additionally, a number of other characteristics of the AIS filter and its implementation in an SS system are analyzed. Namely, its frequency response (before and after filter adaption) and its convergence rate.

Section V summarizes the results of this thesis and presents recommendations for further study.

Appendix A presents a survey of four classes of adaptive algorithms discussing their basic characteristics, advantages, and disadvantages. The steepest descent class of algorithms, in particular the Applebaum and Power Inversion algorithms are analyzed to show how they adaptively change the filter weights.

Finally, Appendix B presents a description of the computer simulation along with flowdiagrams for the communications simulator which was utilized for this thesis effort.

## II. Spread Spectrum System Principles (Refs.4,8)

A SS system is one in which the transmitted signal is spread in frequency to a bandwidth much greater than the information bandwidth. In a conventional communications system, a digital symbol of time duration  $T$  is usually transmitted in a bandwidth of  $W = 2/T$ . This digital pulse has only one amplitude and phase state over the interval  $T$  and is considered to have only a single "degree of freedom". Interference and jamming waveforms can resemble digital symbol waveforms and cause performance problems. SS systems protect against performance degradation by increasing the number of "degrees of freedom" of each data symbol according to a pseudonoise sequence. This requires increased transmission bandwidth.

SS techniques have made possible the development of jam resistant communication systems with multiple access, low probability of intercept (LPI), and high resolution ranging. SS signals are generated via special modulation techniques. There are many types of SS systems and many reasons for utilizing different types of SS modulation. However, there exists a common principle in all SS applications: that is rejection of interference, or conversely, improved signal detectability is achieved at the expense of increased transmission bandwidth. The basic types of SS modulation include direct sequence (DS), frequency hop (FH), time hop

(TH), and any hybrid combination of these modulation schemes.

In a DS system, the information data is added modulo two to a higher speed PN code sequence. The combined information and PN code are then used to suppress-carrier modulate an RF carrier (ie. BPSK, QPSK, or MSK). Or, equivalently, the information data can be used to suppress-carrier modulate an RF carrier. The combined information and RF carrier are then used to modulate a PN code.

Frequency hopping is the periodic changing of the frequency or frequency set associated with a transmission. A PN code determines successive frequency sets. If the data modulation is multiple FSK, then two or more frequencies are in the set that changes at each hop. For other data modulation schemes, a single center or carrier frequency is changed at each hop (Ref.24:65).

Time hopping is a technique used to obtain spectral spreading by channelizing the carrier through the use of time slots that use a burst of transmission within the slot. The PN code selects the slot in which the transmitted pulse occurs.

Additionally, any combination of these modulation techniques can be employed, as is often the case.

### Spread Spectrum System Model

The baseline components of a DS modulated SS communications system employing binary phase shift keyed (BPSK) signaling are illustrated in Figure 1 where:

- $d(t)$  is the digital data sequence ( $\pm 1$ ).
- $E/T$  is the signal power.
- $PN(t)$  is the PN code sequence ( $\pm 1$ ).
- $\omega_0$  is the carrier frequency (rad/sec).

Multiplication of the bipolar binary data sequence by a carrier results in a phase shift of zero or  $\pi$  radians. The phase modulated carrier is then multiplied by the PN spreading sequence,  $PN(t)$ . The rate of the PN code is typically on the order of megabits per second, while the rate of the message waveform is typically on the order of kilobits per second. As a result of this modulation of the information signal by the PN code sequence, the power in the transmitted signal is spread in frequency over a bandwidth corresponding to the PN clock frequency. Because the transmitted energy is spread over a wide bandwidth, the SNR at the receiver input is low. Thus, to the unwanted observer, the signal appears to be wideband noise.

The receiver has a reference code generator which is a replica of the transmitted spreading code. The reference PN code generator, when synchronized with the received spreading

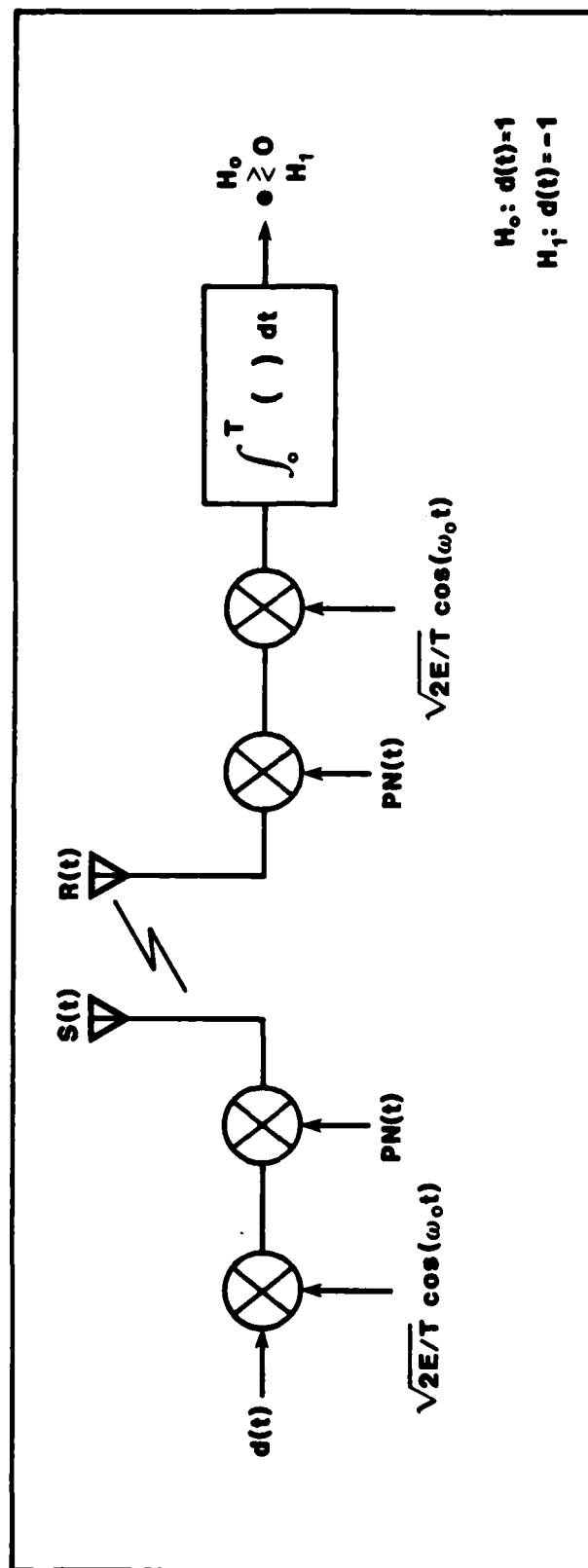


Figure 1. Direct Sequence Spread Spectrum Communications Model.

code, is used to strip the PN code off the signal as illustrated in Figure 2. The received signal,  $R(t)$ , is first multiplied by the synchronized reference code and then passed through a correlation detector whose output is the sufficient statistic,  $e^1$ . Using a threshold device and the sufficient statistic, a decision is made as to which of two hypotheses is correct. Under one hypothesis,  $H_0$ , a message bit  $d(t) = 1$  is detected. Under the other hypothesis  $H_1$ , a message bit  $d(t) = -1$  is detected.

It is intuitively obvious that the difference between SS systems and conventional systems is the multiplication by the PN code sequence at the transmitter and receiver. At this point, a description of the characteristics of PN sequences will be presented, since they are so important in SS system implementation.

### Characteristics of PN Sequences

The terms pseudorandom (PR) or pseudonoise (PN) are coined for this class of sequences because the sequence generates sample statistics similar to a random noiselike

---

<sup>1</sup> A sufficient statistic is a value which provides enough information about an observation to enable a proper decision about what message was sent (Ref.13:63).

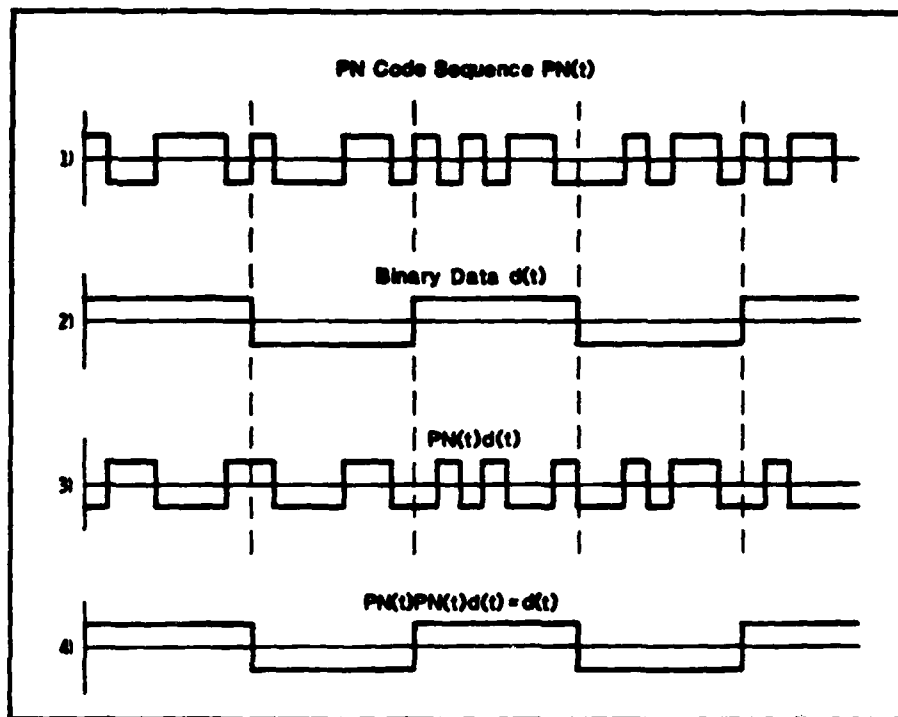


Figure 2. Data Modulation/Demodulation of a PN Sequence.

waveform. However, the sequences are both deterministic and periodic. A completely random binary sequence could be generated by using successive tosses of a coin and writing a 1 when a head appears and a 0 when a tail appears.

The type of sequence under study is the random binary sequence  $PN(t) = \pm 1$ . This class of sequences exhibits three randomness postulates (Refs. 8:10 and 11:1):

1) The Balance Property. The number of plus ones will be approximately equal to the number of minus ones.

2) The Run Property. Among the runs of consecutive ones and zeroes, about one-half of the runs of each kind are of length one, one-fourth of each kind are of length two,



one-eighth are of length three, and so on.

3) The Correlation Property. The expectation of the autocorrelation function of the sequence is maximum at the origin and decreases rapidly away from the origin.

The PN binary sequence is generated using shift registers and tapping the output back to the input. The output of the shift registers will be a PN sequence of ones and zeroes called chips. This sequence will repeat itself every  $2^N - 1$  chips for an N-bit shift register. For the model under study, the PN sequence consists of chips of  $T_c$  seconds duration, and amplitude  $\pm 1$ . It is assumed that the sequence is continuous, that the positive and negative chips occur with equal probability, and that successive pulses are statistically independent. Figure 3a illustrates an arbitrary portion of a typical PN sequence.

The autocorrelation function of the PN sequence,  $R_{PN}(\tau)$ , is the time average of the sequence multiplied by a time shifted version of itself (Ref.16:301). The autocorrelation function is given by

$$R_{PN}(\tau) = \lim_{T \rightarrow \infty} \frac{1}{2T} \int_{-T}^T PN(t)PN(t+\tau)dt \quad (1)$$

where  $\tau$  is the amount of time shift.

From the randomness property 1, it is clear that for  $|\tau| > T_c$ , the average value of  $PN(t) \cdot PN(t+\tau)$  is approximately zero since its instantaneous value has an equal

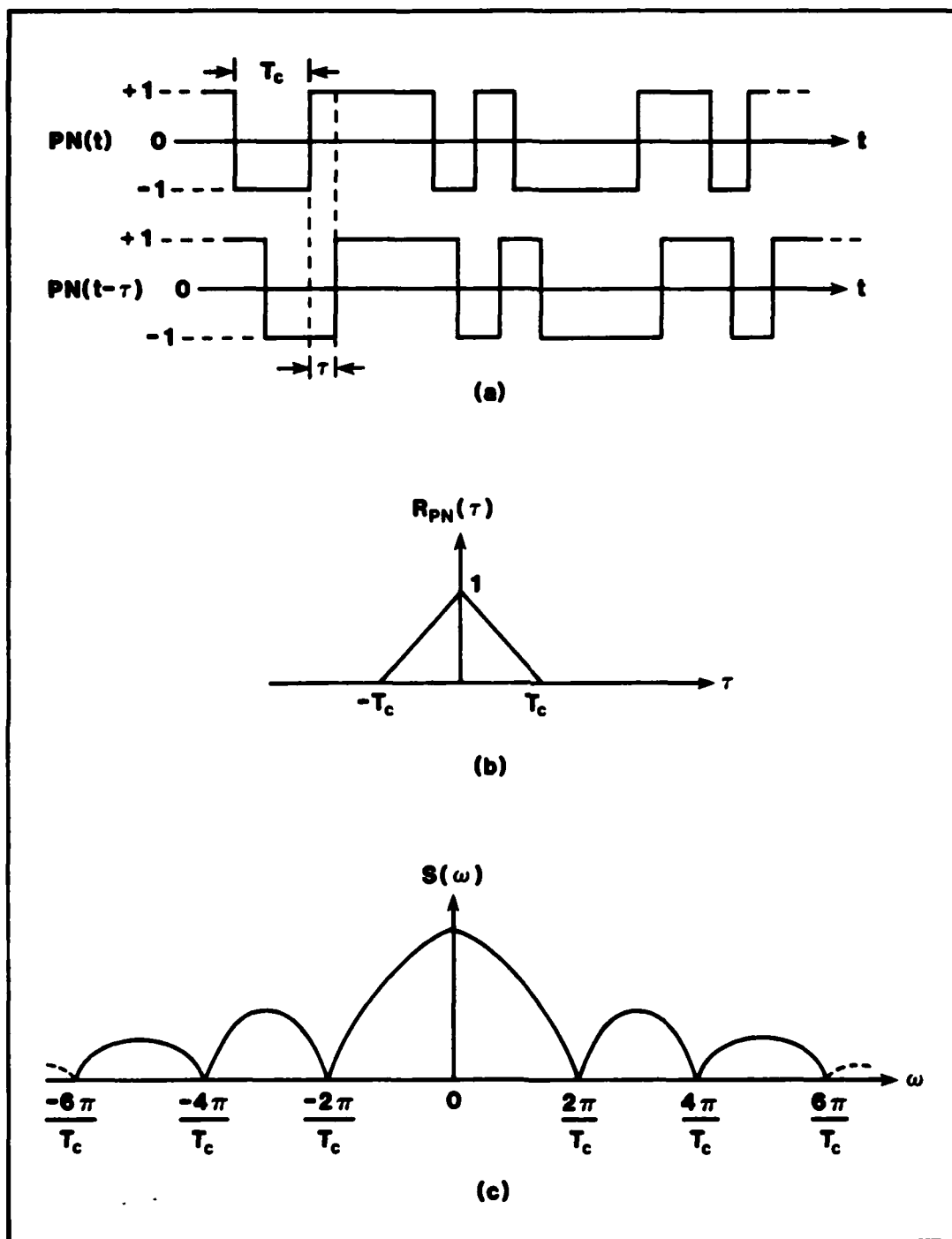


**Figure 3. Autocorrelation Function and Power Spectral Density of a PN Sequence**

**(a) PN Code Sequence**

**(b) Autocorrelation Function**

**(c) Power Spectral Density.**

probability of being plus one or minus one. On the other hand, for  $|\tau| \leq T_c$ , the average value over one chip of  $PN(t) \cdot PN(t+\tau)$  is given by the area of the overlapping part of the displaced chips divided by  $T_c$ , as illustrated in Figure 3a. This area is given by  $T_c - |\tau|$ , so

$$R_{PN}(\tau) = \begin{cases} \frac{1}{T_c} (T_c - |\tau|) & \text{for } |\tau| \leq T_c \\ 0 & \text{for } |\tau| > T_c \end{cases} \quad (2)$$

as illustrated in Figure 3b.

The power spectral density (PSD),  $S_{PN}(\omega)$ , for a PN sequence is found as a consequence of the Wiener - Khintchine theorem applied to the autocorrelation function  $R_{PN}(\tau)$ :

$$S_{PN}(\omega) = \int_{-\infty}^{\infty} R_{PN}(\tau) e^{-j\omega\tau} d\tau \quad (3)$$

Because  $R_{PN}(\tau)$  is an even function, the PSD can be expressed, utilizing Euler's formula, as

$$S_{PN}(\omega) = \int_{-\infty}^{\infty} R_{PN}(\tau) \cos(\omega\tau) d\tau \quad (4)$$

Further, substituting  $R_{PN}(\tau)$  and making use of symmetry yields

$$\begin{aligned}
 S_{PN}(\omega) &= \frac{2}{T_c} \int_0^{T_c} (T_c - |\tau|) \cos(\omega\tau) d\tau \\
 &= T_c \frac{\sin^2(\omega T_c/2)}{(\omega T_c/2)^2}
 \end{aligned}
 \tag{5}$$

The PSD,  $S_{PN}(\omega)$ , is shown in Figure 3c.

### Spread Spectrum System Performance

In reference to Figure 1, the transmitted waveform of the SS system model is given by

$$S(t) = \sqrt{2E/T} \, d(t)PN(t)\cos(\omega_c t) \quad 0 \leq t \leq T
 \tag{6}$$

where  $T$ , the message bit interval, is an integer multiple of  $T_c$ , the code bit interval. The received signal can be represented by

$$R(t) = S(t) + n(t)
 \tag{7}$$

where  $n(t)$  is zero mean, white Gaussian noise (WGN) with a PSD of  $S_n(\omega) = N_0/2$  (watts/Hz), and is independent of the PN code. Assuming code synchronization, the received waveform is multiplied by a stored replica of the code to produce the

following:

$$\begin{aligned}
 R'(t) &= \sqrt{2E/T} \, d(t)PN^2(t)\cos(\omega_0 t) + PN(t)n(t) \\
 &= \sqrt{2E/T} \, d(t)\cos(\omega_0 t) + n'(t)
 \end{aligned}
 \tag{8}$$

The autocorrelation of  $n'(t)$  is given by

$$\begin{aligned}
 R'(t_1, t_2) &= E \{ n'(t_1)n'(t_2) \} \\
 &= E \{ PN(t_1)PN(t_2) \} E \{ n(t_1)n(t_2) \} \\
 &= R_{PN}(t_1 - t_2)(N_0/2) \delta(t_1 - t_2)
 \end{aligned}
 \tag{9}$$

The delta function allows a non-zero value only when  $t_1 = t_2$ , thus

$$\begin{aligned}
 R'(t_1 - t_2) &= R_{PN}(0)(N_0/2) \delta(t_1 - t_2) \\
 &= (N_0/2) \delta(t_1 - t_2)
 \end{aligned}
 \tag{10}$$

Therefore,  $n'(t)$  is WGN. This is supported by Ziemer and Tranter in their work showing that any linear operation on a Gaussian process yields a Gaussian process (Ref.28:305). The problem is thus reduced to a threshold detection problem of determining whether  $H_0$  or  $H_1$  is true using binary antipodal signaling in WGN. The probability of error  $P(E)$  is given by

$$P(E) = \text{erfc} \left( \sqrt{2E/N_0} \right) \quad (11)$$

where the message bits are assumed equally likely and where the complement error function (erfc) is given by

$$\text{erfc}(x) = \frac{1}{\sqrt{2\pi}} \int_x^{\infty} \exp(-y^2/2) dy \quad (12)$$

Therefore, for WGN, the performance of a SS system is identical to a conventional system.

The performance characteristics of an SS system become obvious in the presence of a strong, narrowband, interfering signal centered about the carrier frequency. Assume the interfering signal,  $I(t)$ , to be zero mean and Gaussian with a PSD,  $S_I(\omega)$ , as illustrated in Figure 4. Also, assume the interfering signal to be uncorrelated with the PN code. The analysis would be incorrect for a repeat jammer because of the correlation between the PN code and jammer.

The received signal is now given by

$$R(t) = S(t) + n(t) + I(t) \quad (13)$$

further,

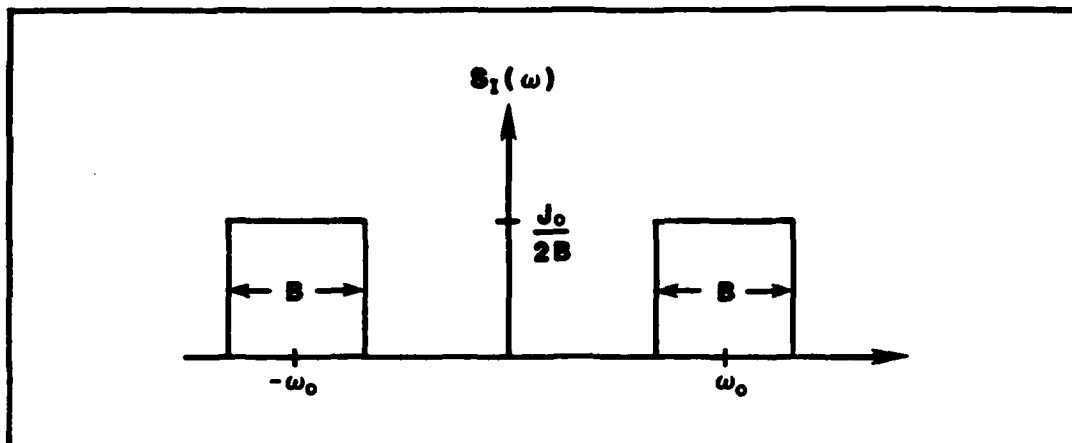
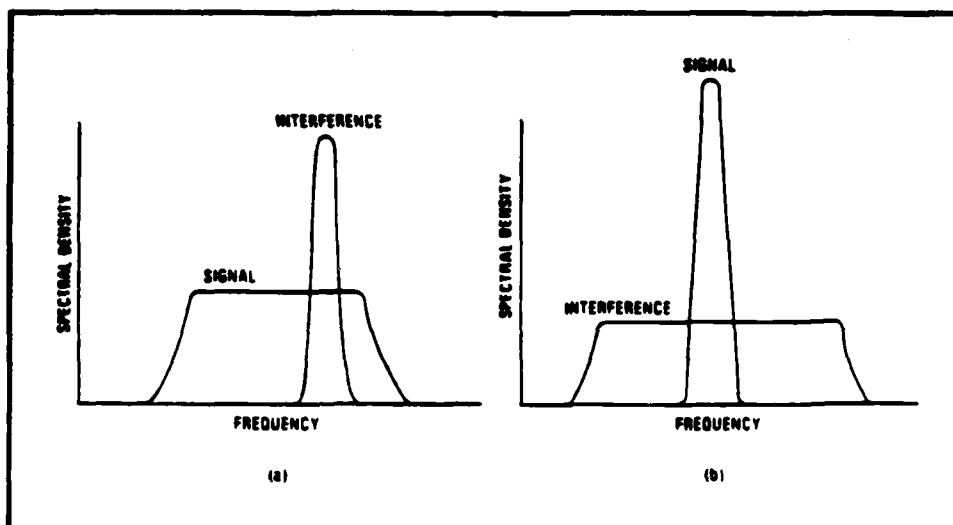


Figure 4. Power Spectral Density of Interfering Signal,  $I(t)$ .

$$\begin{aligned}
 R'(t) &= \sqrt{2E/T} \quad d(t)PN^2(t)\cos(\omega_0 t) + PN(t) [n(t) + I(t)] \\
 &= \sqrt{2E/T} \quad d(t)\cos(\omega_0 t) + n''(t)
 \end{aligned}
 \tag{14}$$

Multiplication of the received signal by the reference PN code strips the code off the signal and reduces the interference as qualitatively illustrated in Figure 5. Figure 5a shows the relative spectra of the received signal and interference. Multiplication by the reference PN code produces the spectra qualitatively depicted in Figure 5b at the input to the correlation detector. The message signal bandwidth is reduced from  $W$  (the PN code bandwidth) to  $B$  (the original message bandwidth), while the interference energy is spread over a bandwidth exceeding  $W$ .

The autocorrelation of  $n''(t)$  is given by



**Figure 5. Spectra of Desired Signal and Interference**

**(a) Received Signal**

**(b) Correlation Detector Output (Ref. 24:27).**

$$\begin{aligned}
 R''(t_1, t_2) &= E \{ n''(t_1) n''(t_2) \} \\
 &= E \{ PN(t_1) PN(t_2) \} \\
 &\quad \cdot E \{ [n(t_1) + I(t_1)] [n(t_2) + I(t_2)] \}
 \end{aligned}
 \tag{15}$$

$$\begin{aligned}
 R''(t_1, t_2) &= R_{PN}(t_1 - t_2) \left[ E \{ n(t_1) n(t_2) \} + E \{ n(t_1) I(t_2) \} \right. \\
 &\quad \left. + E \{ I(t_1) n(t_2) \} + E \{ I(t_1) I(t_2) \} \right]
 \end{aligned}
 \tag{16}$$

Because  $n(t)$  and  $I(t)$  are independent of each other, the autocorrelation can be written as



$$R''(t_1, t_2) = R_{PN}(t_1 - t_2) \left[ (N_0/2) \delta(t_1 - t_2) + R_I(t_1 - t_2) \right] \quad (17)$$

The autocorrelation of the interfering signal,  $R_I(\tau)$ , is found by taking the inverse Fourier transform of  $S_I(\omega)$  with  $\tau = t_1 - t_2$ , that is

$$\begin{aligned} R_I(\tau) &= \frac{1}{2\pi} \int_{-\infty}^{\infty} S_I(\omega) e^{j\omega\tau} d\omega \\ &= \frac{1}{2\pi} \int_{\omega_0 - B/2}^{\omega_0 + B/2} (J_0/2B) e^{j\omega\tau} d\omega \\ &= J_0 \frac{\sin(\pi B\tau)}{\pi B\tau} \cos(\omega_0\tau) \end{aligned} \quad (18)$$

The autocorrelation of  $n^*(t)$  then transforms to the following:

$$\begin{aligned} R''(\tau) &= R_{PN}(\tau) (N_0/2) \delta(\tau) + R_{PN}(\tau) J_0 \frac{\sin(\pi B\tau)}{\pi B\tau} \cos(\omega_0\tau) \\ &= (N_0/2) \delta(\tau) + R_{PN}(\tau) J_0 \frac{\sin(\pi B\tau)}{\pi B\tau} \cos(\omega_0\tau) \end{aligned} \quad (19)$$

For the case of narrowband jamming,  $B \rightarrow 0$ ; thus  $R''(\tau)$  reduces to the following:

$$R''(\tau) = (N_0/2) \delta(\tau) + R_{PN}(\tau) J_0 \cos(\omega_0 \tau) \quad (20)$$

The PSD of  $n''(t)$  is given by

$$\begin{aligned} S''(\omega) &= \int_{-\infty}^{\infty} (N_0/2) \delta(\tau) e^{-j\omega\tau} d\tau + \int_{-\infty}^{\infty} R_{PN}(\tau) J_0 \cos(\omega_0 \tau) e^{-j\omega\tau} d\tau \\ &= (N_0/2) + (J_0 T_c / 2) \frac{\sin^2[(\omega - \omega_0) T_c / 2]}{[(\omega - \omega_0) T_c / 2]^2} \\ &\quad + (J_0 T_c / 2) \frac{\sin^2[(\omega + \omega_0) T_c / 2]}{[(\omega + \omega_0) T_c / 2]^2} \end{aligned} \quad (21)$$

$S''(\omega)$  is illustrated in Figure 6. The bandwidth of  $PN(t)I(t)$  is much wider than the bandwidth of  $PN(t) \cdot s(t)$  because the data pulse duration,  $T$ , is typically several orders of a magnitude greater than the code pulse deviation,  $T_c$ . Over the message bandwidth, the PSD of  $PN(t) \cdot I(t)$  is approximately flat and is processed by the correlation detector as an additive WGN term. Using this approximation, the PSD of  $n''(t)$  becomes

$$S''(\omega) = (N_0/2) + (J_0^2 T_c / 2) \quad (22)$$

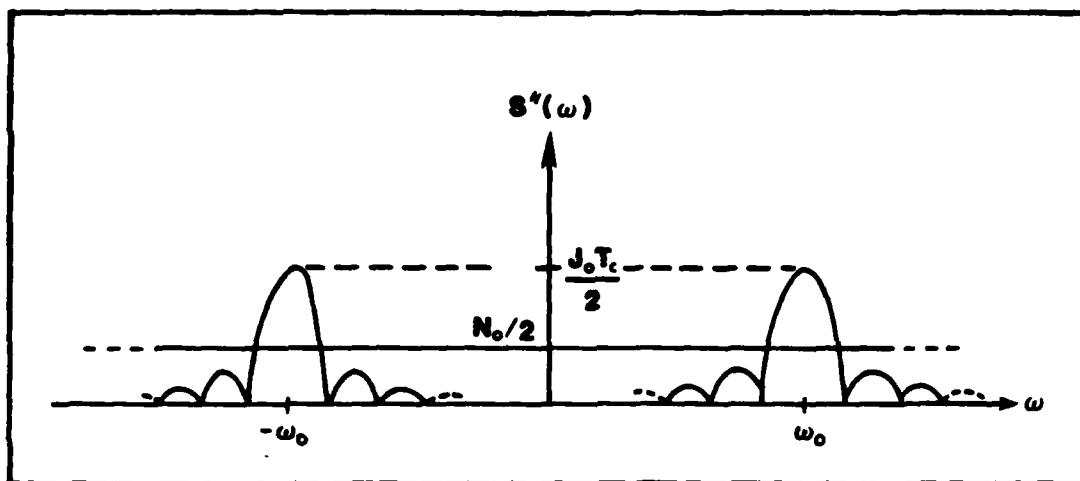


Figure 6. Power Spectral Density of  $n''(t)$ .

The probability of error,  $P(E)$ , in deciding if the transmitted message was a plus one or a minus one, is given by

$$P(E) = \text{erfc} \left[ \sqrt{2E/(N_0 + J_0 T_c)} \right] \quad (23)$$

The improved performance due to SS techniques can be determined by comparing the above  $P(E)$  with the case when no PN code is used.

If a PN code is not utilized in the system, corresponding to the case when  $PN(t) = 1$ , then the autocorrelation of the noise as  $B \rightarrow 0$  becomes

$$R''(\tau) = (N_0/2) \delta(\tau) + J_0 \cos(\omega_0 \tau) \quad (24)$$

and the PSD of the noise becomes

$$S''(\omega) = (N_0/2) + J_0/2 \delta(\omega + \omega_0) + J_0/2 \delta(\omega - \omega_0) \quad (25)$$

The mean and variance of the sufficient statistic,  $e$ , must be found in order to determine the  $P(E)$  for this case of no PN code. From the communications system model of Figure 1, the sufficient statistic becomes

$$\begin{aligned} e &= \int_0^T R'(t) \sqrt{2E/T} \cos(\omega_0 t) dt \\ &= 2E/T \int_0^T d(t) \cos^2(\omega_0 t) dt + \sqrt{2E/T} \int_0^T n(t) \cos(\omega_0 t) dt \\ &\quad + \sqrt{2E/T} \int_0^T I(t) \cos(\omega_0 t) dt \end{aligned} \quad (26)$$

The conditional means are given by

$$\begin{aligned} E\{e/H_0\} &= 2E/T \int_0^T E\{d(t)/H_0\} \cos^2(\omega_0 t) dt \\ &\quad + \sqrt{2E/T} \int_0^T E\{n(t)/H_0\} \cos(\omega_0 t) dt \\ &\quad + \sqrt{2E/T} \int_0^T E\{I(t)/H_0\} \cos(\omega_0 t) dt \\ &= 2E/T \int_0^T \cos^2(\omega_0 t) dt = E = \bar{e}_0 \end{aligned} \quad (27)$$

and similarly

$$E \{e/H_1\} = -E = \bar{e}_1 \quad (28)$$

The conditional variances of the sufficient statistic are equal (Ref.25:177), that is

$$\begin{aligned} \text{Var} (e/H_0) &= \text{Var} (e/H_1) \\ &= 2 E/T \int_0^T \int_0^T R''(t,u) \cos(\omega_0 t) \cos(\omega_0 u) dt du \\ &= (EN_0/2) + (EJ_0 T/2) = \sigma^2 \end{aligned} \quad (29)$$

Therefore, the PDF of the sufficient statistic is Gaussian with mean  $\bar{e}_0$  or  $\bar{e}_1$ , and variance  $\sigma^2$ . The  $P(E)$  in estimating the correct message sent is as follows:

$$\begin{aligned} P(E) &= P(e > 0/H_1)P(H_1) + P(e < 0/H_0)P(H_0) \\ &= P(e < 0/H_0) \\ &= \frac{1}{\sqrt{2\pi} \sigma} \int_{-\infty}^0 \exp \left[ -\frac{1}{2} \frac{(x - \bar{e}_0)^2}{\sigma^2} \right] dx \\ &= \text{erfc} \left[ \sqrt{\frac{2E}{N_0 + J_0 T}} \right] \end{aligned} \quad (30)$$

or

$$\begin{aligned}
 P(E) &= P(e > 0 / E_1) \\
 &= \frac{1}{\sqrt{2\pi} \sigma} \int_0^{\infty} \exp \left[ -\frac{1}{2} \frac{(x - \bar{x}_1)^2}{\sigma^2} \right] dx \\
 &= \operatorname{erfc} \left[ \sqrt{2E/N_0 + J_0 T} \right]
 \end{aligned}
 \tag{31}$$

Equations (23) and (31) are now compared to show the effect of the PN code on system performance. If  $N_0$  is considered negligible, then the effect of the narrowband interference on the system performance was reduced from  $J_0 T$  to  $J_0 T_c$ . The improvement gained through this use of a PN code can be expressed as the ratio

$$\frac{J_0 T}{J_0 T_c} = \frac{T}{T_c} = PG
 \tag{32}$$

and is called the processing gain (PG) of the SS system. Since the RF transmitted bandwidth equals  $1/T_c$ , and the data bandwidth equals  $1/T$ , PG can be equivalently expressed as  $B_{RF}/B_{data}$ .

The above analysis depicts how a SS system achieves interference rejection, and that the PG is the quantitative measure of this capability. Thus, a SS system can operate at the lower signal-to-noise ratio

$$[S/N]_{ss} = \frac{1}{PG} [S/N]_{data} \quad (33)$$

where  $[S/N]_{data}$  is that needed by a conventional receiver for the same message modulation. The receiver can operate at very low S/N ratios if PG is large.

The principles of SS systems that have been presented in this section should be adequate to present to the reader the technical basis of SS for this thesis study. In the next section, further interference suppression techniques will be presented which complement the interference suppression capability already inherent in SS systems.

### **III. SAW Adaptive Interference Suppression Techniques**

Further interference rejection in a SS system can be realized by the insertion of a pre-detection filter. An adaptive pre-detection filter in its basic form is a device which adjusts its internal parameters and optimizes its performance according to the statistical characteristics of its input and output signals. The internal parameter adjustment is accomplished via a series of variable settings controlled by an adaptive algorithm (Ref.27:616).

Several devices, other than SAW devices, have been considered for application to the interference rejection problem. They are charge-coupled devices (CCDs), magnetostatic wave (MSW) devices, and acousto-optic devices.

#### **Alternative Technologies**

Since its beginning in 1969, the CCD has been used for many applications including signal processing, optical and infrared imaging, and digital memory applications (Ref.9:392). The CCD device easily adapts to implement transversal filters, however, the disadvantages of the CCD approach are the lower frequency of operation and the tolerance on sample time required for wide bandwidth and high dynamic range (Ref.22:2-3). Further, the external circuitry required for programming the filter tap weights would make up



approximately 90 percent of the programmable transversal filter (PTF), creating a problem for its construction into a monolithic chip. It is clear then that the CCDs projected performance in the foreseeable future is far below that required for PTFs and wideband interference suppression.

Magnetostatic waves are slow, dispersive, magnetically dominated electromagnetic waves which propagate in magnetically biased ferrite materials at frequencies of 1-20 GHz (Ref.14:506). These MSWs can be exploited in devices offering instantaneous bandwidths of up to 2.2 GHz at microwave center frequencies from 0.5 to 20 GHz (Ref.14:506). MSW devices have lower propagation loss than SAW devices, however, below 3 GHz SAW devices are superior. At present, MSW devices are not suitable for interference suppression, and they are still in the research and development stage.

Acousto-optic spectrum analysis techniques have become popular in the past few years as low cost, small size methods of performing spectral analysis on wideband signals with high probability of interception. These methods are applicable to intercept and radar warning receivers, but in communications receivers, dynamic range is severely limited due to optical scattering (Ref.22:2-4). Decoding of SS waveforms becomes impossible because phase information is not available at the detector output unless a complex holographic system is employed. Although acousto-optic spectrum analyzers possess acceptable frequency and bandwidth characteristics, the

limited dynamic range and absence of phase information in the analyzers appropriate for adaptive interference suppression renders acousto-optics inappropriate for the filtering operation under study in this thesis effort.

### SAW - Programmable Transversal Filter Technology

SAW devices possess characteristics that make them a robust choice for programmable transversal filter (PTF) implementation in SS systems. The SAW AIS filter has the potential to revolutionize the field of partially secure, antijam communications. Adjustable tap weights on this device allow any transfer function (bandpass or bandreject response) within the overall bandwidth and time duration of the device to be realized. A SAW PTF model has been constructed by Texas Instruments to cover the frequency band 200-300 MHz with a minimum resolution of 12.5 MHz (Ref.22:2-4). This PTF can be converted to an AIS filter by implementing measurement and feedback paths to iteratively alter the frequency response which selectively suppresses undesired waveforms. Selection of an adaptive algorithm to accomplish the measurement and feedback functions was carried out by Texas Instruments. Four classes of algorithms exist in the literature which can perform the required adaptive filtering, however because of hardware constraints imposed by the PTF, certain algorithms are more suitable for use in this application than others. A computer simulation model of the

existing breadboard PTF enabled Texas Instruments to choose the AIS algorithm which best exploits the advantages of the existing technology and minimizes the effects of device limitations.

The steepest descent (Refs.1,2,6,10,26,27) class of algorithms, in particular the Applebaum and the power inversion algorithms, are considered by Texas Instruments as the most suitable for AIS PTF implementation for the reasons stated in the assumptions sub-section of section I. A survey of the four classes of adaptive algorithms presenting their basic characteristics, advantages, and disadvantages is given in Appendix A.

#### SAW Device Theory

Elastic waves are the basis for SAW filter operation because they travel in suitable solids with negligible loss and at velocities, typically, of  $10^3$  to  $10^4$  meters-per-second. This leads to operating frequencies of from 30 to 800 MHz for practical SAW filters (Ref.12:1).

SAW technology has reduced the size and weight of filters because surface waves travel at velocities four or five orders of magnitude lower than electromagnetic waves. This reduction in size is proven with typical values of wave velocity,  $v$ , and frequency,  $f$ , as follows:

For elastic waves the intertap spacing,  $\lambda$  is given by

$$\lambda = v/f = \frac{3000 \text{ m/sec}}{300 \text{ MHz}} = 10\mu\text{m}$$

(34)

For electromagnetic waves  $\lambda$  is given by

$$\lambda = \frac{3 \times 10^8 \text{ m/sec}}{300 \text{ MHz}} = 1\text{m}$$

(35)

Rayleigh waves are the type of elastic waves employed in SAW filters because they can propagate along the free surface of a solid and still remain confined to the vicinity of that surface. If the solid is piezoelectric, then an elastic wave traveling on its surface produces an electric wave so that a traveling electric field extends above the surface and can interact with any metal electrodes on its surface (Ref.12:1). This generation of an electric field is the "piezoelectric effect" and is formally stated as follows: In certain crystals, mechanical strain produces a proportional electric polarization and, conversely, an applied electric field produces a proportional mechanical strain (Ref.12:5).

SAW waves are generated and detected by means of an interdigital transducer (IDT). The IDT is made up of metal contacts periodically spaced on the surface of a

piezoelectric material (or substrate). A basic SAW device is shown in Figure 7. The typical width of each electrode is  $\lambda/4$ , the spacing between adjacent electrodes is  $\lambda/4$ , and the spacing between alternate electrodes is  $\lambda$  where  $\lambda$  equals the wavelength of the substrate (Ref.9:390). When a radio frequency (RF) voltage is applied to the input IDT, electric fields are set up within the substrate and these electric fields generate stress patterns via the piezoelectric effect. Therefore, the substrate has elastic waves traveling in both directions normal to the electrodes. The output IDT, employed for the detection process, utilizes the same configuration as the input IDT.

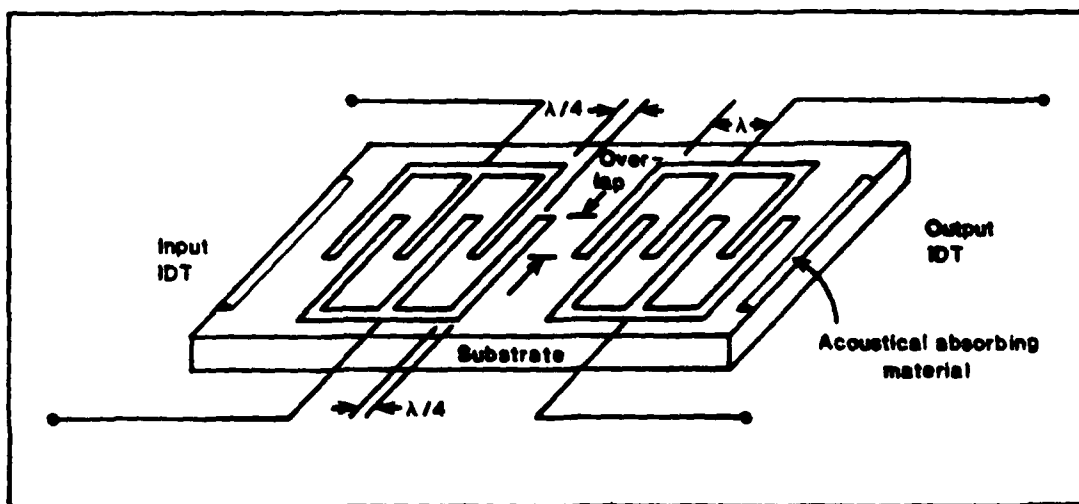


Figure 7. Typical SAW Device (Ref. 9:390).

The SAW-PTF under study in this thesis is one of the filters presently under study by Texas Instruments. The existing SAW filter is based on a lithium niobate ( $\text{LiNbO}_3$ )

substrate consisting of a conventional wideband input IDT at 250 MHz and a 16 tap output electrode array which samples the SAW at a 200 MHz rate (Ref.22:2-10). The sample rate of 200 MHz was chosen from the concept of sub-harmonic sampling. That is, the sample rate equals twice the usable bandwidth of the filter, or  $2 \times 100$  MHz. The programmability of this transversal filter allows a single filter to operate as a bandpass, band-reject, adaptable, or matched filter.

It should be pointed out that although silicon (Si) or  $\text{LiNbO}_3$  based technologies provide high levels of integration, even higher levels of integration and speed are needed for microcircuit applications in the late 1980s and 1990s. Also, there has been some concern about the levels of natural and nuclear radiation hardness not achievable with Si microcircuits, especially in those deployed in space applications. Gallium arsenide (GaAs) based technologies are being developed to afford the electronics engineer with the capability of higher speed, more integrated, and greater radiation hardened microcircuits than is presently available with Si or  $\text{LiNbO}_3$  devices (Ref.17:76-78).

The operation of the PTF consists of four parts. The four parts are SAW excitation, SAW detection, tap weighting, and tap weight distribution. A SAW is excited via a wideband input IDT. The wave is sampled once each wavelength by a detector array of  $1/200$  MHz = 5 Nsec spaced output electrodes. The PTF detector array is illustrated in Figure 8

with ground electrodes removed for clearness. The sampled RF potential in each tap is amplified and weighted before being summed with the other tap signals. This amplification and weighting of the RF signal is accomplished through the use of dual-gate field effect transistors (FETs). Each output electrode is connected to the high frequency gates of two dual-gate FETs, one for each phase. The RF potential is applied to the first gate (inner gate) of the two dual-gate FETs, and the individual tap weight control voltages are applied to the second gate (outer gate). The FETs are connected sequentially to two drain buses. One drain bus being positive, and the other being negative. The FETs choose which bus the RF potential is sent to, and also allow for variable tap weight amplitudes. If the upper FET control gate voltage is increased (e.g. biased on), then a positive weight is produced. On the other hand, if the lower control gate voltage is biased on, then a negative weight is produced.

The key to realizing an arbitrary frequency response, that is a fixed bandwidth  $\sin x/x$  function, with a SAW filter is to determine the appropriate weighting voltages of the IDT electrodes. Because the SAW filter can be thought of as a discrete time sampling device with finite impulse response (FIR), the large body of digital filter theory can be applied to SAW filter design (Ref.20:132).

The PTF under study has achieved the translation of

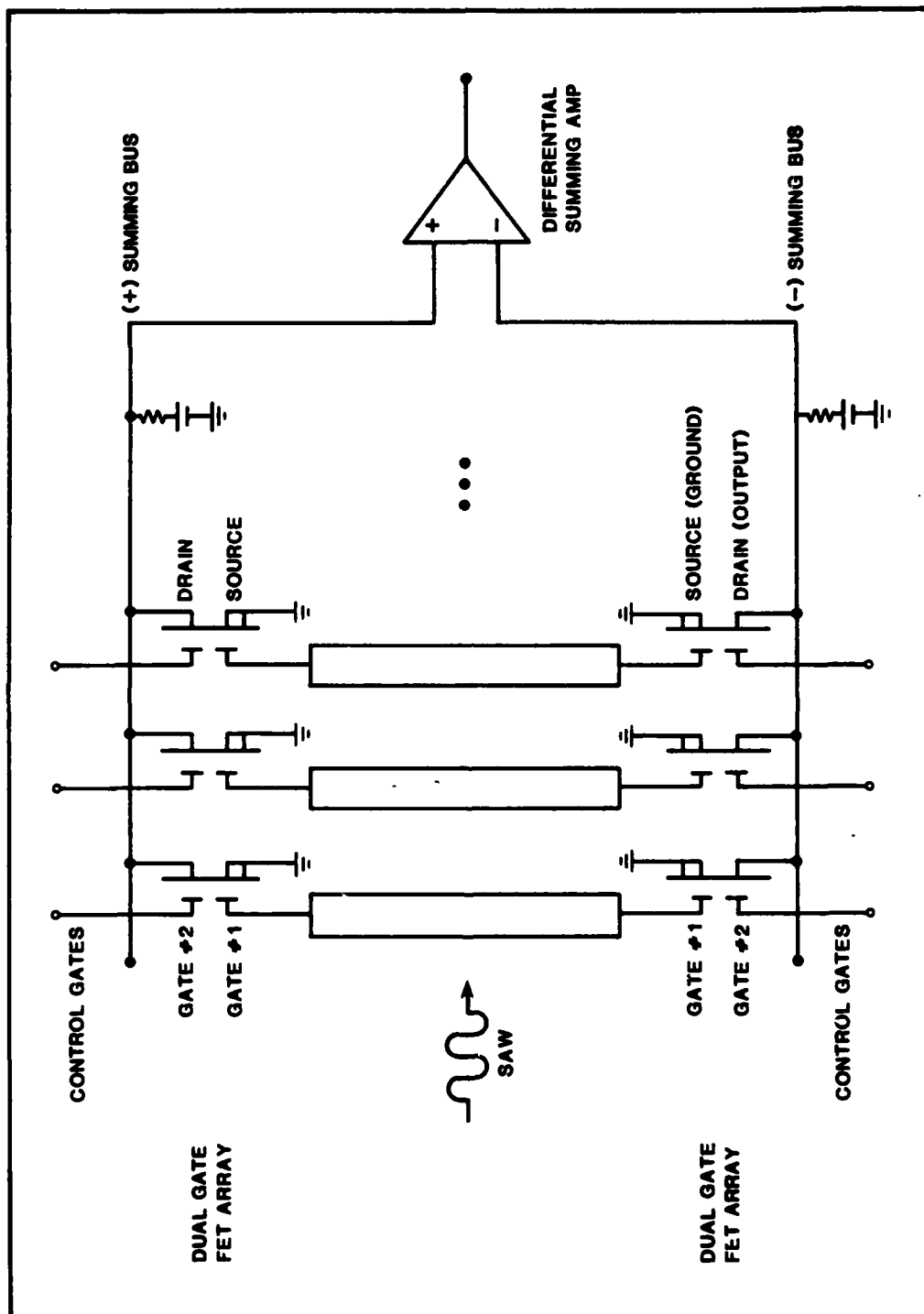


Figure 8. PTF Biphas Detector Array (Ref. 22:2-10).



its  $\sin x/x$  frequency response to any center frequency from 200 to 300 MHz. This frequency response translation is illustrated step by step in Figure 9. An infinite set of delta functions in the time domain transforms to an infinite set of delta functions in the frequency domain, but separated by the inverse of the time sample ( $\Delta t$ ). The PTF under study has 16 time domain samples, or tap weights, so the infinite set of time domain delta functions are time gated to 16 delta functions as shown in Figure 9b. This time gating transforms to the  $\sin x/x$  response in the frequency domain. Control over placement of these  $\sin x/x$  responses is accomplished by modulating the tap weights with a slowly varying cosine function whose frequency equals the difference between the spatial sampling,  $f_0 = 200$  MHz, and the desired center frequency,  $f_c$ . This modulating by a cosine function is shown in Figure 9e. The frequency range of interest is then bandpass filtered as shown in figure 9f.

The tap weights in the time domain are given by:

$$h(t_n) = \cos \left[ 2\pi t_n (f_c - f_0) \right] \quad (36)$$

where  $t_n = n \cdot \Delta t$ . A sample tap weight calculation for a 275 MHz center frequency is as follows:

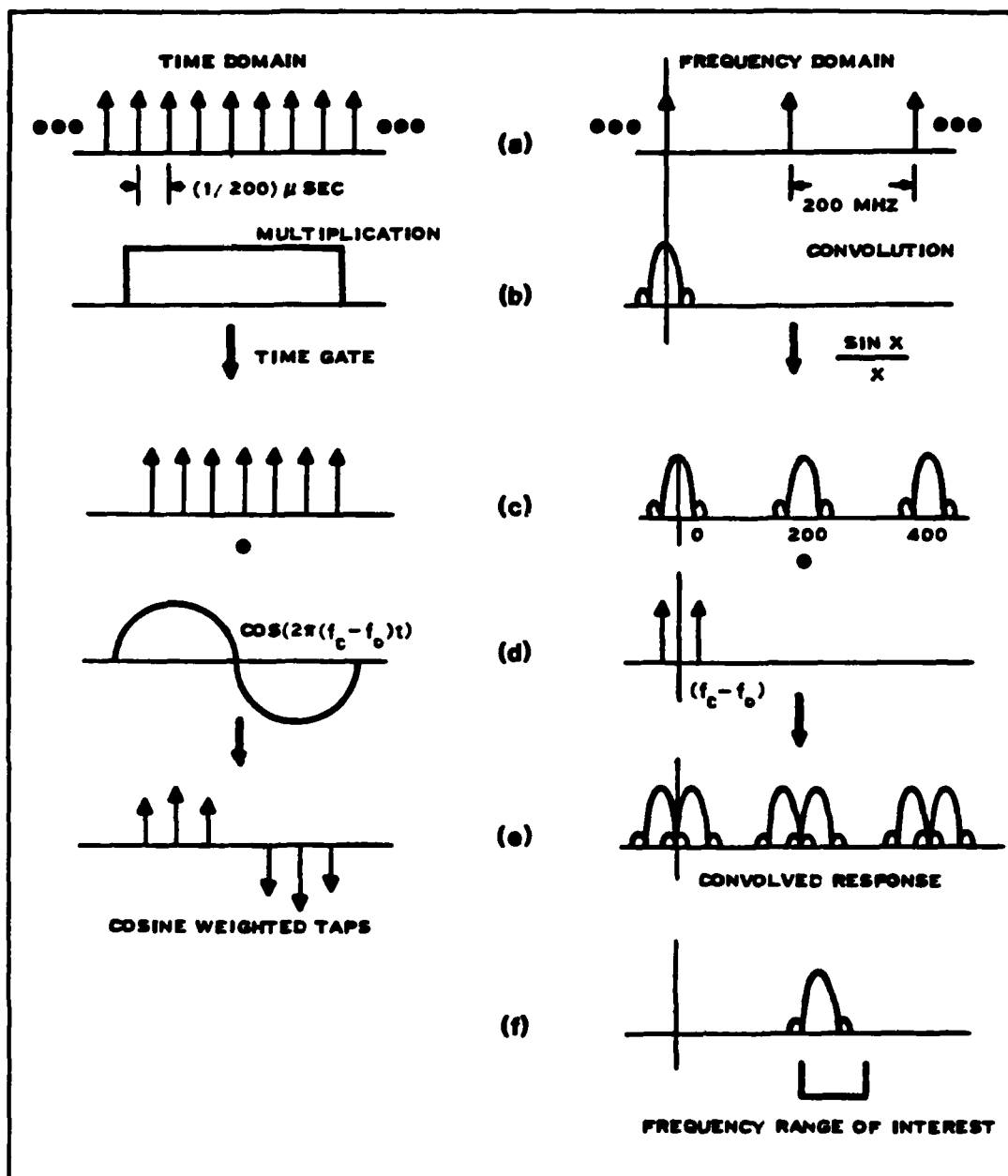


**Figure 9. PTF Frequency Translation**  
 (a) An Infinite Set of Time and Frequency Domain Delta Functions  
 (b) Time Window Function  
 (c) Gated Delta Functions  
 (d) Multiplication by  $\cos(2\pi(f_c - f_o)t)$   
 (e) Cosine Modulated Tap Weights  
 (f) Filtered Frequency Domain (Ref. 22:2-13).

$$\begin{aligned}
h(t_n) &= \cos [2\pi n \Delta t (275-200)] \\
&= \cos [2\pi n \cdot 75/200] \\
&= \cos [n3\pi/4] \\
&= 1.0, -0.707, 0.0, 0.707, -1.0, 0.707, 0.0, -0.707, \text{ etc.} \\
&\hspace{15em} (37)
\end{aligned}$$

A hybrid PTF has been designed and built by Texas Instruments on a  $\text{LiNbO}_3$  substrate. The experimental tap weight linear control range was found to be greater than 40 dB. This is illustrated in Figure 10 where normalized RF output voltage from the dual-gate FET drain is plotted as a function of offset control gate voltage from gate #2. Also, the tap switching speed, from +1 to -1, was found to be approximately 100 ns (Ref.22:2-12).

#### Programmable Transversal Filters Utilizing Adaptive Interference Suppression Techniques

As mentioned previously, four classes of adaptive algorithms exist which can be implemented to iteratively "null out" jamming and/or interfering signals in communications systems. The steepest descent class of algorithms, in particular the Applebaum and Power Inversion algorithms, were chosen for implementation to perform the adaptation because of their minimization of both hardware constraints and convergence time (Ref.22:2-21).

Several configurations for implementing steepest descent algorithms with the PTF have been considered.

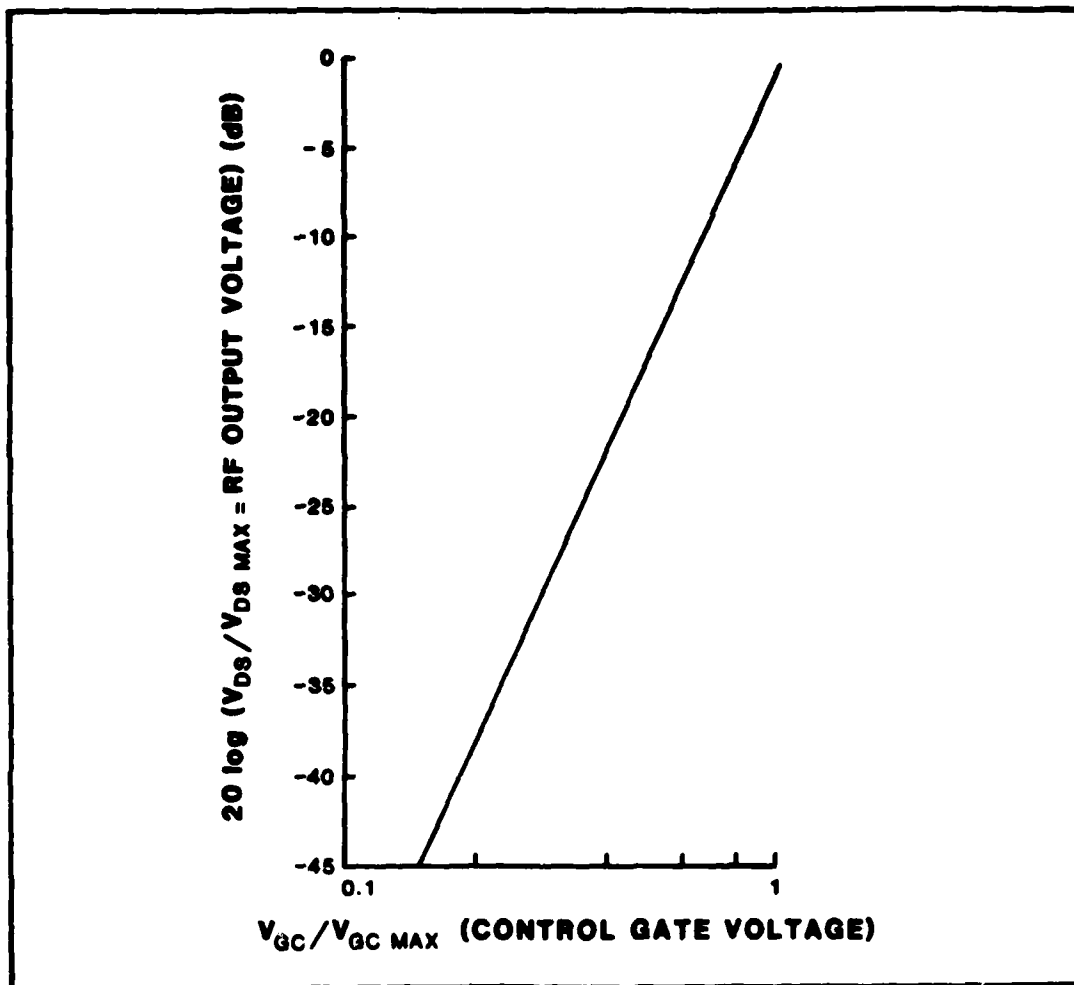


Figure 10. Tap Weight Control Range (Ref. 22:2-16).

Basically, there are two types of approaches; one involves access to individual tap outputs while the other does not provide for individual access to tap outputs.

The configuration which utilizes access to individual tap outputs employs a processor for each tap and can thus realize simultaneous adjustment of all tap weights as

illustrated in Figure 11. Simultaneous tap weight adjustment creates the advantage of fast adaptation time, however, it introduces the difficulty of simultaneous equalization and hardware complexity. Further, the increased hardware complexity required for individual tap access to the 200-600 tap PTFs of the near future would make this configuration impractical.

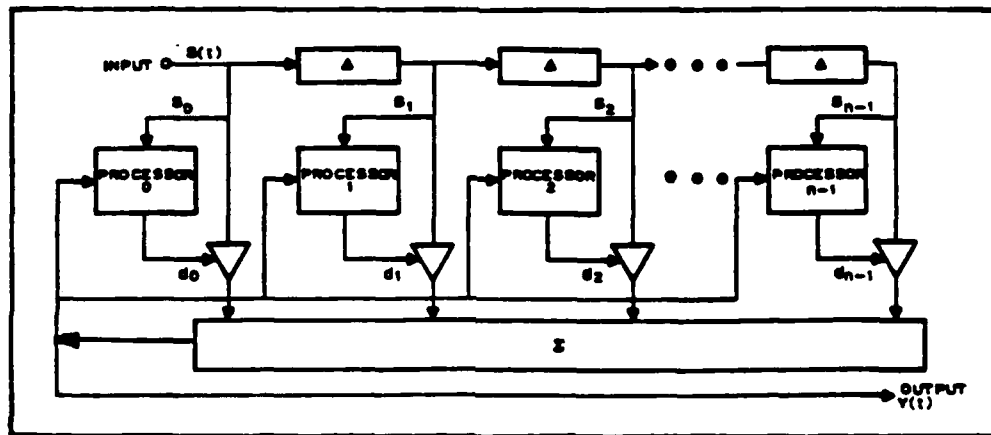
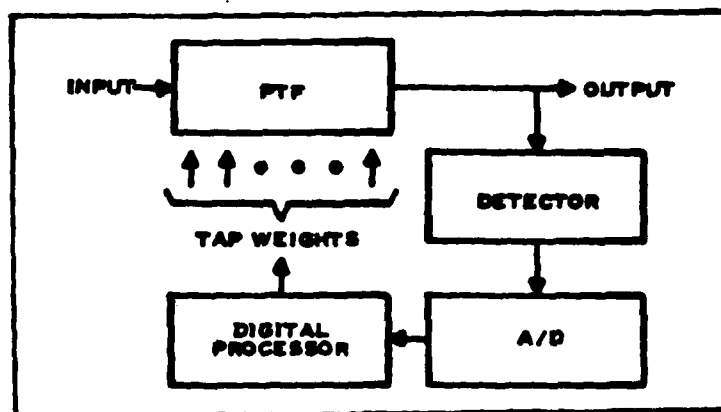


Figure 11. Configuration Utilizing Access to Individual Tap Outputs for Simultaneous Tap Weight Adjustment (Ref. 22:2-26).

A better configuration which does not require access to individual tap outputs is illustrated in Figure 12. Adaption is accomplished using the PTF output which creates the disadvantage of this configuration in that the filter response is not available during adaptation.

Texas Instrument's proposed baseline adaptive PTF configuration and the one chosen for study in this thesis utilizes two PTFs as shown in Figure 13. One PTF is employed to both monitor interference and compute the desired tap



**Figure 12. Configuration Utilizing a Single PTF Without Access to Individual Tap Outputs (Ref. 22:2-27).**

weights for the other PTF, which is utilized for interference suppression. This overcomes the limitation of the previous configuration in Figure 12 by allowing for access to the filter output while the adaptation is taking place.

The full scale proposed adaptive PTF configuration is illustrated in Figure 14. The main PTF is implemented with complex weights and consists of two PTFs. The incoming RF signal is split into its in-phase (I) and quadrature (Q) components by a quadrature hybrid 3 dB splitter. In this way, both the in-phase and quadrature channel PTFs are implemented with real weights. The complex weight implementation produces an improved nulling capability, minimum distortion in the adapted response, and doubles the usable bandwidth of the filter for constant intertap delay. The weight vector driving this filter, via the data processor, consists of a superposition of quiescent weights and perturbation weights.

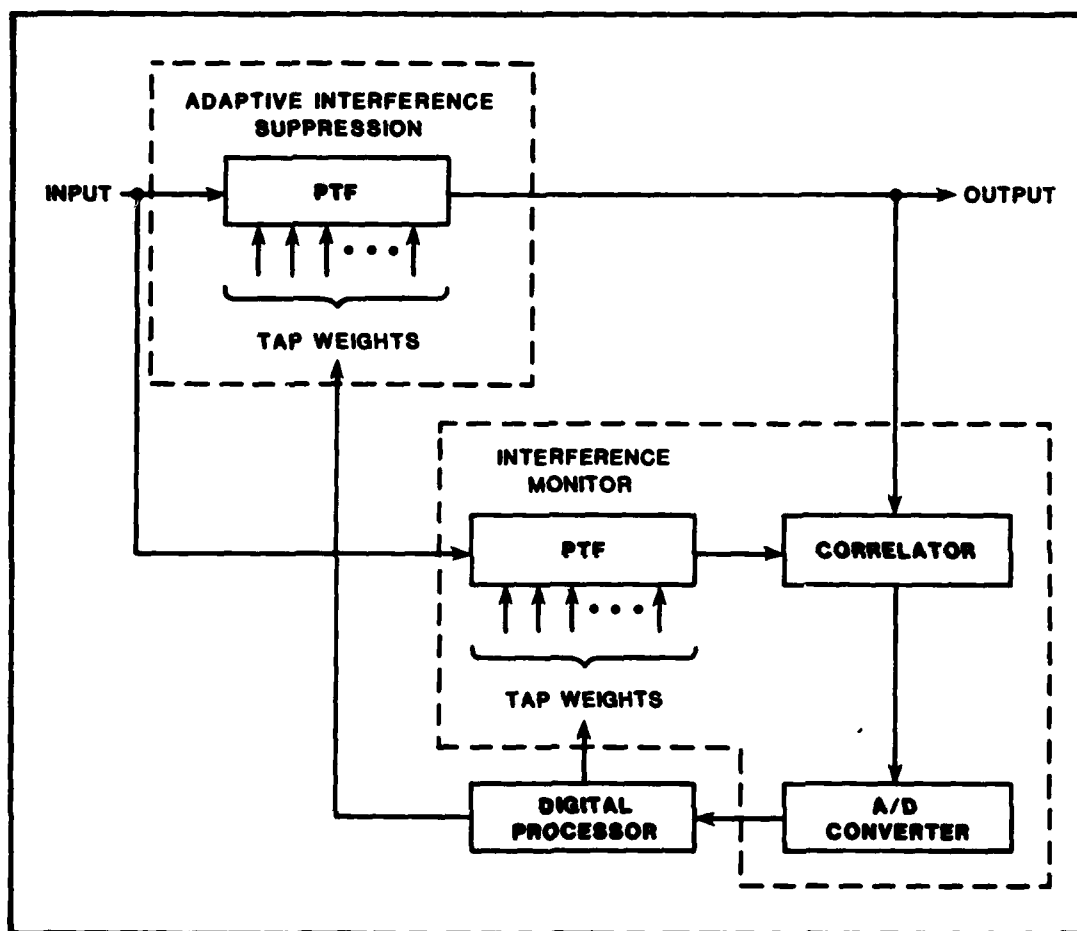


**Figure 13. Configuration Utilizing Two PTFs: One For Interference Monitoring and One For Adaptive Interference Suppression (Ref. 22:2-27).**

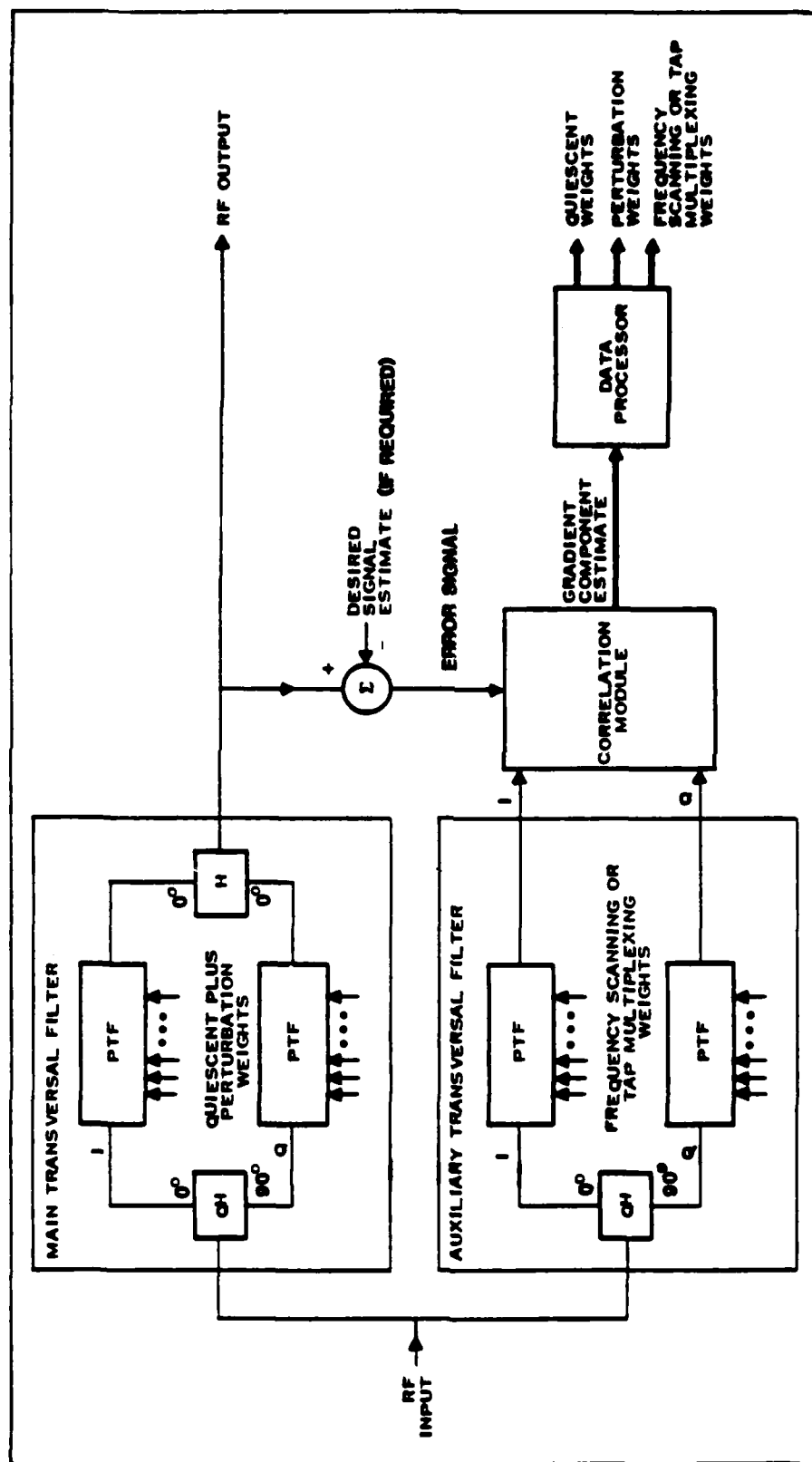


Figure 14. Full Scale Adaptive Transversal Filter Block Diagram (Ref. 22:2-20).



The quiescent weights are selected for the Applebaum algorithm, based on the desired signal spectrum, to produce the desired frequency response of the filter. That is, the quiescent weights use some form of "a priori" knowledge about the desired signal. The perturbation weights are selected and are continuously altered due to the adaptive algorithm to place notches or band-stops in the spectral regions of the jammers or interfering signals.

The auxiliary transversal filter is identical to the main transversal filter in theory. This filter permits access to the RF signal at any of the taps by setting the gain at the desired tap to unity and the gain of all other taps to zero. The use of the auxiliary filter allows for sequential implementation of the least mean squared (LMS) algorithms in the time domain without direct access to individual taps in the main filter. Further, this filter can be utilized in the frequency scanning mode of operation to allow implementation of the LMS algorithms in the frequency domain, that is, the filter continuously scans the input RF signal searching for a change in interference statistics. The configuration for implementation of several adaptive algorithms in either the time or frequency domain is illustrated in Figure 15.

The correlation module performs a cross-correlation between the outputs of the main and auxiliary filters. The correlation output is sampled resulting in a component of the

gradient vector (see Appendix A for a theoretical explanation of the gradient vector) which incidently determines the perturbation weights. For each iteration of the adaptive algorithm, the complex valued components of the gradient vector are estimated by sequencing through each of the tap outputs for the time domain, or by sequencing through each of the frequency passbands for the frequency domain.

The data processor performs the necessary operations to output three types of weighting vectors. The first type is the quiescent weight vector for use in the main filter to produce the desired frequency response characteristics of the filter. The second type is either the frequency scanning weight vector (utilized in the frequency domain) or the tap element multiplexing weight vector (utilized in the time domain) for use in the auxiliary filter. The third type is a perturbation weight vector (modified version of the estimated gradient vector from the correlation output) for use in addition to the quiescent weight vector in the main filter.

These modifications to the estimated gradient vector to produce the perturbation weight vector as mentioned above are of three types: first is a scaling of the vector to achieve both loop stability and acceptable adaption time; second is an iteration-by-iteration dithering of the vector direction and magnitude to increase steepest descent acceleration; and third is the transformation of the gradient vector from the time domain to the frequency domain if the

• POWER INVERSION ALGORITHM

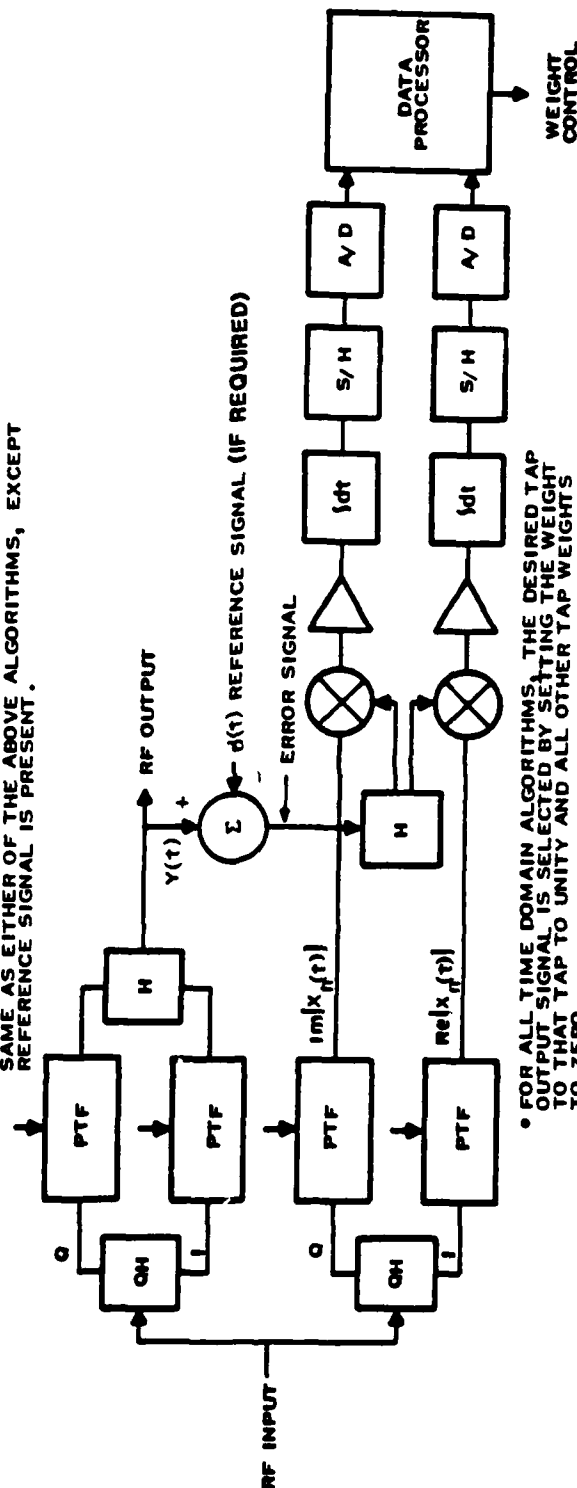
CENTER TAP WEIGHT ALWAYS SET TO UNITY, OTHER TAP WEIGHTS ARE INITIALLY SET TO ZERO, NO REFERENCE SIGNAL

• APPLEBAUM ALGORITHM

TAP WEIGHTS ARE INITIALLY SET TO GIVE DESIRED BANDPASS AND BANDSTOP CHARACTERISTICS, NO REFERENCE SIGNAL

• WIDROW ALGORITHM

SAME AS EITHER OF THE ABOVE ALGORITHMS, EXCEPT REFERENCE SIGNAL IS PRESENT.



• FOR ALL TIME DOMAIN ALGORITHMS, THE DESIRED TAP OUTPUT SIGNAL IS SELECTED BY SETTING THE WEIGHT TO THAT TAP TO UNITY AND ALL OTHER TAP WEIGHTS TO ZERO.

• FOR ALL FREQUENCY DOMAIN ALGORITHMS, THE TAP WEIGHTS ARE SET TO SCAN A NARROW PASSBAND AT DESIRED CENTER FREQUENCY  $f_c$ .

Figure 15. Implementation of Adaptive Algorithms in the Time or Frequency Domain (Ref. 22:2-24).

auxiliary filter is used in the frequency scanning mode of operation (Ref.22:2-30).

#### Implementation of the Applebaum Algorithm in the Frequency Domain

Implementation of adaptive algorithms in the frequency domain can increase the convergence rate as explained in Appendix A. The configuration for implementation of several adaptive algorithms in the frequency domain is illustrated in Figure 15. For the case of the Applebaum algorithm, the tap weights of the main filter are set to give the desired passband and stopband frequency response characteristics while the auxiliary filter is set in the frequency scanning mode. The region scanned by the auxiliary filter is separated into distinct passbands where a portion of these bands are associated with the desired signal spectrum and the others with possible interference signals. The passbands that make up the desired signal spectral region can either be used in the interference suppression operation or bypassed altogether to prevent any suppression of the desired signal. At any passband position,  $i$ , the output of the auxiliary filter,  $z_i(t)$ , is correlated with the output of the main filter,  $y(t)$ , and this result is scaled by the loop gain constant,  $\alpha$ . The data processor outputs a perturbation weight vector whose elements are given by

$$\Delta W_n = -\alpha Z_i^*(t) Y(t) e^{j2\pi\Delta(n-1)f_i}$$

$$n = 1, 2, \dots, N \quad (38)$$

where  $\Delta$  is the tap delay,  $f_i$  is the scan frequency,  $Y(t)$  is the main filter output signal,  $*$  indicates a finite time integration, and  $N$  is the number of taps. This perturbation vector is added to the previous weight vector in the main filter for each  $i$ th passband region.

Several techniques can be utilized to enhance the convergence rate of this algorithm, that is to decrease the number of iterations required to suppress the interfering signals. For instance, frequency scanning across the spectrum can be performed to estimate the strength of the interfering signal components. A strategy can then be used to scan through only those spectral regions where interfering components exist. Finally, one passband at a time can be made to adaptively suppress the inband interference before scanning to the next passband.

#### A Consideration of Algorithm Adaption Time

The amount of time required for an adaptive algorithm to establish an adapted state for a new spectrum or jamming signal is termed the adaption time. It is essential to minimize this time, especially in a wartime scenario, since the purpose of the communications system is to rapidly get an understandable message to the intended receiver.

Several factors must be considered when attempting to minimize adaption time.

- An adaptive algorithm with rapid convergence must be employed.
- Measurement of the required algorithmic data must be fast and efficient.
- Computation of the tap weights must be fast and efficient.
- Implementation of the modified weights must be fast and efficient.

The most effective way to decrease adaption time would be to directly adjust individual taps, however, as was mentioned earlier, it would be impractical to provide direct access to the 500 tap PTFs of the near future. Alternatively, external estimation of the interference spectrum followed by the required tap weight adjustments necessary to suppress this interference can be implemented. Further, referencing of stored previous tap weights for a given bandpass can be performed to minimize the number of iterations and thus adaption time.

The next section will be concerned with improved system performance by keying in on minimization of the desired signal degradation as well as minimization of algorithm convergence rate. An analysis of a SS communications computer simulation with the AIS-PTF included will be presented to achieve the above goals.

#### **IV. Analysis of Adaptive Interference Suppression**

This section deals with the performance of the AIS filter. The improvement in SS system performance when utilizing the AIS filter is determined in terms of the SNR at both the input and output of the correlation detector. SNR is the most convenient performance index for obtaining numerical results. Additionally, a number of other characteristics of the AIS filter and its implementation in a SS system are analyzed. Namely, its frequency response (before and after filter adaption), the receiver correlation response (before and after adaption), the pre-detection signal plus jammer plus noise spectrum (before and after filter adaption), and its convergence rate.

To the extent that it is possible, an analytical evaluation of a particular combination of modulation, spectral spreading, jamming, AIS filtering, and demodulation schemes will provide an engineer with much insight into the improved system performance that can be gained through an AIS filter. However, analytical evaluations are usually not adequate enough to analyze a complete SS system under all of the expected modes of operation that might be encountered in real life (Ref.5:2). It is obvious then, that one way to evaluate a SS system under all the expected modes of operation is to build it. However, this alternative can be quite costly. Still yet another alternative is to create a

set of software packages which can act as a SS communication simulator. This was the alternative chosen for this thesis effort. The analysis that follows is based on computer generated data.

A description of the communications simulation along with system simulation flowdiagrams is given in Appendix B.

It should be noted that computer simulation models are usually exploited during early stages of system design and development where a scaled model may be used. In later stages, a simulation model of an entire SS system would require a prohibitive amount of computer time and memory (Ref.23:1081).

#### Pre-Detection SNR Improvement Due to AIS Filter

In order to demonstrate the effectiveness of the AIS filter, the pre-detection SNR of the receiver is compared with and without the suppression filter for various user entered parameters in the computer simulation. A summarized list of the computer parameters is given in Table I where several abbreviations are used: power inversion (PI), Applebaum (A), time (T), and frequency (F). Also, Cases 20 through 22 are used to assess the transversal filters performance with nominal filter fabrication and circuitry errors. Tap weight word length (quantization error) has been considered in all 22 cases. The remaining four errors under consideration are explained with the use of Figure 16. The



Table I  
Summary of Computer Simulation Parameters for the 22 Cases Analyzed

Case #	Algorithm	Domain	Signal BW(MHz)	# of Jammers	Location of Jammer(MHz)
1	PI	F	10	1	222
2	PI	F	10	1	246
3	PI	F	50	1	222
4	PI	F	50	1	246
5	A	F	10	1	222
6	A	F	10	1	246
7	PI	T	10	1	246
8	A	T	10	1	246
9	PI	F	10	1	250
10	PI	F	10	1	249
11	PI	F	10	1	248
12	PI	F	10	1	247
13	PI	F	10	2	222,246
14	PI	F	50	2	222,246
15	A	F	10	2	222,246
16	A	T	10	2	222,246
17	PI	F	10	3	222,246,266
18	A	F	10	3	222,246,266
19	A	T	10	3	222,246,266
20	Case 2 With Nominal Filter Errors				
21	Case 15 With Nominal Filter Errors				
22	Case 18 With Nominal Filter Errors				

$$A_n = W_n \pm Y_n \quad (40)$$

where  $W_n$  is the quantized tap weight and  $Y_n$  is the tap weight error for a given tap. The summing delay error is represented as  $\delta_n$  for a given tap. The phase error between the in-phase (I) and quadrature (Q) channels is represented as  $\Delta\phi$ .

The pre-detection performance without the filter is obtained by passing the desired PN spread spectrum signal plus jamming through the filter with its quiescent tap weights set to an all-pass response. The computer generated value of SNR prior to the first iteration of the adaptive algorithm is the SNR of the signal plus jamming passed through the filter with an all-pass response.

Pre-detection SNR is computed in the computer simulation in terms of signal-to-jamming ratio (SJR). The computer generated value of SJR (calculated in the main program; see Appendix B) does not include the band limited Gaussian noise (BLGN) power. To do so would require much more computer memory and processing time. However, BLGN with bandwidth equal to the signal bandwidth is impressed on the SS signal (in subroutine SPS; see Appendix B) after the filter tap weights have been calculated in the main program. BLGN can be seen on the signal plus jammer plus noise figures in this section. Also, the correlation response includes the

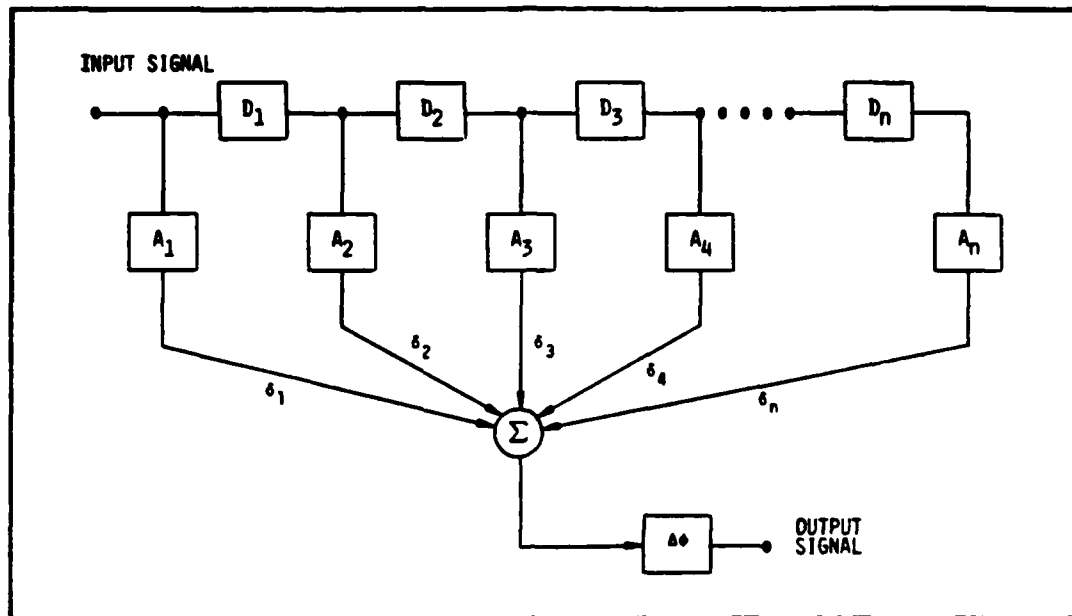


Figure 16. PTF Device Model

errors are introduced in the simulation as Gaussian random variables as can be seen in subroutine PTF of Appendix B. The intertap delays,  $D_n$ , have errors associated with each tap as represented in the equation

$$D_n = \Delta \pm \alpha_n$$

(39)

where  $\Delta$  is the correct intertap delay equal to 5 Nsec and  $\alpha_n$  is the intertap delay error for a given tap. The tap weight generation errors are represented in the equation

effects of BLGN since correlation is just the product (in the frequency domain) of the signal plus jammer plus noise spectrum with a replica of the desired signal.

It should be noted that from earlier research on adaptive arrays discussed by Schewegman and Compton (Ref.18:9), the depths of the nulls formed in the filter response are limited by system input noise, quantization error, and filter fabrication and circuitry error. The error contribution due to system input noise is of the same order of magnitude as the combined quantization and implementation errors. Therefore, neglecting the system input noise in the calculation of the adapted filter response will cause an error in the maximum null depth of about 3 dB.

Interference suppression due to the AIS filter does not include the processing gain (PG) of the SS signal correlator. The spread spectrum PG is due to the matched filter correlation operation which spreads the interference and despreads the desired signal in frequency. Further interference suppression provided by the PG of the SS signal correlator will be discussed in the next section.

There are many combinations of the user entered parameters, as can be seen in Table V of Appendix B. Some of the more relevant combinations of input parameters (as summarized in Table I) are used to produce the following system performance results.

The computer generated values of SJR both before any

filter adaption occurs and after 35 iterations of the adaptive algorithm are listed in Table II for the 22 cases. Also, the AIS filter pre-detection improvement factor (IF), defined as the difference between the post-adaption and pre-adaption SJRs, is given in Table II for the 22 cases. All jammers are CW and have a power level of 30 dB greater than the signal.

The pre-adaption signal plus jammer plus noise spectrum for Case 1 is illustrated in Figure 17. The CW jammer is seen to be located out-of-band, that is, the center frequency of the jammer is greater than 10 MHz (the PN clock frequency) from the SS signal center frequency of 250 MHz. It is believable that an out-of-band jammer should have a less detrimental effect on the desired signal than an in-band jammer. This is shown by comparing the post-adaption SJR for Cases 1 and 2. The quiescent PTF response for the power inversion algorithm is initially set for an all-pass response to pass the desired wideband PN signal. The algorithm produces this all-pass response by setting the center filter tap weight to unity gain and all other tap weights to zero as explained in Appendix A. The algorithm iteratively adjusts the filter tap weights to place a null on the jammer. The adapted filter response after 35 iterations is illustrated in Figure 18 with a null at 222 MHz. The post-adaption signal plus jammer plus noise spectrum is shown in Figure 19. Comparing with Figure 17, the total jammer power is seen to

Table II  
Pre-detection SJR Before and After Filter Adaption  
and Improvement Factor

Case #	Pre-adaption SJR(dB)	Post-adaption SJR(dB)	Pre-detection IF(dB)
1	-30.0	18.6	48.6
2	-30.0	2.8	32.8
3	-30.0	18.6	48.6
4	-30.0	2.8	32.8
5	-30.0	18.8	48.4
6	-30.0	10.5	40.5
7	-30.0	3.3	33.3
8	-30.0	18.6	48.6
9	-30.0	-30.0	0.0
10	-30.0	-12.0	18.0
11	-30.0	-10.0	20.0
12	-30.0	- 8.0	22.0
13	-33.0	- 9.7	23.3
14	-33.0	- 7.2	25.8
15	-33.0	7.8	40.8
16	-33.0	2.0	31.0
17	-34.8	-16.6	18.2
18	-34.8	1.3	36.1
19	-34.8	- 2.0	32.8
20	-30.0	- 5.6	24.4
21	-33.0	3.3	36.3
22	-34.7	1.0	35.7

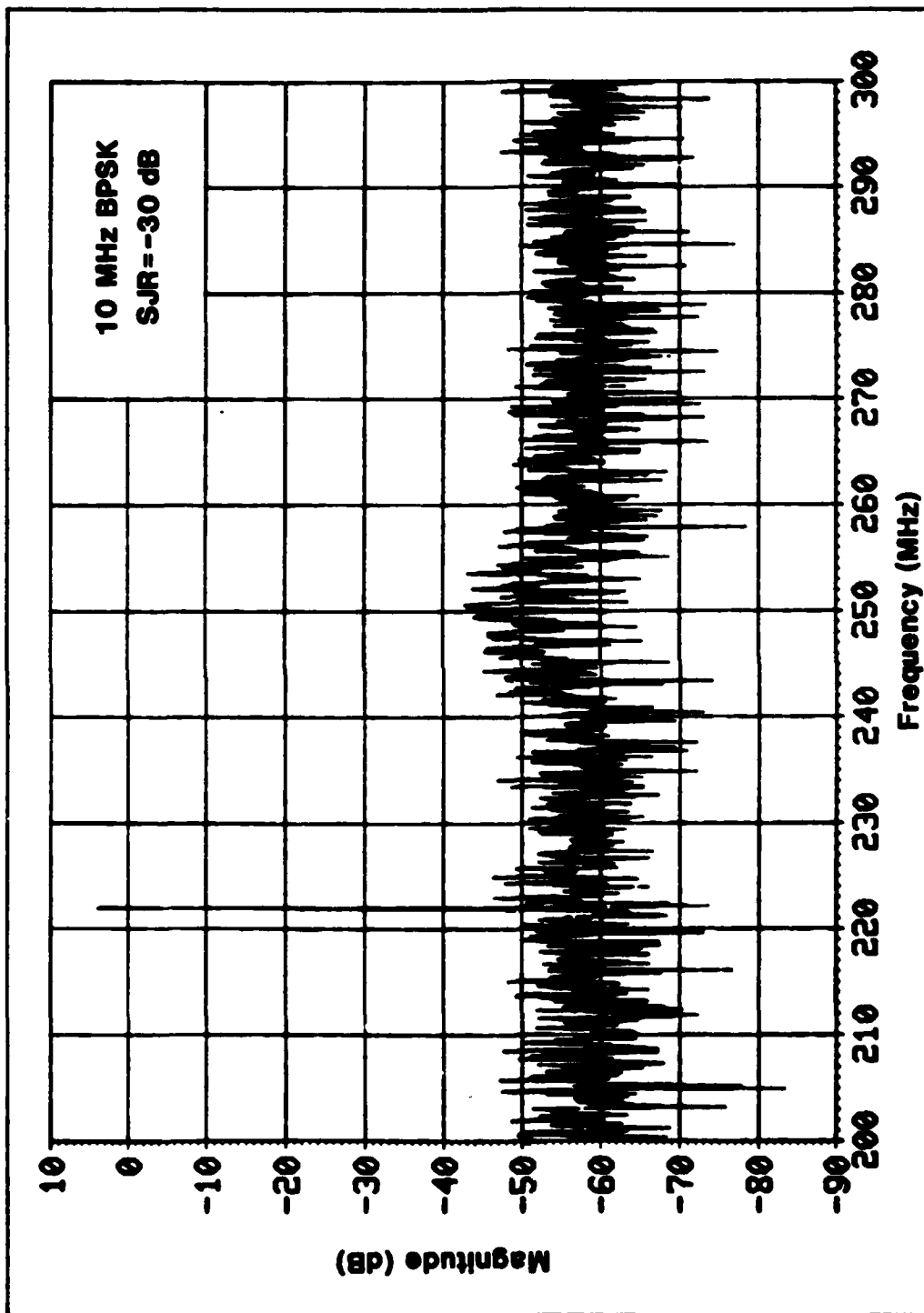


Figure 17. Pre-adaption Signal Plus Jammer Plus Noise Spectrum for Case 1.

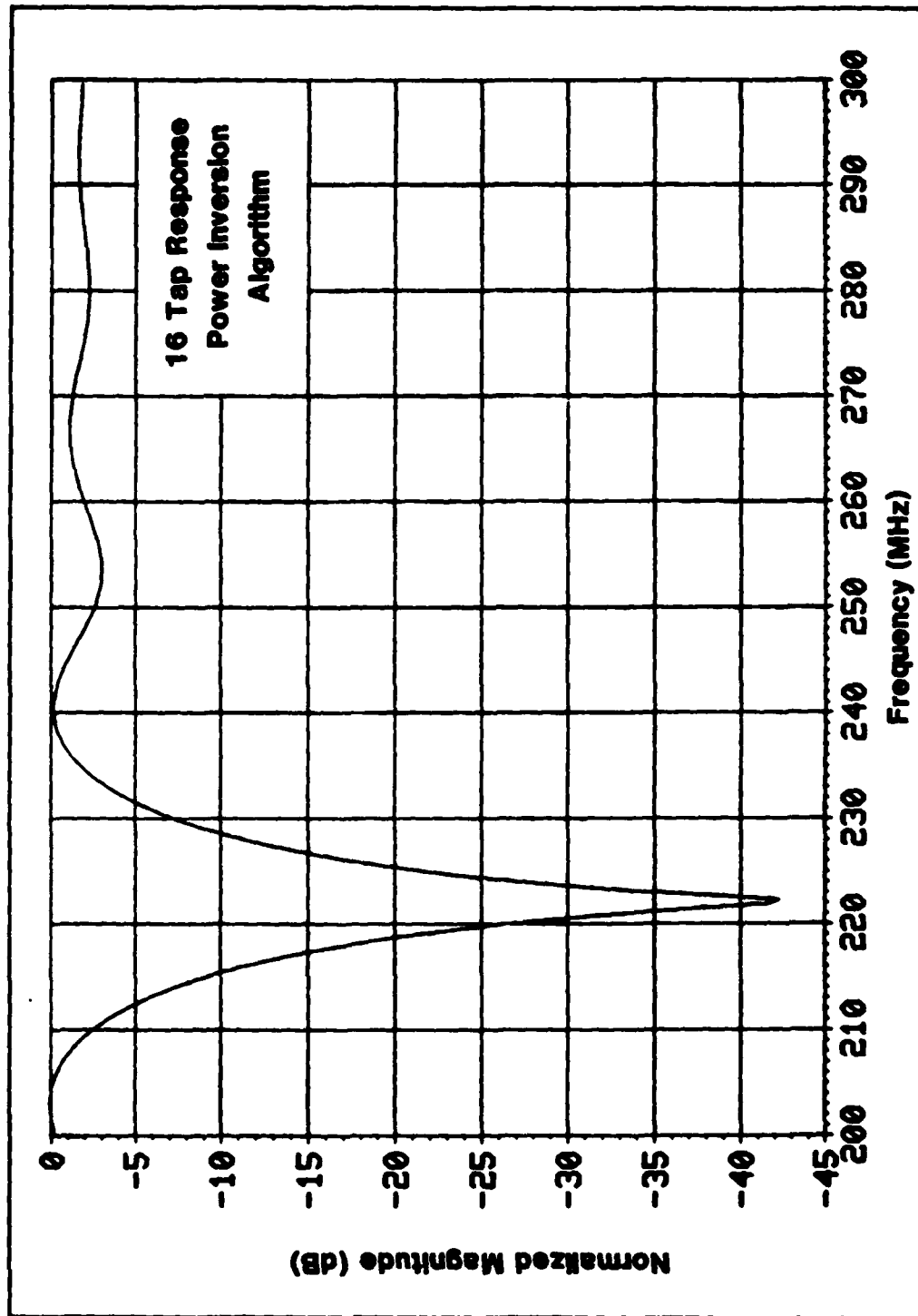


Figure 18. Adapted Filter Response for Case 1.



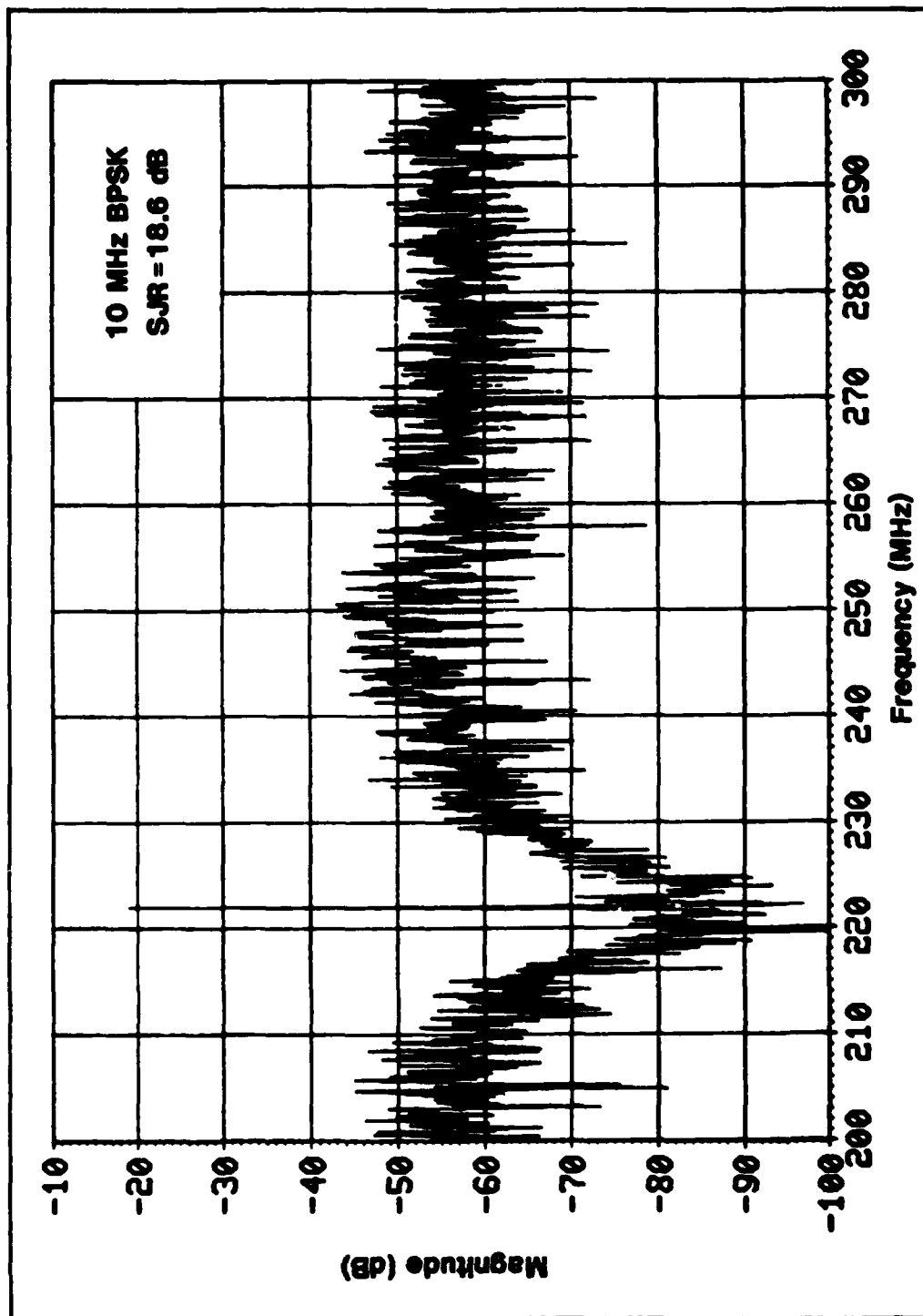


Figure 19. Post-adaption Signal Plus Jammer Plus Noise Spectrum for Case 1.

be decreased.

The pre-adaption signal plus jammer plus noise spectrum of Case 2 is illustrated in Figure 20 where the jammer is seen to be in-band. The adapted filter response after 35 iterations is illustrated in Figure 21 with a null at 246 MHz.

The post-adaption values of SJR for Cases 3 and 4 remained the same as Cases 1 and 2, respectively, even though the SS signal bandwidth was increased to 50 MHz. However, there is a decrease in performance of Case 3 over Case 1 and an increase in performance of Case 4 over Case 2 at the correlation detection output, as will be seen in the next section.

The adapted filter response for Case 6 is illustrated in Figure 22 with a null at 246 MHz. A major factor causing the increase in performance of Case 6 over Case 2 is the 3 dB width of the null. The 3 dB width of the null for Case 6 is about 8 MHz as can be seen in Figure 22. The 3 dB null width for Case 2 is about 21 MHz, as can be seen in Figure 20. There is a greater desired signal degradation in Case 2 than in Case 6 as a result of the increased null width and a subsequent filtering of more signal for Case 2.

The adapted filter response for Case 7 is illustrated in Figure 23 with a null at 246 MHz. There is a slight increase in performance of Case 7 over Case 2. This is due to the null of Case 7 being 60 dB down as opposed to the null

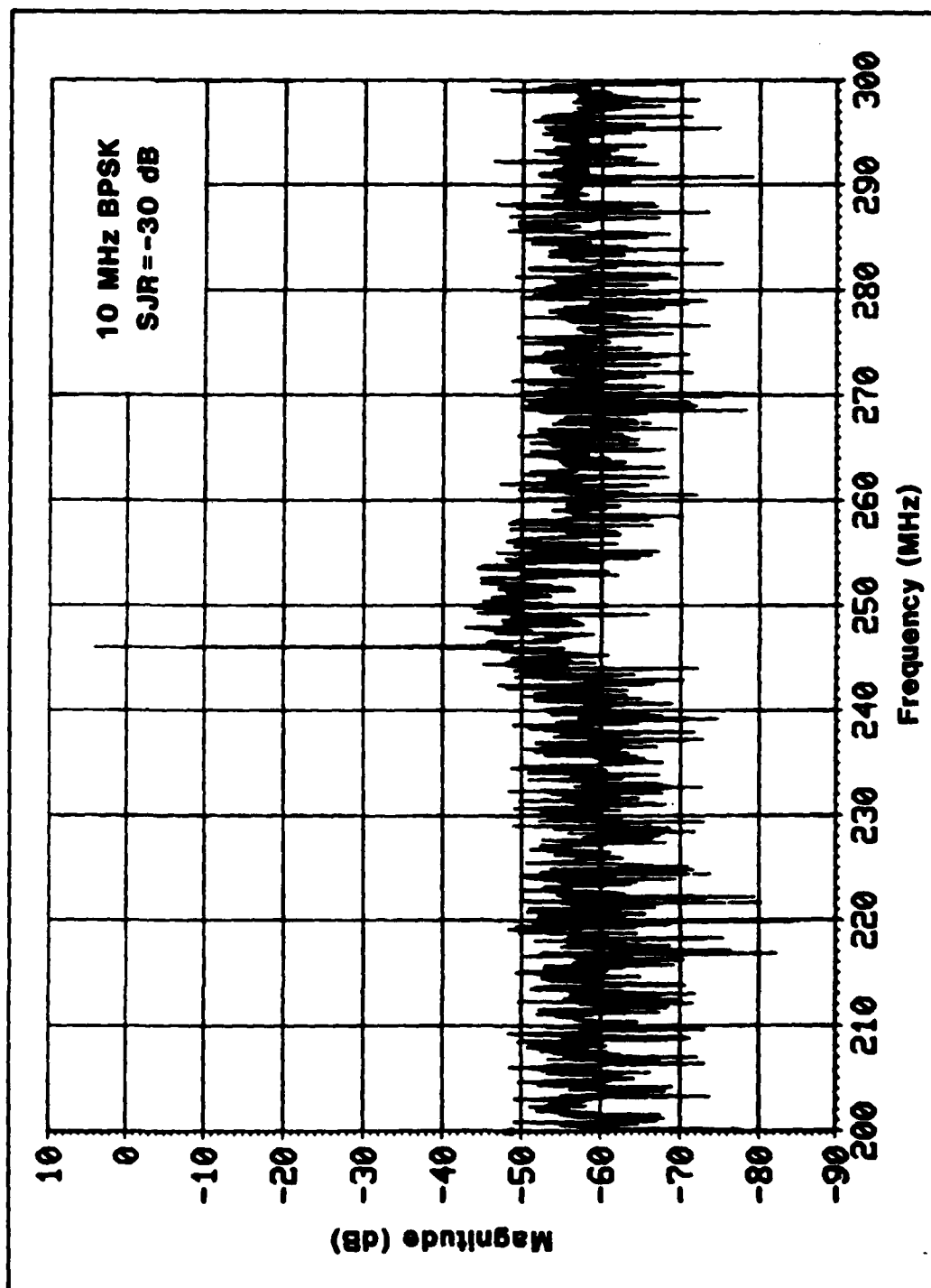


Figure 20. Pre-adaption Signal Plus Jammer Plus Noise Spectrum for Case 2.

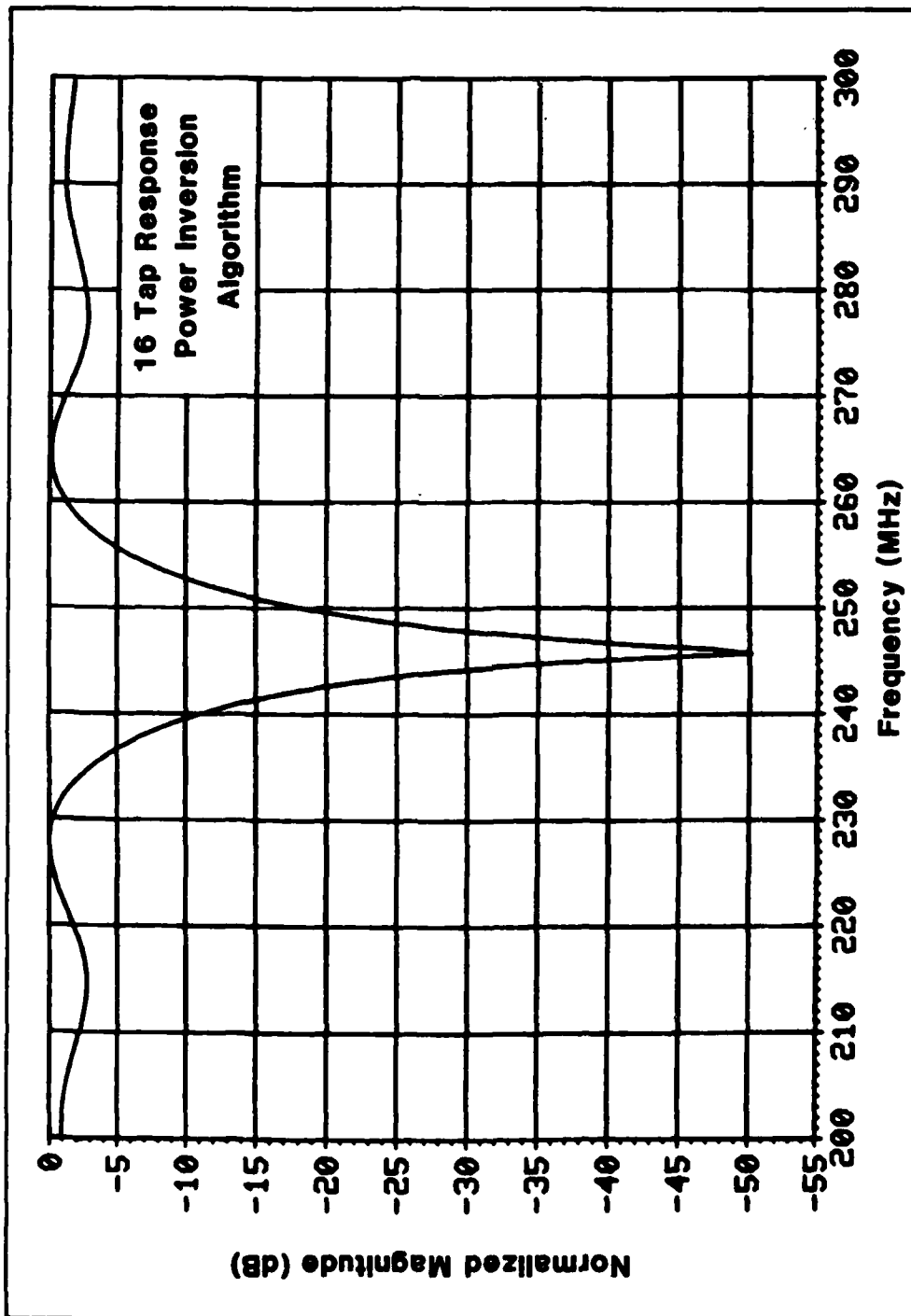


Figure 21. Adapted Filter Response for Case 2.

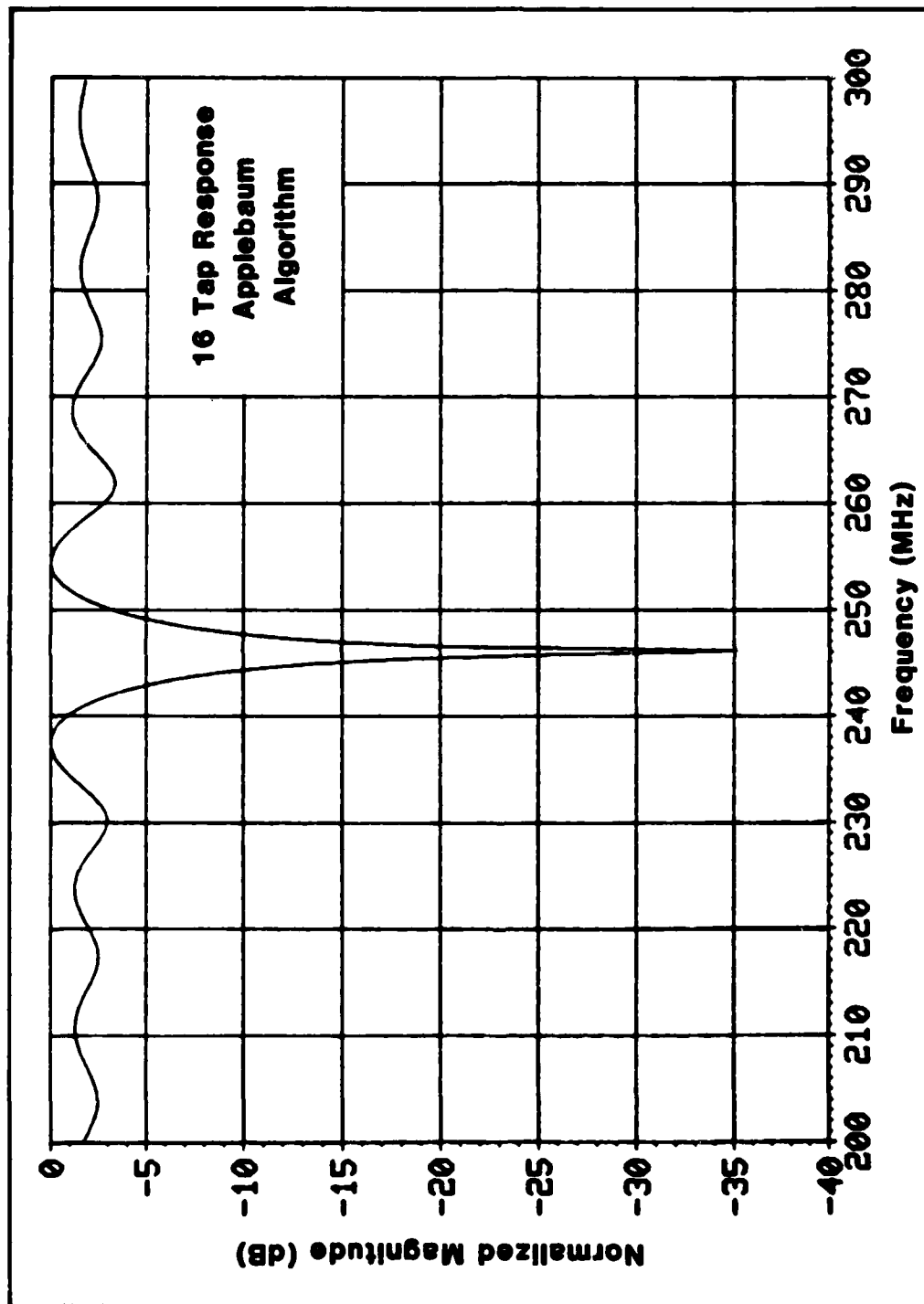
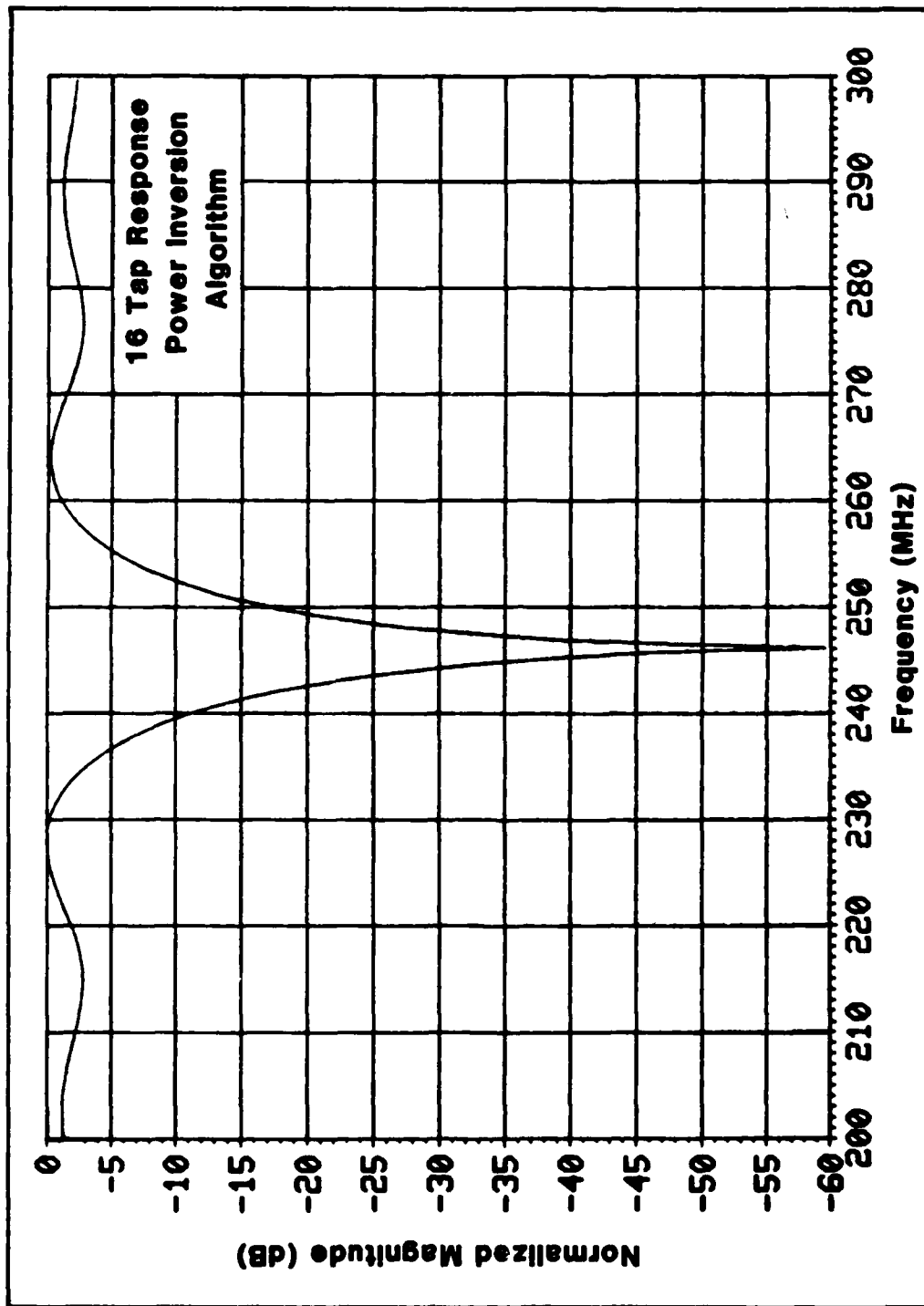


Figure 22. Adapted Filter Response for Case 6.



**Figure 23. Adapted Filter Response for Case 7.**

of Case 2 being 50 dB down. The frequency domain implementation of the adaptive algorithms, as discussed in section III, divides the usable filter bandwidth into several quasi-orthogonal channelized passbands. Since the channelized passbands used to synthesize the adapted filter response are not completely orthogonal to each other, the null depth obtained for the frequency domain algorithm is limited. As a result of this degradation, the null depth of Case 2 is 10 dB less than the null depth of Case 7. Also for this same reason, there is a significant increase in performance of Case 8 (implemented in the time domain) over Case 6 (implemented in the frequency domain).

Case 9 involves a jammer whose center frequency is located at the center frequency of the SS signal. A jammer at this location wreaks havoc on the receiver. The AIS filter is unable to adapt a null on the jammer, and the SJR remains around -30 dB. Because the power inversion algorithm initially sets the center tap weight to unity gain and the remaining taps to zero, it was thought that this symmetric setting of weights might affect the adaption on a centrally located jammer. However, implementation of the Applebaum algorithm with the first filter tap weight set to unity and the remaining taps set to zero revealed the same results on the filters inability to adapt on a centrally located jammer. However, if the CW jammer is impressed 1 MHz or more away from the SS signal carrier frequency, the AIS filter is able

to adapt a null on the jammer to provide improvement as demonstrated in Cases 10 - 12 of Table II.

The pre-adaption signal plus jammer plus noise spectrum of Case 13 is illustrated in Figure 24 where it is seen that one CW jammer is located in-band and the other is located out-of-band. The adapted filter response is illustrated in Figure 25.

When the SS signal bandwidth is increased to 50 MHz, as in Case 14, the SJR improves slightly for the same jamming signals as Case 13.

The adapted filter response for Case 15 is illustrated in Figure 26. A major factor causing the increase in SJR performance in Case 15 over Case 13 is the 3 dB width of the nulls. The Applebaum algorithm of Case 15 is able to achieve 3 dB null widths of about 9 MHz, whereas the power inversion algorithm of Case 13 is able to achieve 3 dB null widths of about 16 MHz. The post-adaption signal plus jammer plus noise spectrum is illustrated in Figure 27 where the total jammer powers are seen to be suppressed from their original powers in the pre-adaption signal plus jammer plus noise spectrum of Figure 24.

A comparison of cases 15 and 16 reveals that a time domain implementation of the Applebaum algorithm does not perform as well as a frequency domain implementation of the Applebaum algorithm for the case of two jammers. However, it is suspected that if the algorithm is allowed to adapt for



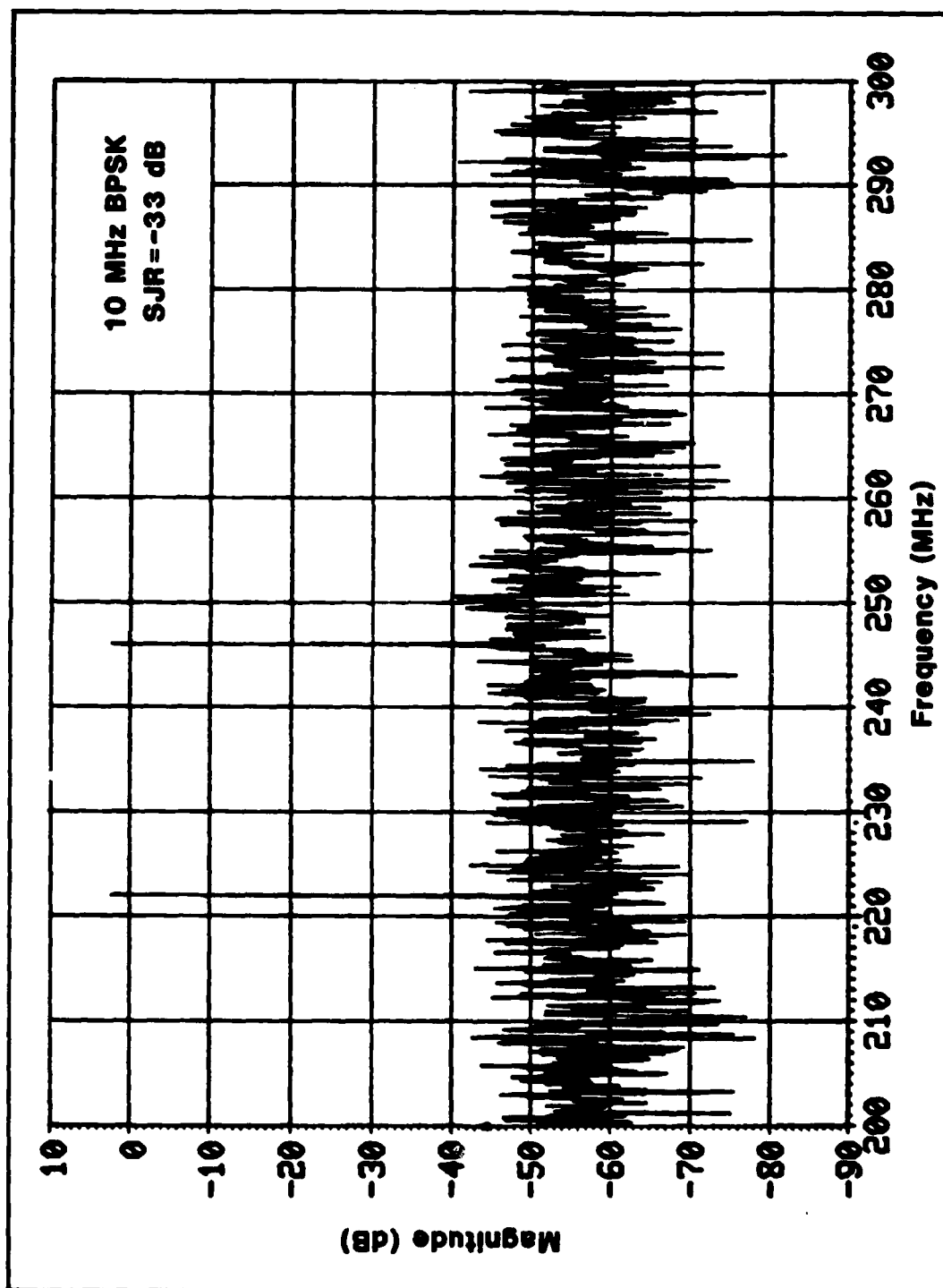


Figure 24. Pre-adaption Signal Plus Jammer Plus Noise Spectrum for Case 13.

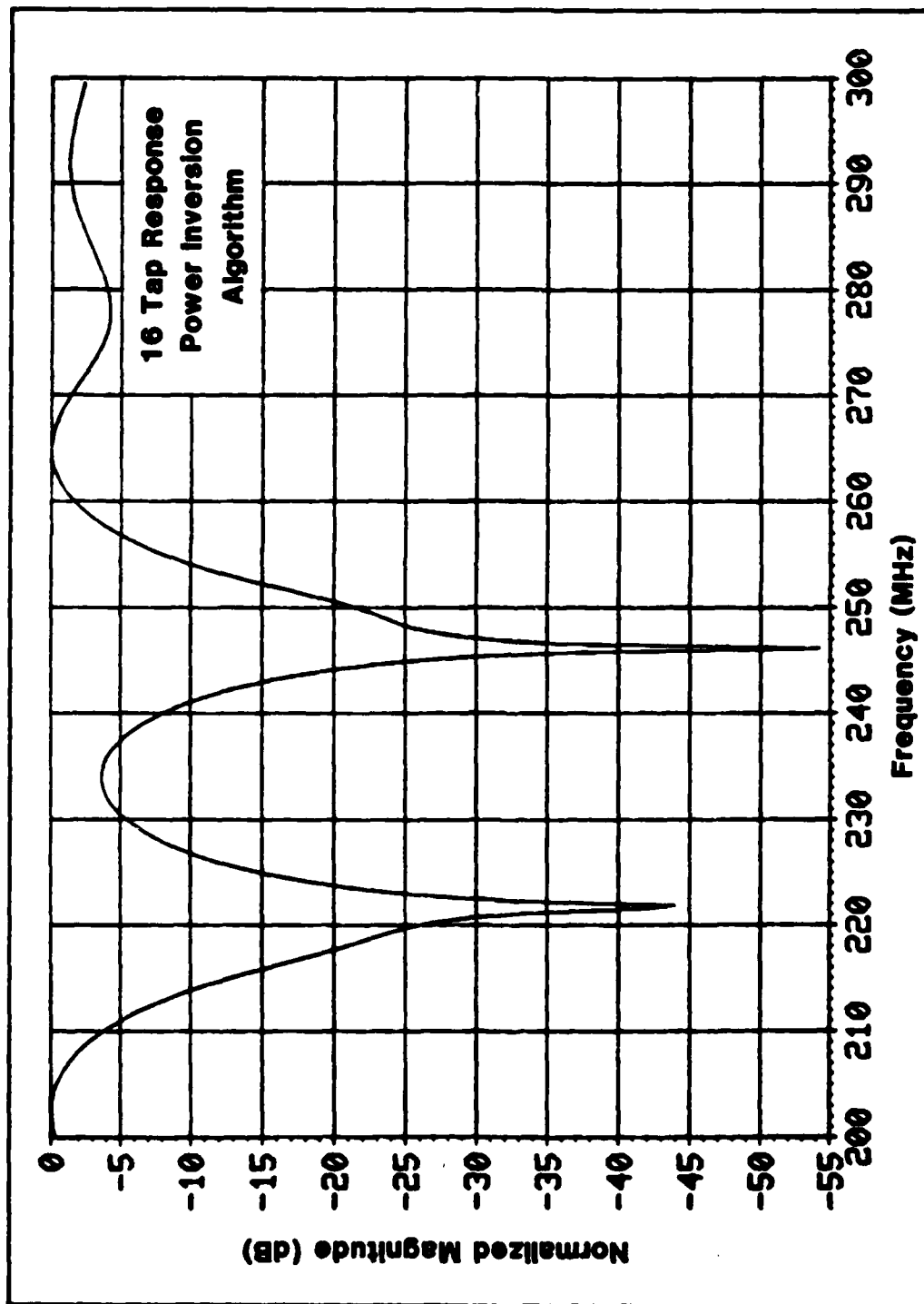


Figure 25. Adapted Filter Response for Case 13.

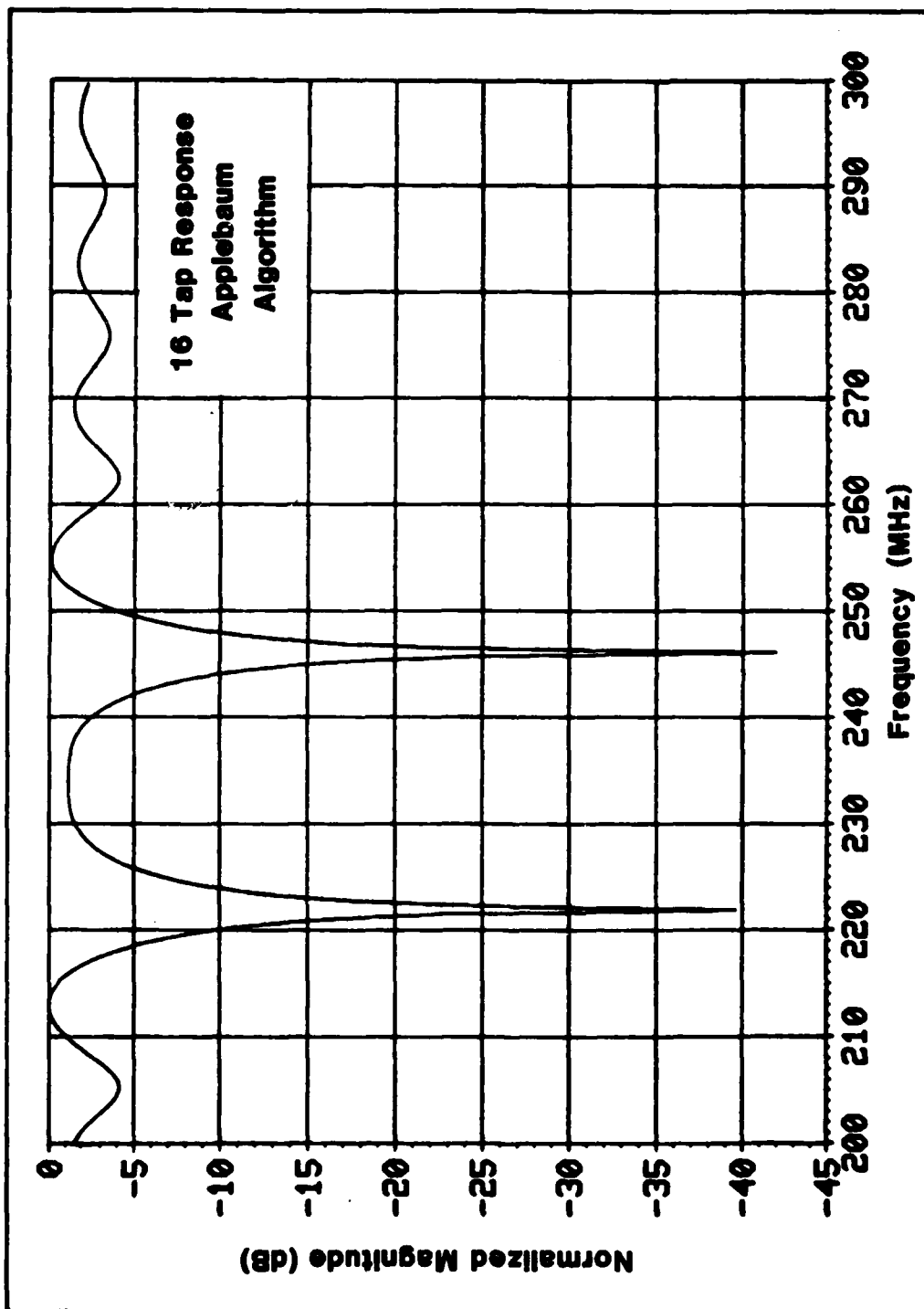


Figure 26. Adapted Filter Response for Case 15.

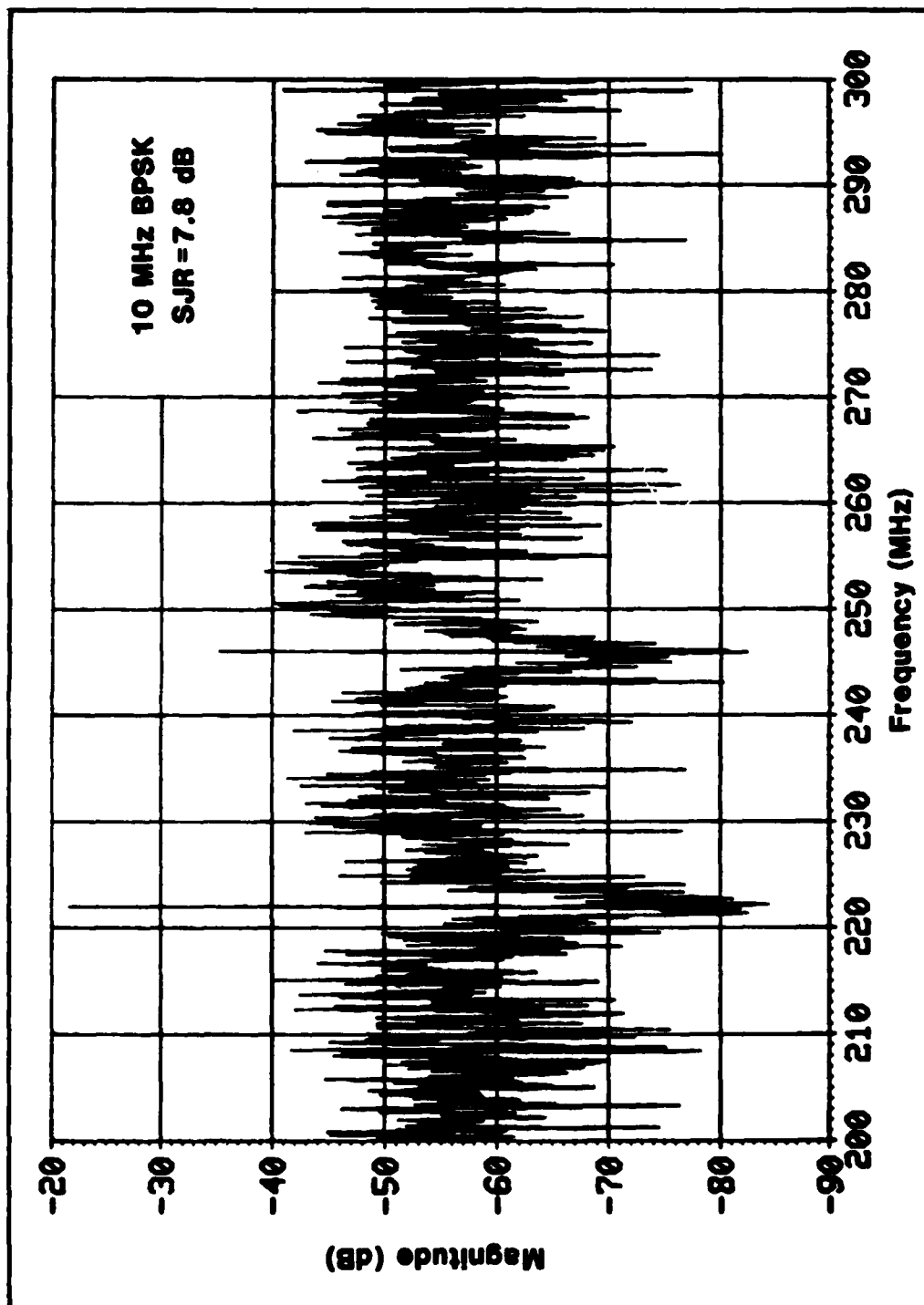


Figure 27. Post-adaption Signal Jammer Plus Noise Spectrum for Case 15.

more than 35 iterations, then the time domain implementation will yield increased performance over the frequency domain implementation as was the case for one jammer.

The pre-adaption signal plus jammer plus noise spectrum of Case 17 is illustrated in Figure 28 where it is seen that one CW jammer is located in-band and the other two are located out-of-band. The adapted filter response is given in Figure 29. The post-adaption signal plus jammer plus noise spectrum is illustrated in Figure 30 where the three jamming signals are seen to be suppressed from their original powers in the pre-adaption signal plus jammer plus noise spectrum of Figure 28.

The adapted filter response for Case 18 is illustrated in Figure 31. A major factor causing the increase in performance of Case 18 over Case 17 is the magnitude of the lobes in the adapted filter response. The magnitude of the filter response lobe between 245 MHz and 265 MHz for Case 17 is 17 dB down from that of Case 18. Thus, more desired signal is filtered in Case 17. Also, the average 3 dB width of the nulls for Case 18 is about 10 MHz as opposed to about 14 MHz for Case 17.

A comparison of Cases 18 and 19 reveals that a time domain Applebaum implementation does not perform as well as a frequency domain Applebaum implementation for the case of three jammers. However, it is suspected that if the algorithm is allowed to adapt for more than 35 iterations,

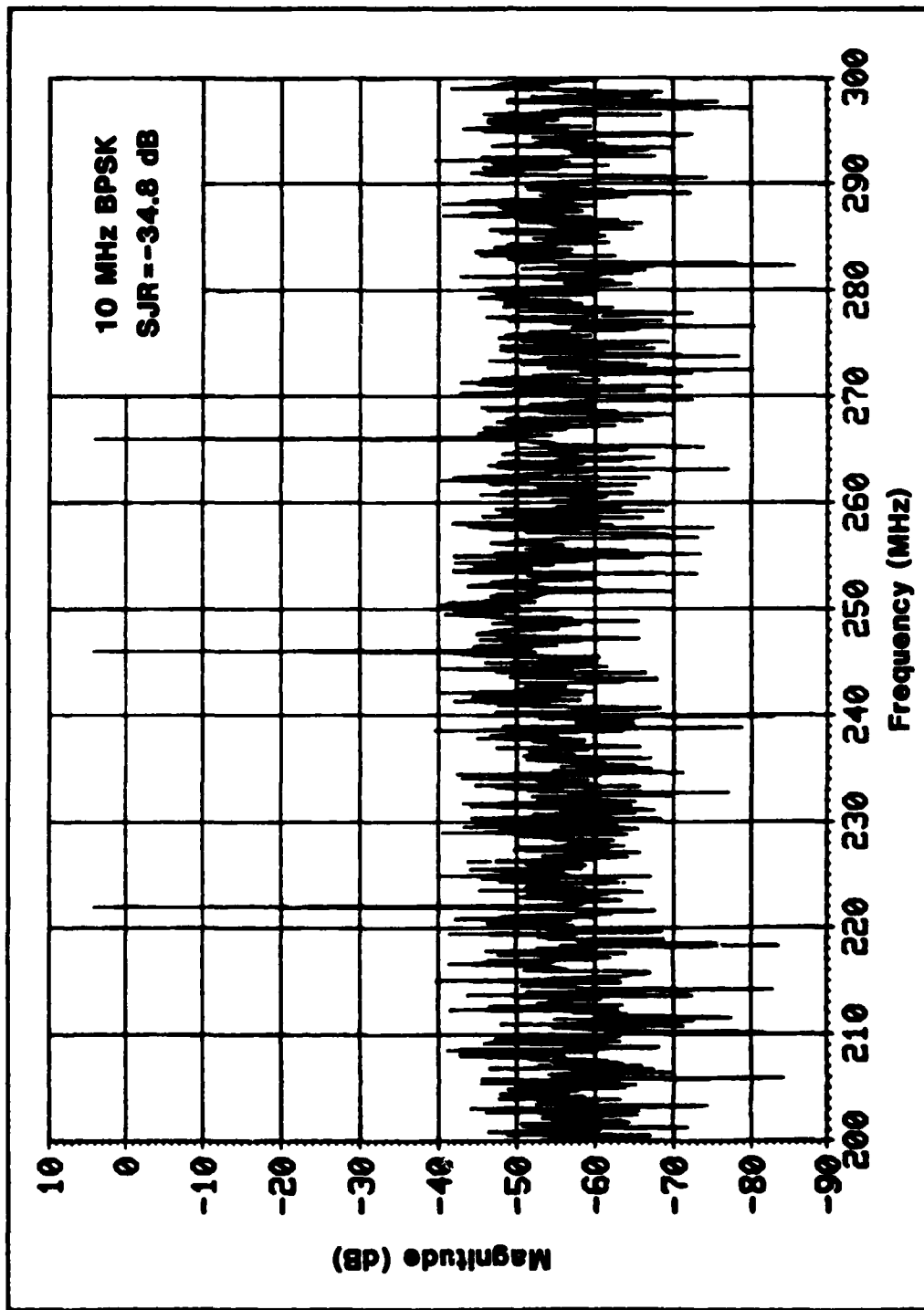


Figure 28. Pre-adaption Signal Plus Jammer Plus Noise Spectrum for Case 17.

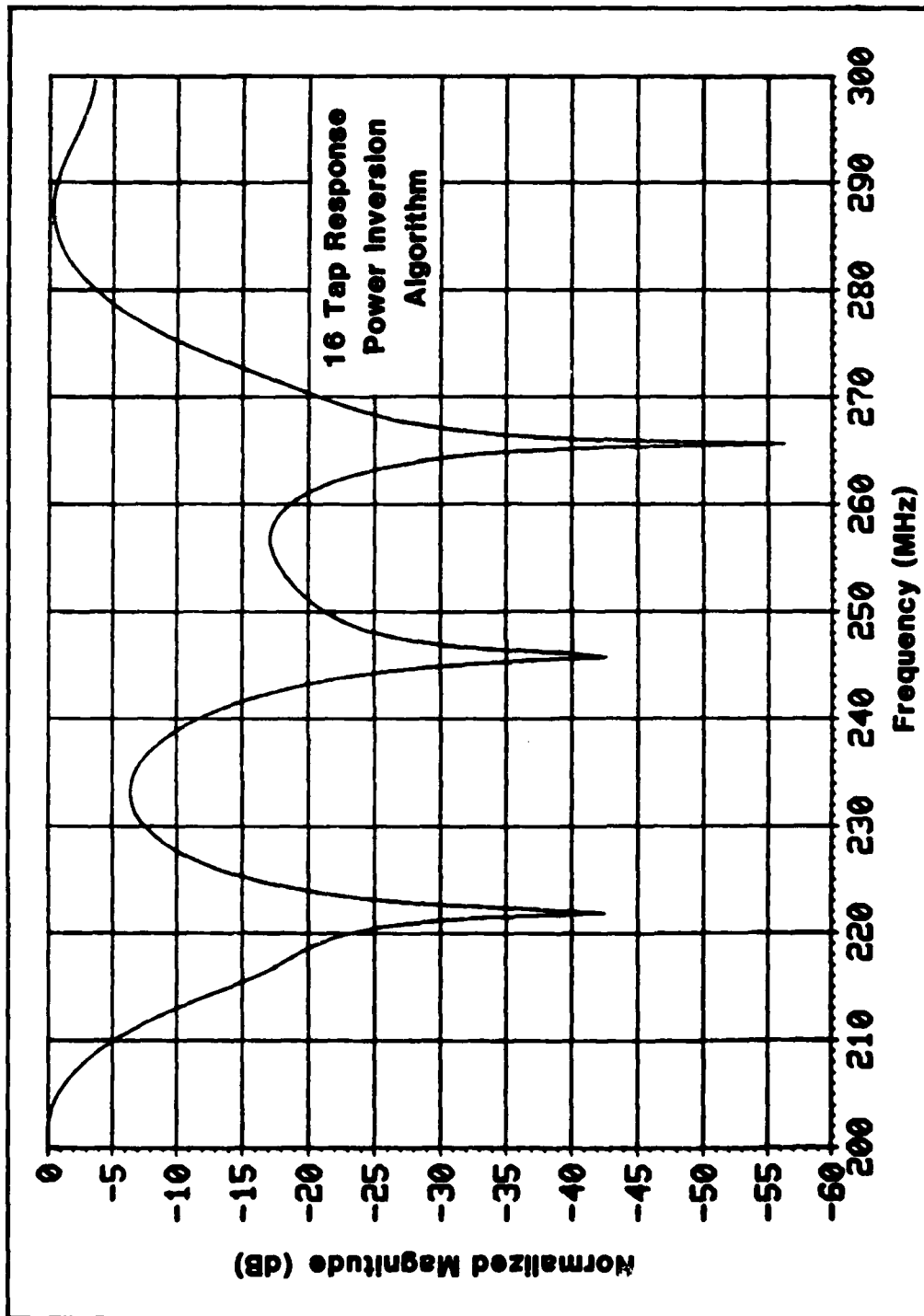


Figure 29. Adapted Filter Response for Case 17.

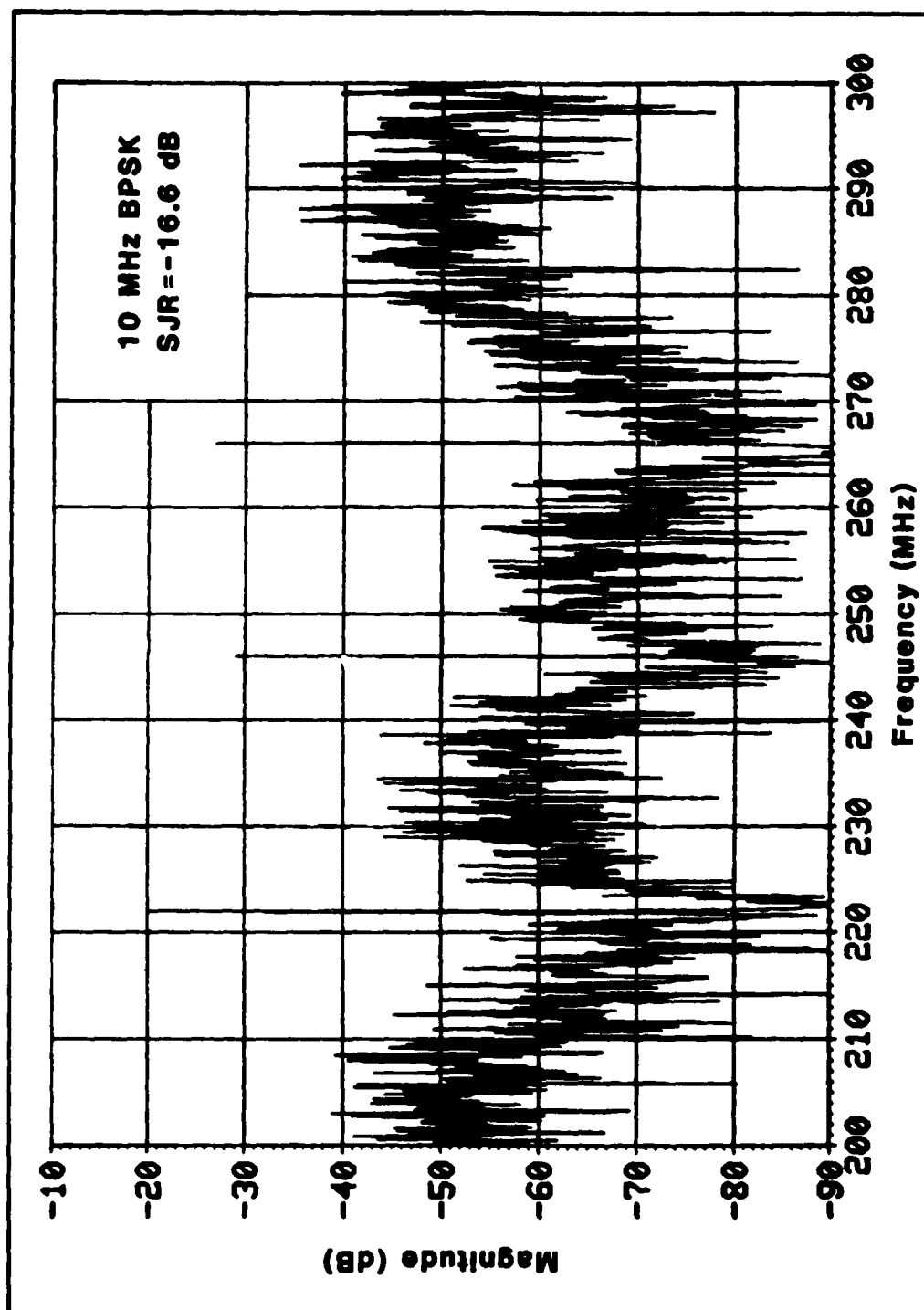


Figure 30. Post-adaption Signal Plus Jammer Plus Noise Spectrum for Case 17.



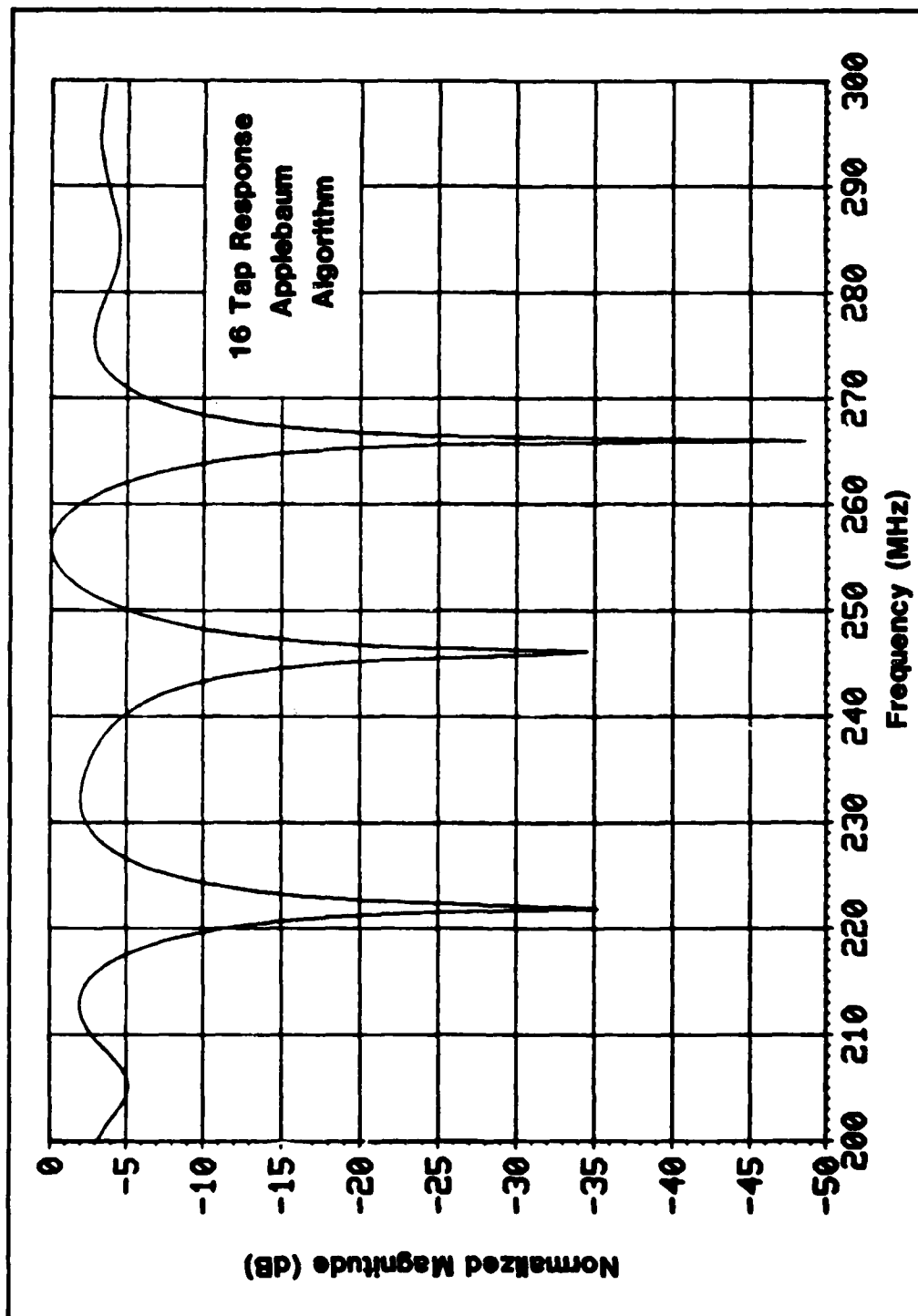


Figure 31. Adapted Filter Response for Case 18.

then the time domain implementation will yield increased performance over the frequency domain implementation as was the case for one jammer.

Cases 20 through 22 are used to assess the transversal filters performance with nominal filter fabrication and circuitry errors. The nominal filter errors chosen for these cases are 8 bits for tap weight word length (quantization error),  $\alpha_n$  = random intertap delay error from a normal distribution with  $\sigma_{\alpha n} = 0.017$  Nsec,  $\gamma_n$  = random tap weight generation error from a normal distribution with  $\sigma_{\gamma n} = 0.05W_n$ ,  $\delta_n$  = random summing delay error from a normal distribution with  $\sigma_{\delta n} = 0.03$  Nsec, and  $\Delta\phi = 5\%$  for the phase error between the I and Q channels. In each case, the post-adaption value of SJR calculated with nominal filter errors is less than its respective value of SJR calculated without filter errors. A factor causing this decrease in performance is that the null depths of the adapted filter responses with errors are degraded from their respective responses without errors. For example the adapted filter response for Case 21 is given in Figure 32 where the null depths are seen to be degraded from their depths in Figure 26.

#### Post-Detection SNR Improvement Due to the AIS Filter

In order to determine the post-detection effectiveness of the AIS filter, the post-detection SNR is compared with

AD-A124 903

THE PERFORMANCE OF A PN SPREAD SPECTRUM RECEIVER  
PRECEDED BY AN ADAPTIVE... (U) AIR FORCE INST OF TECH  
WRIGHT-PATTERSON AFB OH SCHOOL OF ENGI... M M SHEPARD  
DEC 82 AFIT/GE/EE/82-62 F/G 17/4

UNCLASSIFIED

NL

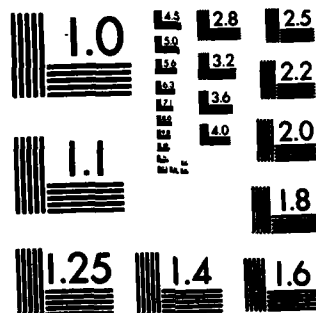
END

DATE

FILED

83

DTIC



MICROCOPY RESOLUTION TEST CHART  
NATIONAL BUREAU OF STANDARDS-1963-A

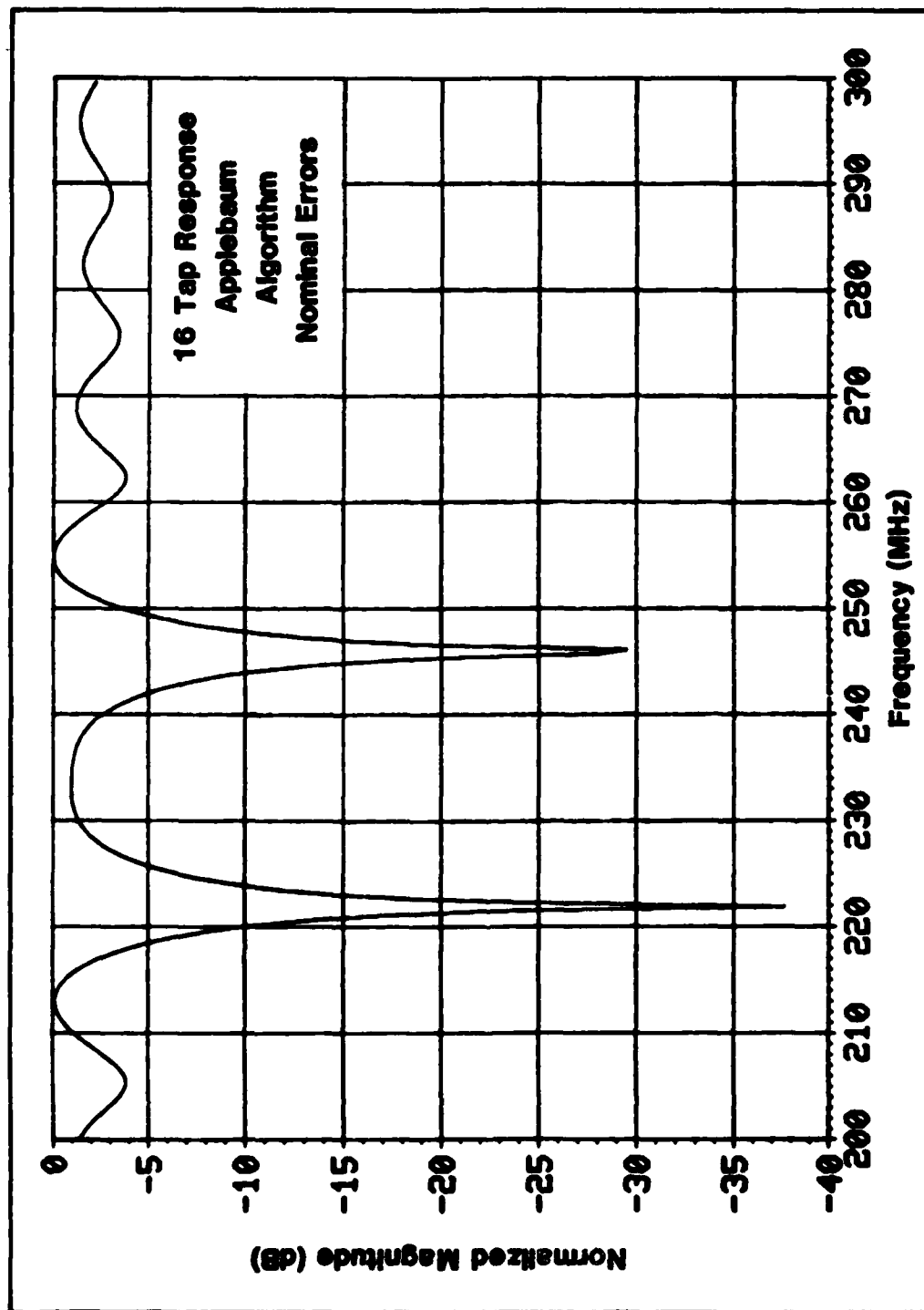


Figure 32. Adapted Filter Response for Case 21.

and without the suppression filter for various user entered parameters in the computer simulation. A summarized list of the computer parameters for the 22 cases is given in Table I.

Post-detection performance without the filter is obtained by passing the desired SS signal plus jamming plus additive BLGN through the filter with its quiescent tap weights set to an all-pass response. The signal plus jamming plus BLGN is then correlated with a replica of the desired signal to produce a pre-adaption correlation response. The performance with the AIS filter is obtained by allowing the filter to iteratively adapt to a frequency response which places nulls on the jammers. The adapted signal plus jamming plus BLGN spectrum is then correlated with a replica of the desired signal to produce a post-adaption correlation response. The performance with the AIS filter is then determined from this correlation response in terms of SNR.

Post-detection SNR is measured in terms of signal-to-jamming plus BLGN ratio (SJNR). The SJNR is calculated from the correlation response plot as the ratio of the magnitude of the correlation peak to the RMS value of the correlation sidelobes on one side of the plot. Also, the computer generated correlation plot is a normalized magnitude plot in that the maximum value is normalized to a magnitude of one. This normalization leads to relative or normalized values of SJNR for post-detection improvement. Also,

post-detection improvement can be determined on the basis of whether or not there is a correlation, and on how high the correlation sidelobes are relative to the peak. The higher the sidelobes, the higher the probability that the detector will make an incorrect decision about what message was sent.

Post-detection improvement is due to both the AIS filter and the PG of the SS signal. The PG, as discussed in Section II, is the ratio of the transmitted RF bandwidth to the data bandwidth. The PG in the computer simulation is the ratio of the number of samples per data bit to the number of samples per PN code chip. The simulation generates 1000 samples/data bit. The number of samples per chip varies according to the user entered value of signal bandwidth, or PN clock frequency  $f_c$ . For a 10 MHz signal, the number of samples per chip, NBW, is given by

$$NBW = \frac{1}{(f_c) (DEL)} = \frac{1}{(10 \text{ MHz}) (5 \text{ Nsec})} = 20 \text{ samples/chip} \quad (41)$$

where DEL is the sampling time. For a 50 MHz signal, NBW is given by

$$NBW = \frac{1}{(50 \text{ MHz}) (5 \text{ Nsec})} = 4 \text{ samples/chip} \quad (42)$$

Thus, for a 10 MHz SS signal, the PG is given by

$$PG = \frac{1000 \text{ samples/data bit}}{20 \text{ samples/chip}} = \frac{50 \text{ chips}}{\text{data bit}} = 17\text{dB}$$

(43)

and, for a 50 MHz SS signal, the PG is given by

$$PG = \frac{1000 \text{ samples/data bit}}{4 \text{ samples/chip}} = \frac{250 \text{ chips}}{\text{data bit}} = 24\text{dB}$$

(44)

The PG can also be expressed as a time-bandwidth product as given by

$$PG = TB = \left( \frac{1000 \text{ samples}}{\text{data bit}} \right) \left( \frac{5 \text{ Nsec}}{\text{sample}} \right) (f_c)$$

(45)

A useful concept in SS communications is jamming margin, JM, given by

$$JM = PG + G_{PTF} - (S/N)_{OUT}$$

(46)

where  $G_{PTF}$  is the gain in interference suppression due to the



AIS filter and  $(S/N)_{OUT}$  is the minimum output SNR required by the detector for a proper decision. A typical value of JM calculated for a 10 MHz SS signal is given by

$$JM = 17 + 30 - 10 = 37dB$$

(47)

Equivalently, the SS system can continue detecting signals even though the signals are 37 dB, but not more, below the jamming.

The computer generated values of normalized post-detection SJNR before and after filter adaption are listed in Table III. Also, the normalized post-detection improvement factor due to the AIS filter, IF, is given in Table III. For the cases that yielded no pre-adaption correlation, the SJNR and IF blocks are left blank, although there is an improvement based on the fact that there is a correlation peak in the post-adaption correlation response.

The pre-adaption correlation response for Case 1 is shown in Figure 33. A correlation peak exists for this case of an out-of-band jammer even without the AIS filter, that is, before any adaption of the all-pass filter occurs to place a null on the jammer. This correlation without the AIS filter is due to the ability of the PG of the SS signal to satisfactorily spread the interference and despread the signal. Improvement of SJNR is realized when the filter is

Table III  
Normalized Post-detection SJNR Before and After  
Filter Adaption and Improvement Factor

Case #	Pre-adaption SJNR(dB)	Post-adaption SJNR(dB)	Post-detection IF(dB)
1	14.6	22.2	7.6
2	-	6.3	-
3	6.0	20.2	14.2
4	3.7	14.8	11.1
5	14.6	22.3	7.7
6	-	9.3	-
7	-	6.7	-
8	-	11.0	-
9	-	-	-
10	-	4.4	-
11	-	4.9	-
12	-	5.8	-
13	-	12.7	-
14	-	17.1	-
15	-	17.6	-
16	-	13.9	-
17	-	7.6	-
18	-	16.5	-
19	-	16.0	-
20	-	2.9	-
21	-	10.9	-
22	-	8.2	-

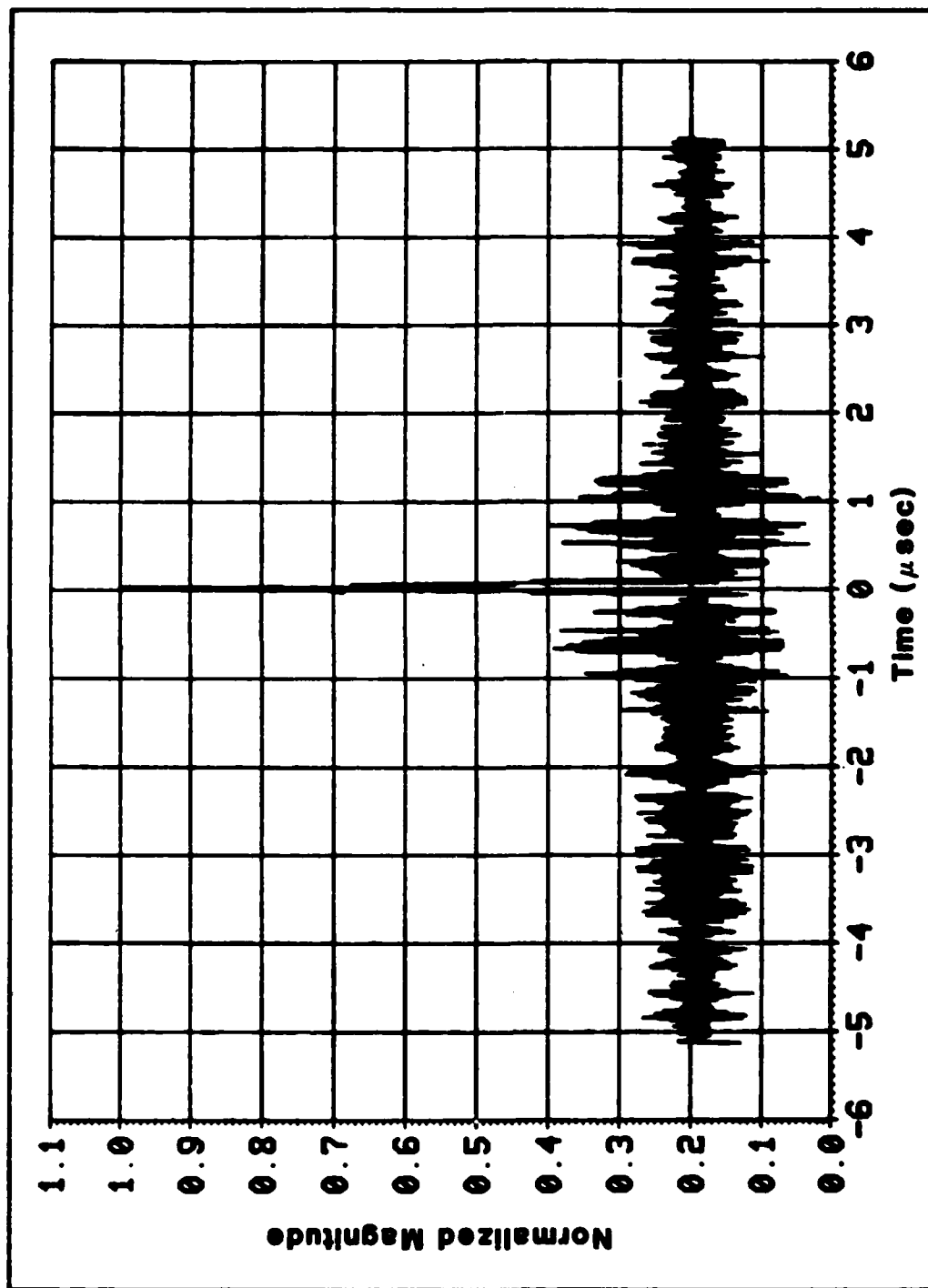


Figure 33. Pre-adaption Correlation Response for Case 1.

allowed to adapt on the jammer. The post-adaption correlation response for Case 1 is shown in Figure 34 where the correlation sidelobes are seen to be decreased.

For Case 2, and in-band jammer case, no correlation exists without the filter as shown in Figure 35. The PG of the SS signal is unable to satisfactorily spread the interference and despread the signal. The sidelobes of the correlation response are up in the threshold region, therefore there is a high probability of false alarm (e.g. incorrect decisions about what message was sent). The post-adaption correlation response for Case 2 is illustrated in Figure 36.

As seen in Table III, there is a decrease in post-adaption SJNR of Case 3 over Case 1, and an increase in post-adaption SJNR of Case 4 over Case 2. These performances are due to the PSD of the SS signal being spread, in Cases 3 and 4, to five times the bandwidth of Cases 1 and 2. Thus, the out-of-band jammer of Case 1 becomes an in-band jammer in Case 3, and the jammer in Case 4 is jamming less signal power than the jammer in Case 1 since the magnitude of signal PSD has decreased.

Case 9 investigates the performance of the AIS filter with a CW jammer located at the center frequency of the SS signal. The AIS filter is unable to provide any improvement for this jamming scenario. However, if the jammer is impressed 1 MHz or more away from the SS signal carrier

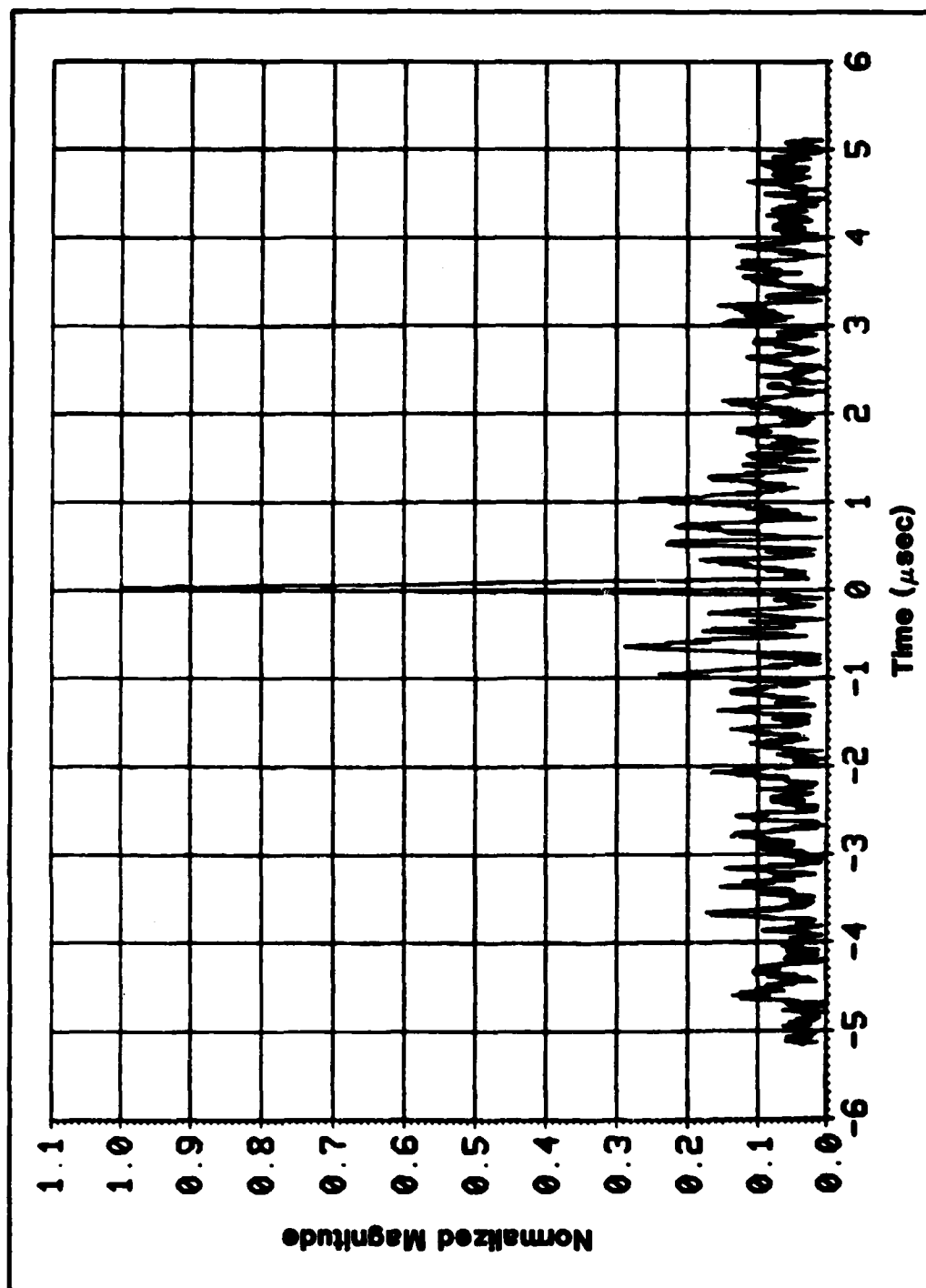


Figure 34. Post-adaption Correlation Response for Case 1.

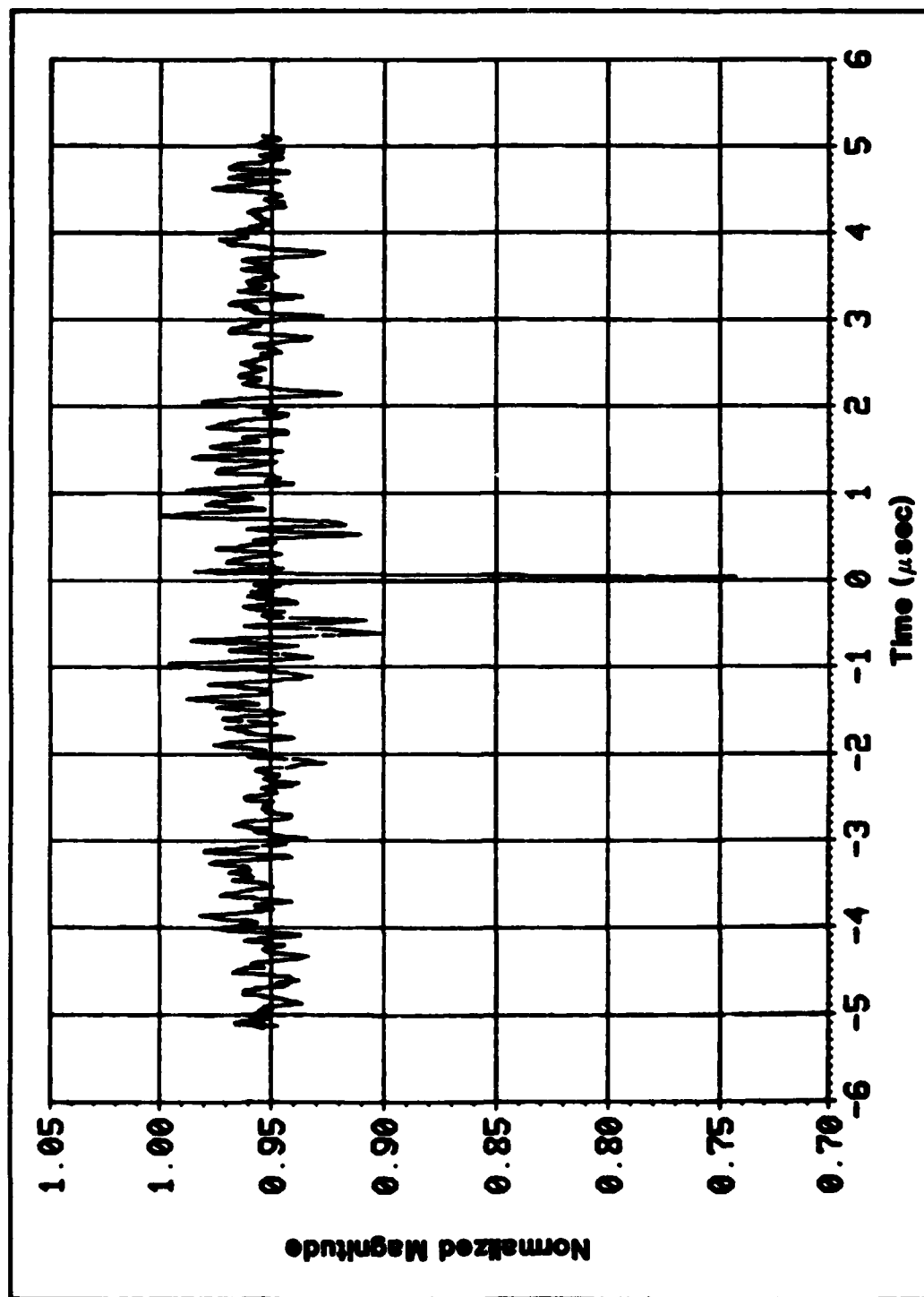


Figure 35. Pre-adaption Correlation Response for Case 2.

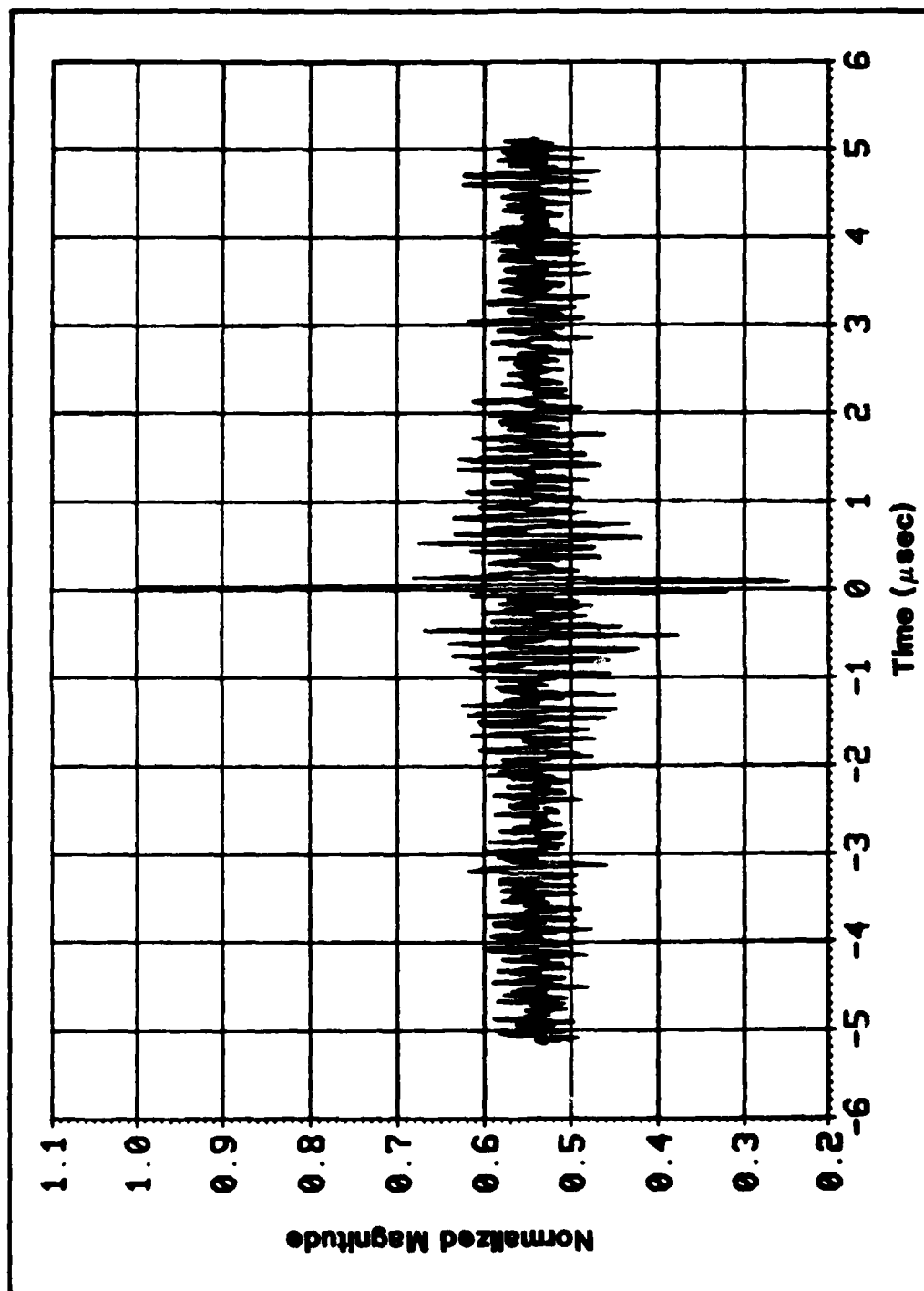


Figure 36. Post-adaption Correlation Response for Case 2.

frequency, the AIS filter is able to provide improvement as demonstrated in Cases 10 - 12 of Table III.

The pre-adaption correlation response for Case 13 is illustrated in Figure 37 where there is no correlation. The PG of the SS signal is unable to spread the two jammers and despread the signal for proper correlation. However, when the filter is allowed to adapt on the jammers, correlation occurs as illustrated in Figure 38.

There is no correlation in Case 18 without the AIS filter as seen in Figure 39. When the filter is allowed to adapt on the three jammers, correlation occurs as illustrated in Figure 40.

When nominal filter fabrication and circuitry errors are introduced, Cases 20 - 22, the magnitude of the post-adaption correlation sidelobes is increased from the magnitude of the post-adaption correlation sidelobes for the respective cases without errors. Thus, there exists a higher probability that the detectors with errors will make an incorrect decision about what message was sent than the detectors without errors.

#### Algorithm Convergence Rate

In this section, Figures 41 through 44 are used to compare the algorithm convergence rates (e.g. the number of iterations required to suppress the jammers) for some of the more relevant cases. The algorithms are allowed to adapt for



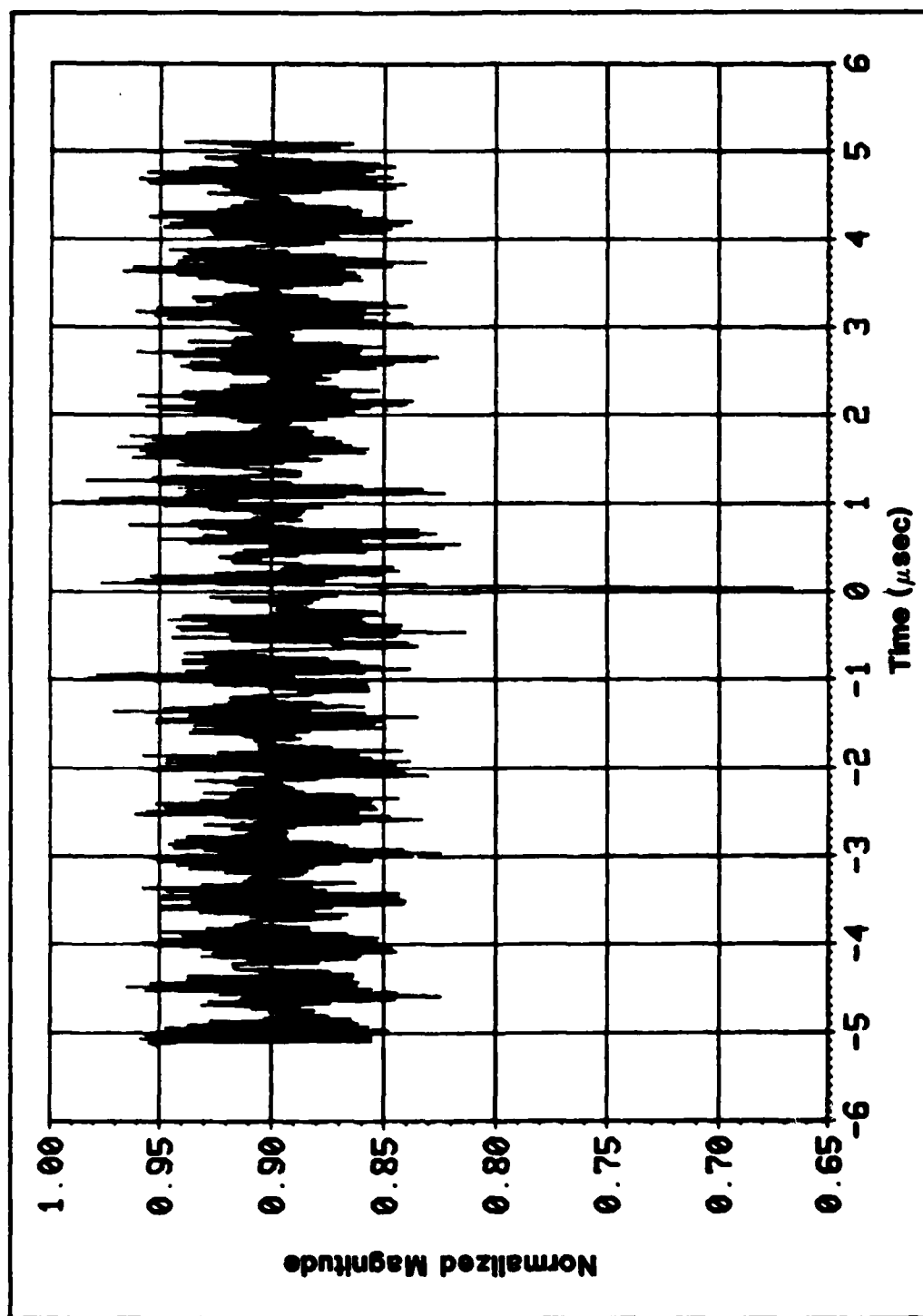


Figure 37. Pre-adaption Correlation Response for Case 13.

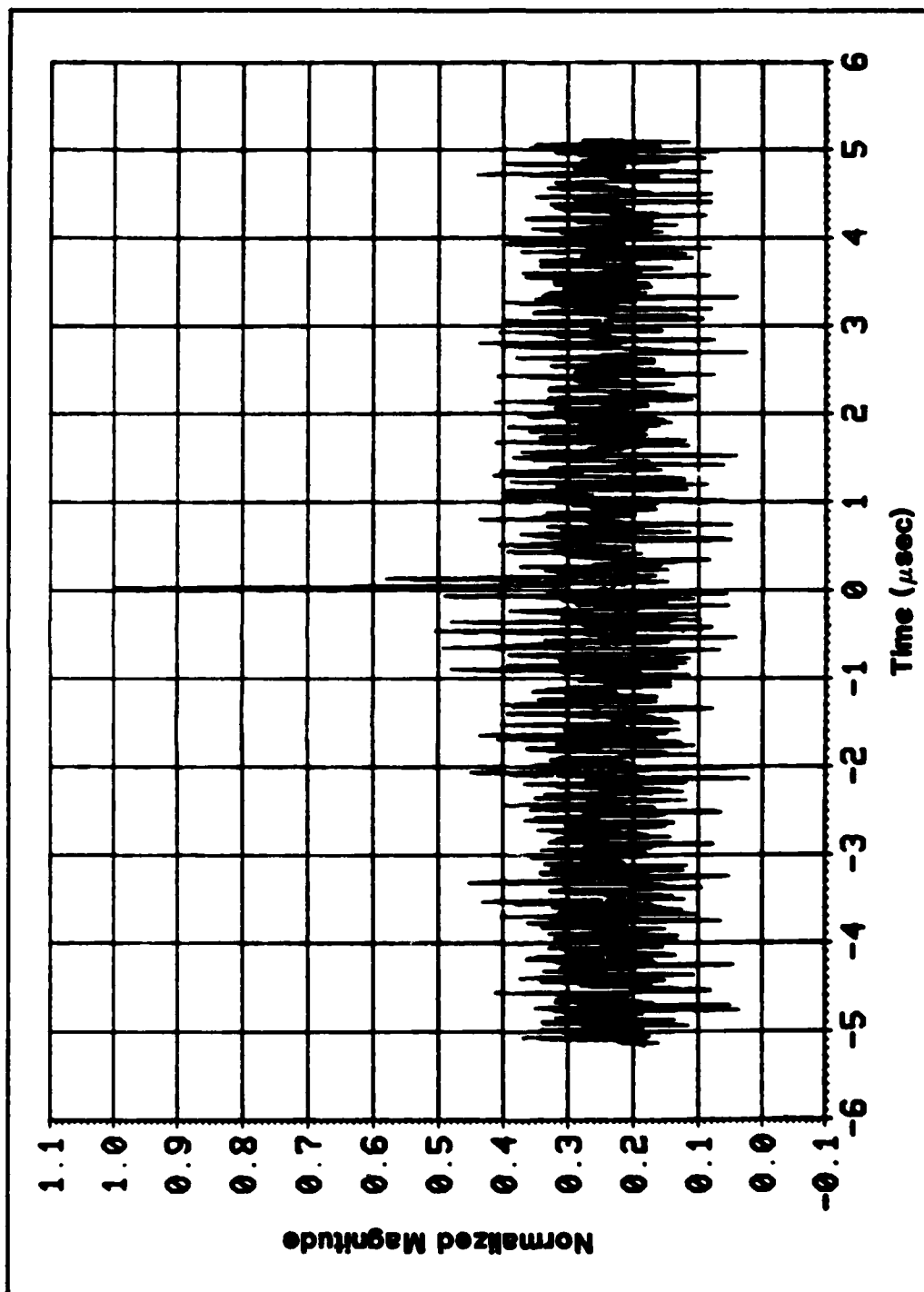


Figure 38. Post-adaption Correlation Response for Case 13.

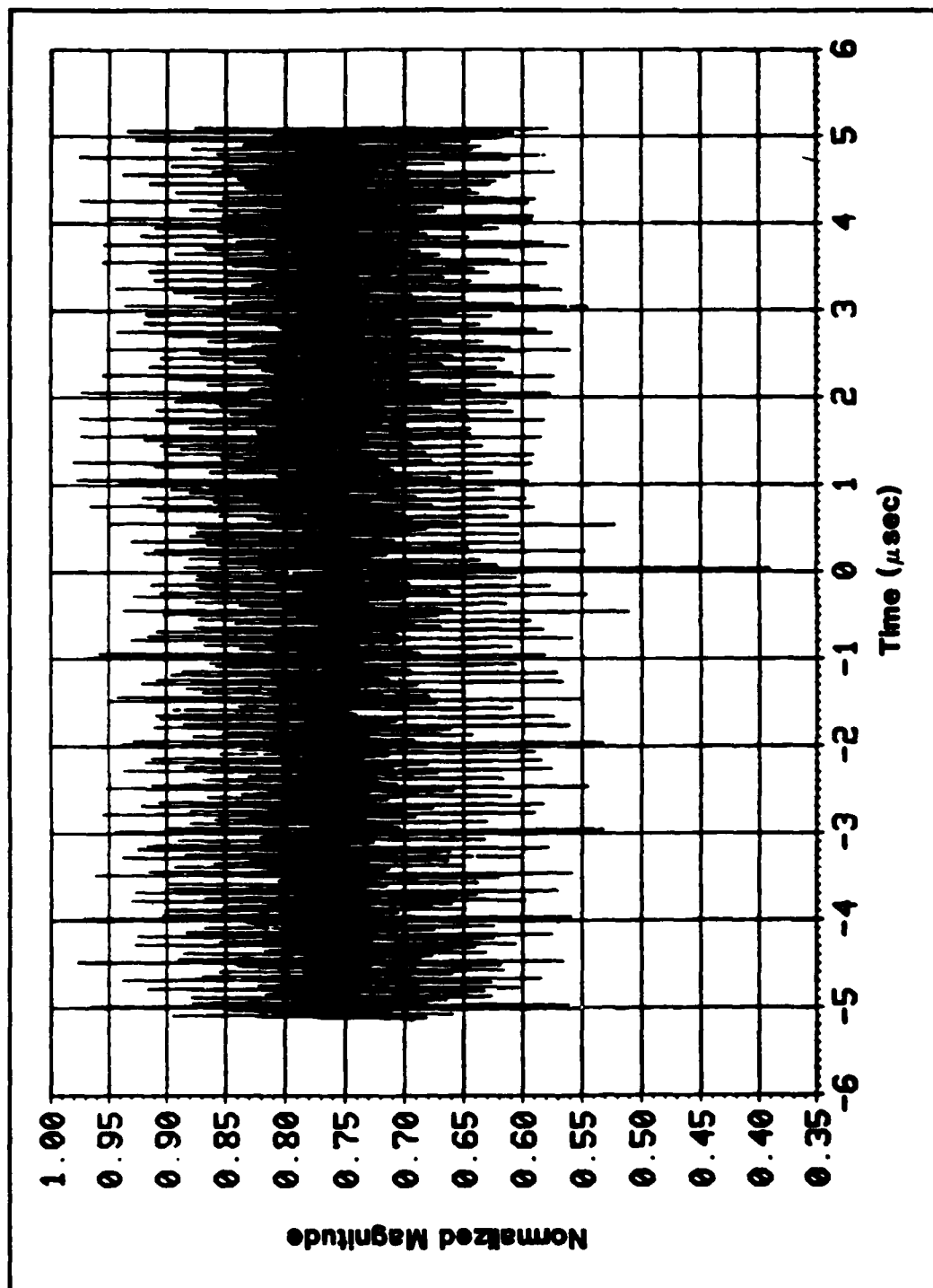


Figure 39. Pre-adaption Correlation Response for Case 18.

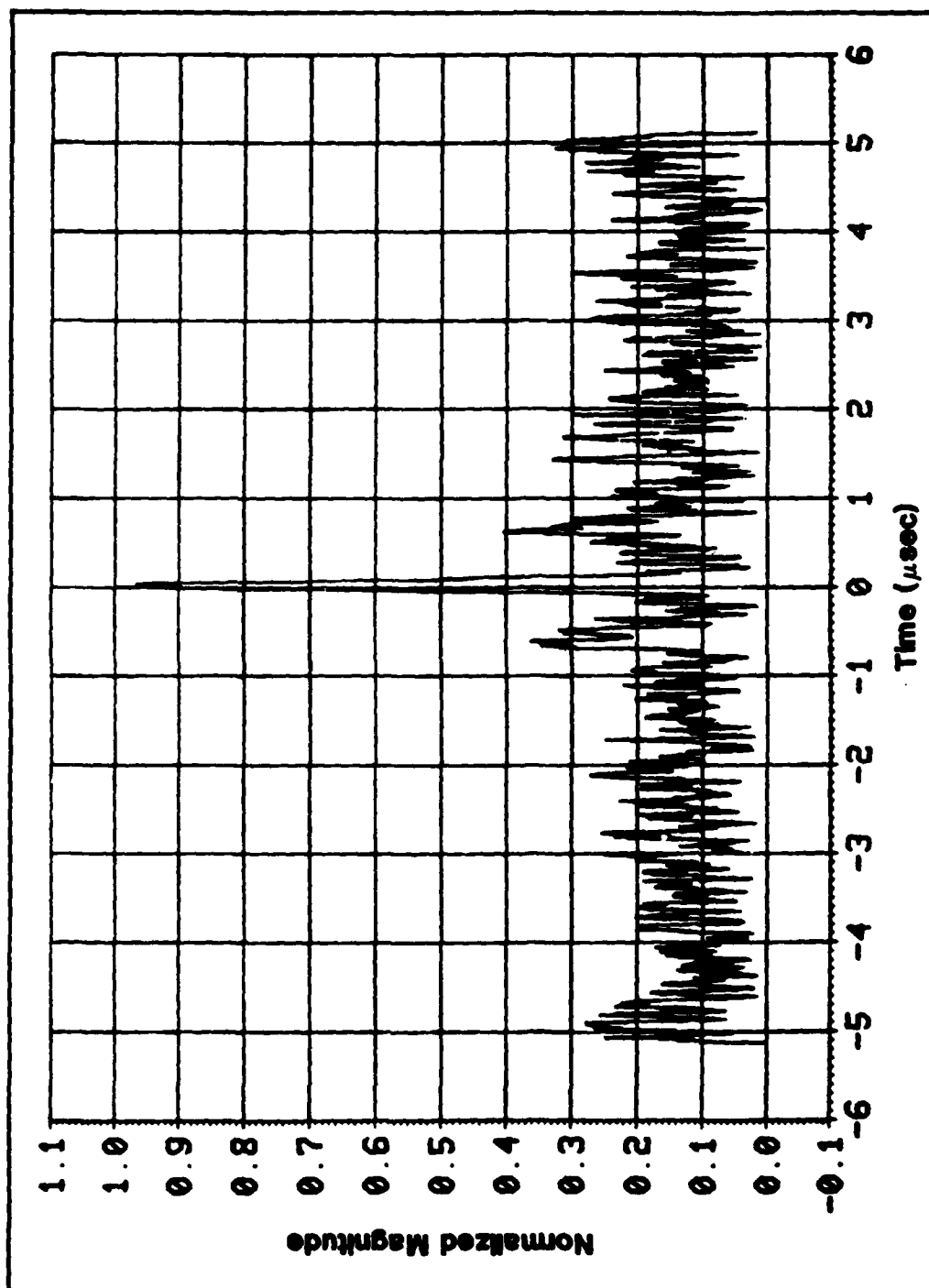


Figure 40. Post-adaption Correlation Response for Case 18.

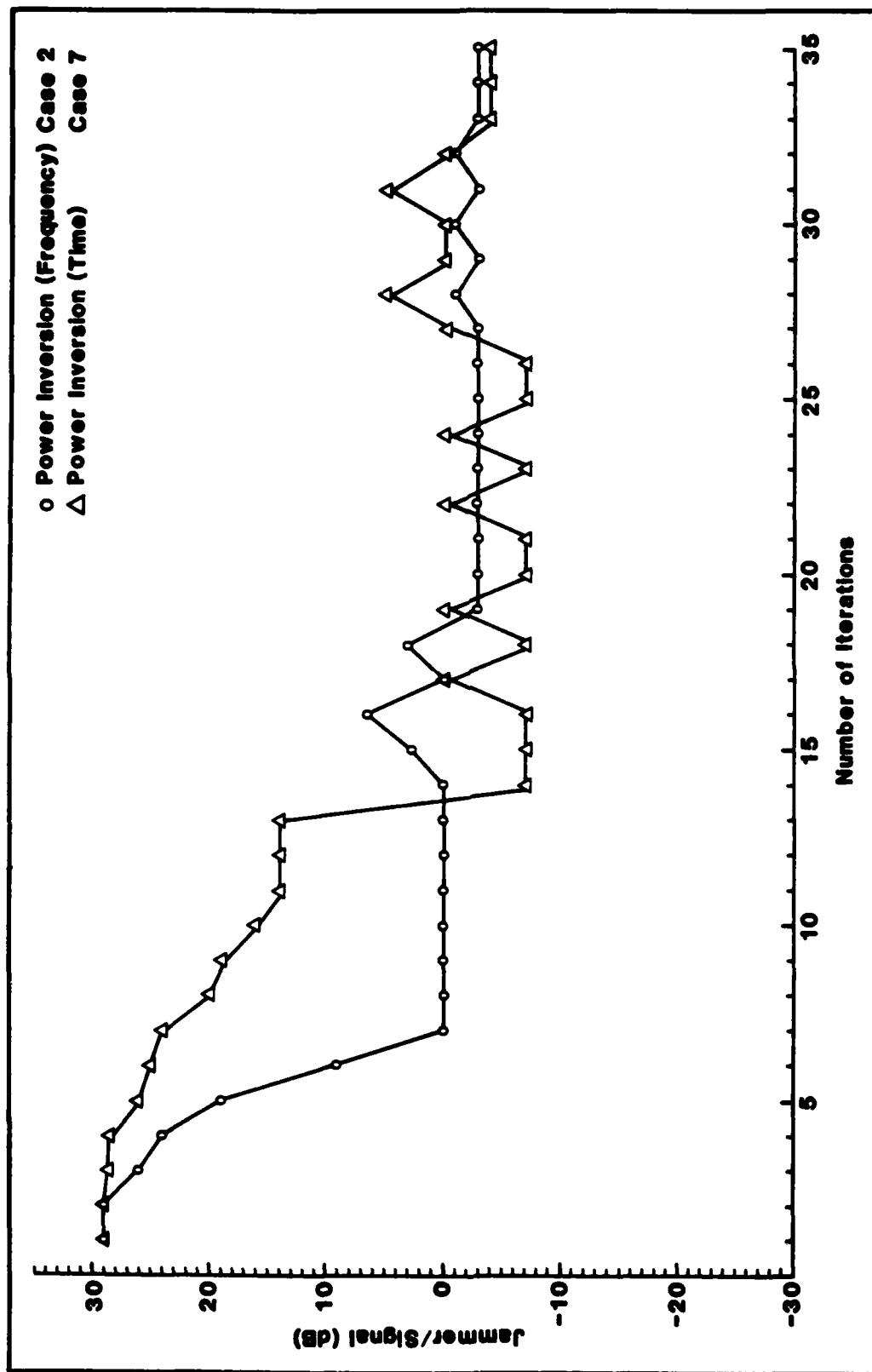


Figure 41. Algorithm Convergence Rate for Cases 2, 7.

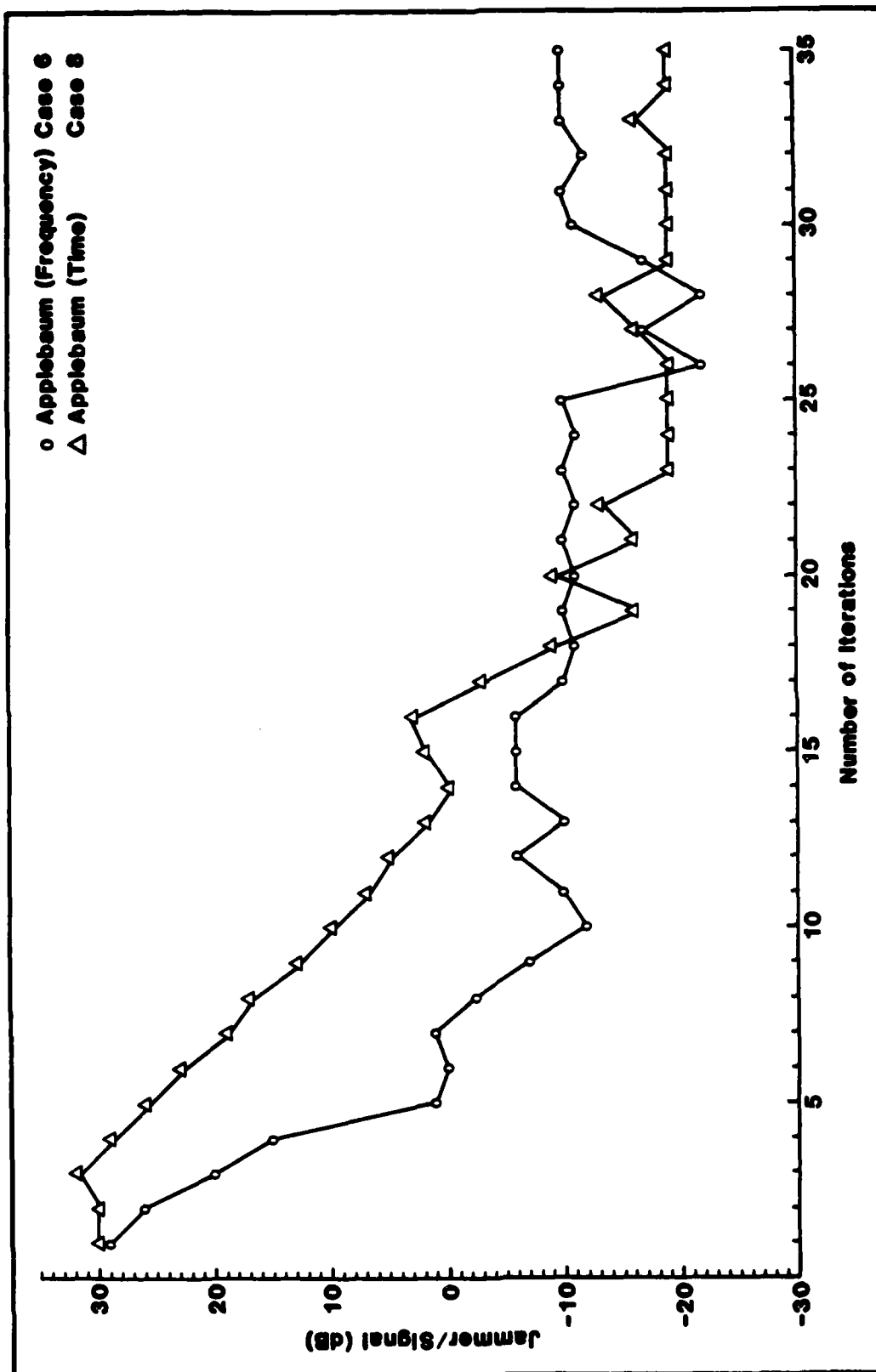


Figure 42. Algorithm Convergence Rate for Cases 6, 8.

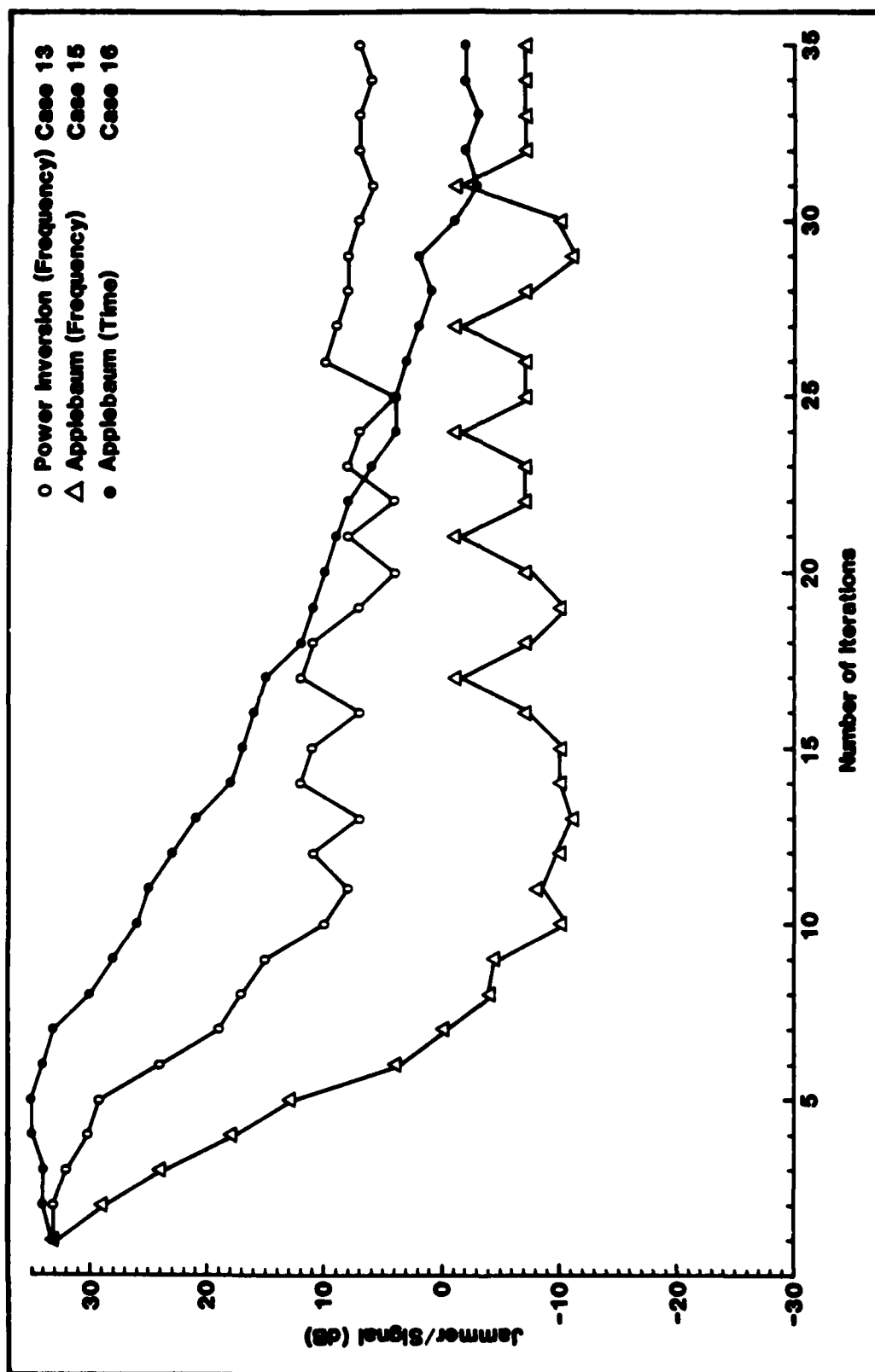


Figure 43. Algorithm Convergence Rate for Cases 13, 15, 16.

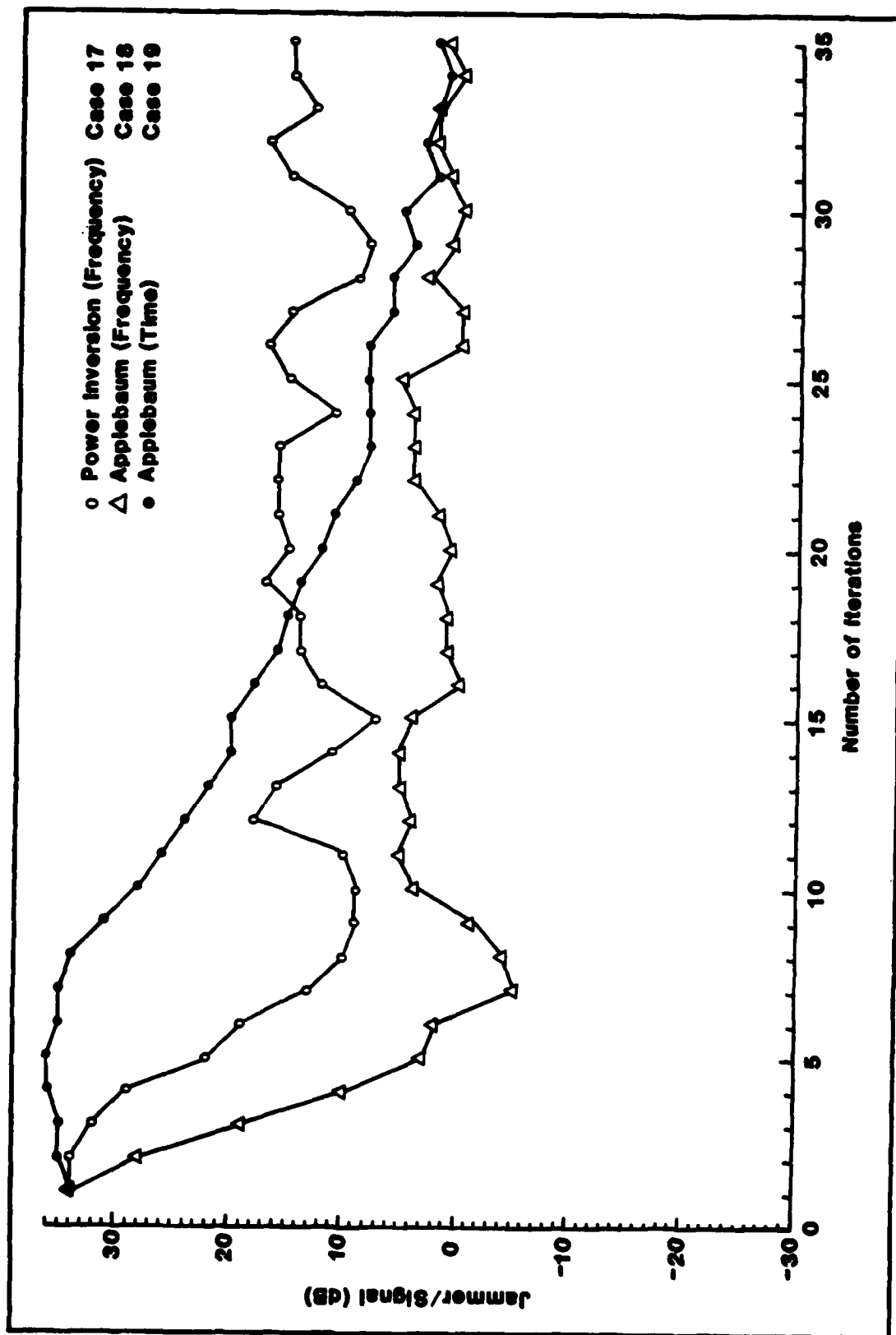


Figure 44. Algorithm Convergence Rate for Cases 17,18,19.



35 iterations which appeared to give a fairly accurate indication of algorithm steady state values of -SJR = jammer-to-signal ratio (JSR).

Figure 41 demonstrates that the power inversion algorithm, implemented in the frequency domain, converges faster than the same algorithm implemented in the time domain. This convergence characteristic is mentioned in Appendix A, and is consistent with Shankar and Peterson's work (Ref.19:124). Although the frequency domain implementation converged faster than the time domain, the time domain yielded lower values of JSR at around 35 iterations for these cases of one CW jammer.

Figure 42 demonstrates that the Applebaum algorithm, implemented in the frequency domain, converges faster than the same algorithm implemented in the time domain. Again, the time domain implementation yielded lower values of JSR at around 35 iterations. A comparison of Figures 41 and 42 shows that either Applebaum algorithm in Figure 42 performed better than either power inversion algorithm of Figure 41.

Figure 43 shows that a frequency domain implementation of the Applebaum or power inversion algorithm converges faster than the time domain implementation of the Applebaum algorithm. Further, the frequency domain implementation of the Applebaum algorithm yielded lower values of JSR at around 35 iterations than the time domain Applebaum implementation for these cases of two CW jammers. However, it is suspected

that the time domain Applebaum implementation will yield lower values of JSR than the frequency domain Applebaum implementation if the algorithm is allowed to adapt for more than 35 iterations.

Figure 44 shows that again the frequency domain implementation of the Applebaum or power inversion algorithm converges faster than the time domain Applebaum implementation. Further, the frequency domain Applebaum implementation yielded lower values of JSR at around 35 iterations than the time domain Applebaum implementation for these cases of three jammers. However, it is suspected that the time domain Applebaum implementation will yield lower values of JSR than the frequency domain Applebaum implementation if the algorithm is allowed to adapt for more than 35 iterations.

## V. Conclusions and Recommendations

### Conclusions

This thesis has shown that a pre-detection adaptive interference suppression (AIS) filter can provide additional improvement against narrowband jamming of PN spread spectrum (SS) signals. Section II presented a theoretical analysis of a SS system model and derived its processing gain (PG). Section III presented several configurations for implementing steepest descent algorithms with the programmable transversal filter (PTF). The configuration utilizing two PTF's, one for interference monitoring and one for adaptive interference suppression, was determined to be the most efficient configuration. Section IV deals with the performance of the AIS filter. A communications simulation (COMSIM) of the AIS filter implemented in a SS system was performed. The performance analysis was carried out in terms of pre-detection SJR, post-detection SJNR, and algorithm convergence rate.

The conclusions drawn in terms of pre-detection SJR are as follows:

(1) The AIS filter provided improvement in SJR for all cases analyzed except the case of a CW jammer located at the center frequency of the desired signal. From the limited data available, no conclusion could be drawn to explain the inability of the filter to adapt to a centrally located

(7) One of the most important limitations to the use of the AIS filter is degradation to the desired signal. As the CW jammer and the desired signal center frequency come together, the attenuation of the desired signal increases causing the SJR to decrease until there is no improvement (Table II, Cases 9-12).

(8) The introduction of nominal filter fabrication and circuitry errors caused the null depths of the adapted filter responses to be degraded from their respective responses without errors.

The conclusions drawn in terms of post-detection SJNR are as follows:

(9) The AIS filter provided improvement in SJNR for all cases except the case of a CW jammer located at the center frequency of the desired signal. Post-detection improvement followed the same patterns as pre-detection improvement.

(10) Post-detection improvement is due to both the AIS filter and the PG of the SS matched filter. It can be noted from Table III, Cases 2 and 4, that for in-band jammers the system performance improvement caused by increasing the PG was 1.5 dB greater than expected. This is due to the constant filter 3 dB null width causing less degradation to the desired SS signal having a greater bandwidth or PG.

(11) The signal at the output of the correlator could not be observed above the interference level before filter

jammer.

(2) The Applebaum adaptive algorithm provided typically 8-16 dB (Tables I and II) greater improvement in SJR than the power inversion adaptive algorithm.

(3) The time domain implementation of the adaptive algorithms, for greater than 33 iterations, provided more improvement in SJR than the frequency domain implementation for the cases of one CW jammer only. However, it is suspected that the same would be true for two or three CW jammers if the adaptive algorithm is allowed to adapt for more than 35 iterations.

(4) The 3 dB widths of the nulls in the adapted filter responses with the Applebaum algorithm implementation are smaller than the 3 dB widths of the nulls in the corresponding power inversion algorithm implementation (e.g. Figures 21, 22, 25, 26, 29, and 31). This is a principal reason that the Applebaum algorithm had better performance than the power inversion algorithm.

(5) Increasing the SS signal bandwidth had little effect on pre-detection SJR.

(6) For the case of three jammers, the adapted filter response lobe between the nulls at 245 MHz and 265 MHz with the power inversion algorithm is 17 dB down from that with the Applebaum algorithm. This is a principle reason that the Applebaum algorithm had better performance than the power inversion algorithm.

adaption occurred for most of the cases analyzed (Table III). This is due to the inadequacy of the spread spectrum PG to overcome the strong jamming signals. However, the AIS filter improved the pre-detection SJR to within the operational range of the correlator.

The conclusions drawn in terms of algorithm convergence rate are as follows:

(12) Both the Applebaum and power inversion algorithms implemented in the frequency domain converged faster than their respective time domain implementations (Figures 41-44). This result is consistent with Shankar and Peterson's work (Ref. 19:124).

(13) The time domain implementation of an adaptive algorithm yielded lower values of jammer-to-signal ratio (JSR), for greater than 33 iterations, than its respective frequency domain implementation for the cases of one jammer (Figures 41 and 42). However, it is suspected that the time domain implementation will yield lower values of JSR for the cases of two or three jammers if the algorithm is allowed to adapt for more than 35 iterations.

### Recommendations

The analysis performed in this thesis provided a variety of information about AIS filter application to SS communications. This information indicates areas where future research might be able to take advantage of the

results obtained in this thesis. Recommendations are as follows:

(1) Additional simulations may be performed to analyze the AIS filter adaptation to a jammer located at the center frequency of the SS signal. The suggested approach is to utilize the final tap weight values of Case 10 as the initial AIS filter tap weights. It is also suggested that the number of iterations be increased to 200.

(2) Channel propagation effects, other than band limited Gaussian noise (BLGN), are not included in the simulation. Multipath and scintillation fading could be implemented in the simulation to assess the AIS filter's performance in a more realistic environment.

(3) Determine the performance improvement that may potentially be realized for AIS filter application to the Integrated Communication, Navigation, Identification Avionics (ICNIA) program at AFWAL/AAAI-3. That is, determine if the filter can provide in-band rejection of jammers on narrowband as well as wideband signals (e.g. JTIDS/FH). This may require cascading an AIS filter with a low sidelobe level PTF.

(4) Expand the computer simulation to include an adaptive null steering antenna with an AIS filter at the output of each antenna element.

(5) Evaluate the AIS filter performance against pulsed, swept, partial band, and barrage jammers.

### Bibliography

1. Applebaum, Sidney P. "Adaptive Arrays," Syracuse University Research Corp., Report SPL TR 66-1 (August 1966).
2. Compton, R.T., Jr. "The Power Inversion Adaptive Array; Concept and Performance," IEEE Transactions on Aerospace and Electronic Systems, AES-15:803-814 (November 1979).
3. Compton, R.T., Jr. "Adaptive Arrays with Constraint Nulls," The Ohio State University ElectroScience Laboratory, Report 3234-3 (September 1972).
4. Dixon, Robert C. Spread Spectrum Systems. New York: John Wiley and Sons, 1976.
5. Drossman, Mel. "Computer Simulation of a Spread Spectrum Communications System," Prepared for US Army Coradcom by S Consulting Services, New York (November 1980).
6. Frost, Otis L. "An Algorithm for Linearly Constrained Adaptive Array Processing," Proceedings of the IEEE, 55: 926-935 (August 1972).
7. Githin, R. D. and F. R. Magee. "Self-Orthogonalizing Adaptive Equalization Algorithms," IEEE Transactions on Communications, Comm-25:666-672 (July 1977).
8. Hall, Thomas J. "Intercept Vulnerability of Direct Sequence Pseudo-Noise Encoded Spread Spectrum Waveforms," Air Force Institute of Technology, MS Thesis, AFIT/GE/EE/79-15 (December 1979).
9. Holmes, Jack K. Coherent Spread Spectrum Systems. New York: John Wiley and Sons, 1982.
10. Kalman, R. E. and N. DeClaris. Aspects of Network and System Theory. New York: Holt, Rhinehard and Winston, 1970.
11. Lord, Peter. "Properties of Pseudo Noise," The Martin Company Electronics Div., Report ER 11683 (March 1961).
12. Matthews, Herbert. Surface Wave Filters: Design Construction and Use. New York: John Wiley and Sons, 1977.
13. Melsa, James L. and D. L. Cohn. Decision and Estimation Theory. New York: McGraw-Hill Book Company, 1978.



14. Owens, J. M., R. L. Carter, and C.W. Smith, Jr. "Magnetostatic Waves, Microwave SAW?," Proceedings of the 1980 IEEE Ultrasonics Symposium, 506-521.
15. Panasik, Carl M. and L. R. Nawman. "Programmable Filter Technology for Integrated Communication Navigation and Identification Systems," Proceedings of the 1982 IEEE National Aerospace and Electronics Conference, 3: 1074-1080.
16. Papoulis, Athanasios. Probability, Random Variables, and Stochastic Processes. New York: McGraw-Hill Book Company, 1965.
17. Phillips, Howard D. "Space-Hardened Microelectronics Bring New Advances," Military Electronics/Counter-measures, 8: 76-78 (August 1982).
18. Schwegman, C. W. and R. T. Compton, Jr. "Power Inversion in a Two Element Adaptive Array," The Ohio State University ElectroScience Laboratory, Report 3433-3 (December 1972).
19. Shankar Narayan, S. and A. M. Peterson. "Frequency Domain Least-Mean-Square Algorithm," Proceedings of the IEEE, 69: 124-126 (January 1981).
20. Slobinik, Andrew J., T. L. Szabo, K. R. Laker. "Miniature Surface-Acoustic-Wave Filters," Proceedings of the IEEE, 67:129-146 (January 1979).
21. Strang, Gilbert. Linear Algebra and its Applications. New York: Academic Press, Inc., 1980.
22. Texas Instruments. "Proposal for Adaptive Interference Suppression Techniques Program," Proposal No. EG81-069, Dallas (October 1981).
23. Toplicar, James R. "Wideband Spread Spectrum Testbed," Proceedings of the 1982 National Aerospace and Electronics Conference, 3:1081-1087.
24. Torrieri, Don J. Principles of Military Communication Systems. Massachusetts: Artech House, Inc., 1981.
25. Van Trees, Harry L. Detection, Estimation, and Modulation Theory: Part I. New York: Prentice Hall, Inc., 1968.

26. Widrow, B, P. E. Montley, L. J. Griffiths, and B. B. Goode. "Adaptive Antenna Systems," Proceedings of the IEEE, 55:2143-2159 (December 1967).
27. Widrow, B. and J. M. McCool. "A Comparison of Adaptive Algorithms Based on the Methods of Steepest Descent and Random Search," IEEE Transactions on Antennas and Propagation, AP-24:615-637 (September 1976).
28. Ziemer, R. E. and W. H. Tranter. Principles of Communications: Systems, Modulation and Noise. Boston: Houghton Mifflin Company, 1976.

## Appendix A

### A Survey of Adaptive Algorithms

Over the past twenty years numerous adaptive algorithms have been developed for the rejection of undesirable energy in communications systems. In the spatial domain, these algorithms have been implemented to achieve null-steering antennas, low sidelobe antennas, and beam steering antennas for interference and jammer suppression. In the temporal domain, these algorithms have been implemented to realize active notch filters, echo cancellation, channel estimation or equalization, and adaptive interference suppression filters.

A majority of the adaptive algorithms were implemented in spatial filtering techniques before temporal filtering techniques became popular. However, the theoretical similarities between spatial and temporal filtering algorithms permitted swift transformation of spatial to temporal algorithms (Refs.1,2,6,10,26).

Temporal domain filters (e.g. the PTF under study in this thesis) are inherently much smaller than spatial domain filters (e.g. adaptive antenna arrays). Further, the physical implementation of some adaptive algorithms requires bulky adaptive hardware. Bulky hardware is more readily acceptable for use in spatial filtering where already large antennas exist than for use in temporal filtering.

Therefore, a practical consideration in choosing an adaptive algorithm for temporal filtering is the physical size of the required adaptive hardware.

#### Principles of the Adaptive Process (Ref.27:616-617)

The adaptive filter illustrated in Figure 45a will be used to present the theoretical basis of the algorithms referenced in this thesis. This adaptive filter is made up of a tapped delay line connected to an adaptive linear combiner. The adaptive linear combiner, as illustrated in Figure 45b, adjusts the gain of the input signals from the delay line and sums them to form an output signal.

The adaptive linear combiner input signal vector is given by

$$x_j^T = [x_{1j} \ x_{2j} \ \dots \ x_{nj}]^T \quad (48)$$

The components of the input signal vector exist simultaneously on all input taps at discrete times as indexed by the subscript  $j$ . The adjustable weighting coefficients  $w_1, w_2, \dots, w_n$  make up the weight vector given by

$$w^T = [w_1 \ w_2 \ \dots \ w_n]^T \quad (49)$$

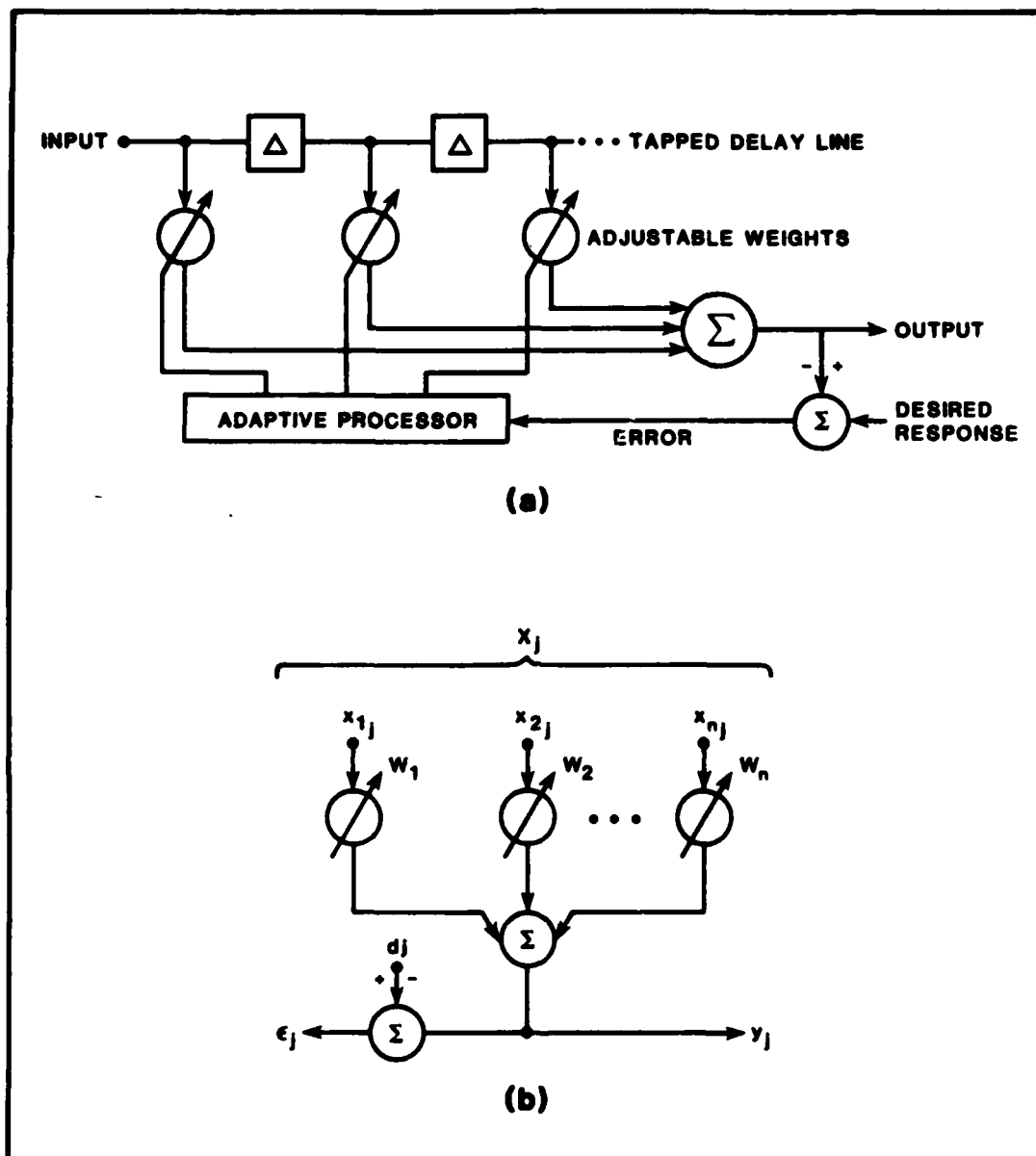


**Figure 45. Adaptive Transversal Filter**  
**(a) Adaptive Filter Configuration**  
**(b) Adaptive Linear Combiner (Ref. 27:616).**

The output signal equals the inner product of  $x_j$  and  $W$  as given by

$$y_j = x_j^T W = W^T x_j \quad (50)$$

The error signal equals the difference between an estimate of the desired signal,  $d_j$ , and the actual output signal,  $y_j$ , as given by

$$\epsilon_j = d_j - y_j = d_j - x_j^T W \quad (51)$$

It is clear that the objective of the adaptive process is to adjust the tap weights of the adaptive linear combiner in order to minimize the mean square of the error  $\epsilon_j$ . Before calculating the mean square of the error, the  $K$ th iteration of the weight vector is expressed as  $W_K$ . The square of the error is then given by

$$\epsilon_j^2 = d_j^2 - 2d_j x_j^T W_K + W_K^T x_j x_j^T W_K \quad (52)$$

The mean or ensemble average of the squared error known as the mean square error (MSE) is given by

$$E[\epsilon_j^2] W_k = E[d_j^2] - 2E[d_j x_j^T] W_k + W_k^T E[x_j x_j^T] W_k \quad (53)$$

Equation 53 is reduced by defining a vector  $P^T$  as the cross-correlation between  $d_j$  and  $x_j^T$  and by defining  $R$  as the input correlation matrix. These two are given by

$$P^T = E[d_j x_j^T] \quad (54)$$

$$R = E[x_j x_j^T] \quad (55)$$

Therefore the simplified MSE is given by

$$\begin{aligned} MSE = \xi_k &= E[\epsilon_j] W_k \\ &= E[d_j^2] - 2P^T W_k + W_k^T R W_k \end{aligned} \quad (56)$$

The MSE is a quadratic function of the weights which can be plotted as a concave hyperparaboloidal surface (Ref.27:617). Adjusting the tap weights relates to descending along this surface with the objective of reaching its minimum point. The technique under consideration here for that purpose is based on gradient methods. The gradient of the MSE,  $\nabla_k$ , can be obtained by differentiating equation 56 as given below

$$\nabla_k = \left\{ \begin{array}{c} \partial E [\epsilon_j^2] / \partial \omega_1 \\ \vdots \\ \partial E [\epsilon_j^2] / \partial \omega_n \end{array} \right\}_{W=W_k} = -2P + 2RW_k \quad (57)$$

The optimal weight vector,  $W_{OPT}$ , is found as usual with simple calculus by setting the first derivative of the MSE to zero. That is, by setting the gradient,  $\nabla_k$ , to zero and solving for  $W$ . In this way the intuitively pleasing result for the optimal weight vector, generally called the Wiener weight vector, is given by

$$W_{OPT} = R^{-1}P \quad (58)$$

#### Description of the Four Classes of Adaptive Algorithms

Adaptive algorithms suitable for use with adaptive filters have been organized into the following four classes:

- Steepest descent algorithms
- Random search techniques
- Sample matrix inversion techniques
- Self-orthogonalizing techniques

#### Steepest Descent Algorithms

The steepest descent class of algorithms is made up of



the power inversion, the Widrow LMS, the Applebaum, and the Frost algorithms as illustrated in Figure 46. These four algorithms vary, depending on the characteristics of the "a priori" information used, the gradient estimation method used, and the method utilized to accelerate the descent in the gradient direction.

The power inversion algorithm assumes that the filter output signal is always noise-like and operates to minimize the power of this output signal (Ref.2). This technique is illustrated in Figure 46a. The term power inversion refers to the ability of the filter to invert the power ratio of the received signals. That is, an interfering signal 40 dB above the desired signal at the filter input comes out of the filter at 40 dB below the desired signal level. Detailed knowledge of the desired signal is not required by this algorithm. The theoretical control law is given by

$$W(k+1) = W(k) - \alpha \left[ x_n(t)^* y(t) \right] \quad (59)$$

where  $k$  denotes the  $k$ th iteration (Ref.22:2-22).  $W(k)$  is the weight vector of the  $k$ th iteration,  $\alpha$  is the loop gain,  $x_n(t)$  is the  $n$ th tap element output where  $*$  indicates a finite time integration, and  $y(t)$  is given by the auxiliary filter by setting the gain of the  $n$ th tap to unity and the gain of all other taps to zero. In the main filter, the center tap

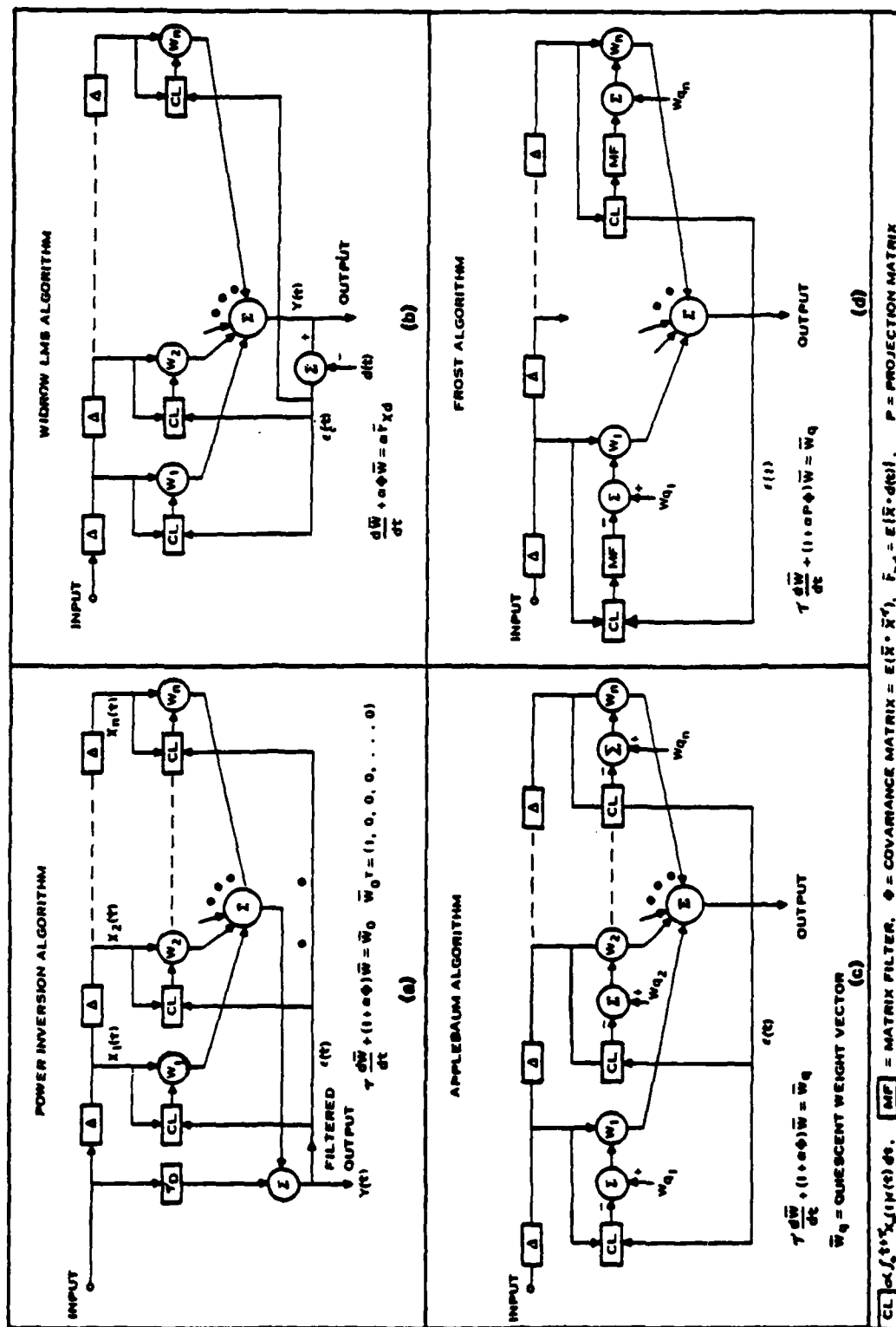


Figure 46. Steepest Descent Adaptive Algorithms (Ref. 2.2:2-23).

where  $\Delta W(k+1)$  is the perturbation weight vector,  $W(k)$  is the weight vector at the  $K$ th iteration,  $W_q$  is the quiescent weight vector,  $\alpha$  is the loop gain,  $x_n(t)$  is the  $n$ th tap element output,  $y(t)$  is the filter output, and  $\beta$  is a weighting used to minimize the deviation of the adapted weight vector from the quiescent weight vector.

The Widrow LMS algorithm operates to minimize the MSE between the filter output signal and an estimate of the desired signal (Refs.10,19,22,27). An estimate of the desired signal is subtracted from the filter output signal to generate an error signal,  $\epsilon(t)$ , as depicted in Figure 46d. The weights are iteratively adjusted by the feedback loop at each of the taps until the correlation between the error signal and each of the tap outputs is minimized. For any deviation between the actual and an estimate of the desired signal, the residual desired signal components in the feedback error signal path will be considered as interfering components and will be suppressed. Therefore, a good estimate of the desired signal is essential with this algorithm. The algorithmic weight control law is given by

$$W(k+1) = W(k) - \alpha [y(t) - d(t)] \cdot x_n^*(t) \quad (61)$$

where  $W$  is the tap weight vector,  $\alpha$  is the loop gain,  $y(t)$  is the main filter output signal,  $d(t)$  is an estimate of the

weight is initially set to unity gain and all other tap weights to zero. This creates an all-pass response for the main filter. The control law then iteratively adjusts the N-1 tap weights to null the interfering signals within the filter passband. It should be noted that in Figure 46a the first tap is constrained to unity gain, which is optimal for some applications. However, it is optimal in this thesis application to initially set the center tap to unity gain because the center frequency of the desired signal is located in the center of the filter bandpass.

The Applebaum algorithm operates to maximize the output signal to jammer plus noise ratio (SJNR) (Ref.1). This algorithm is illustrated in Figure 46c. The algorithm initiates the maximization of the output SJNR ratio by first setting the filter tap weights to maximize the response to the desired signal. The algorithm then operates to minimize the total power output from the filter, similar to the power inversion algorithm. This algorithm also attempts to minimize the time duration (adaption time) in translating from the quiescent to the adapted filter transfer function. No reference signal is required for this algorithm. The Applebaum algorithm tap weight control law is given by

$$\Delta W(k+1) = \beta \left[ W(k) - W_q \right] - \alpha \left[ x_n^*(t)y(t) \right] \quad (60)$$

desired signal,  $x_n(t)$  is the  $n$ th tap element output, and  $y(t) - d(t)$  is the error signal,  $e(t)$ .

The Frost algorithm, illustrated in Figure 46d, places certain constraints within the filter passband which tend to leave the passband unchanged, even in the presence of strong interfering signals in the passband (Refs.6,22:2-24).

An advantage of the steepest descent class of algorithms is that a constant loop gain or step size is realized in the descent operation. This simplifies implementation, but increases convergence rate (e.g. the number of iterations required to obtain adaption). The convergence characteristic of steepest descent algorithms is controlled by the eigenvalues<sup>2</sup> of the input signal covariance matrix. These eigenvalues control the time constants of several decaying components in the filter output during the adaptive process (Ref.22:2-24). Convergence rate can be decreased by implementing the LMS algorithms in the frequency domain as opposed to the time domain (Ref.19:124). This improved convergence rate can be obtained because the outputs from each of the frequency bands are partially decorrelated from each other resulting in a

---

<sup>2</sup> An eigenvalue of the input signal covariance matrix  $X$ , is defined as  $\lambda$  in the characteristic equation: determinant  $(X - \lambda I) = 0$  where  $I$  is the identity matrix (Ref.21:183).

diagonally dominant input signal covariance matrix. The proposed PTF structure allows easy implementation (e.g. simplicity in required hardware) of the steepest descent algorithms which makes their use in adaptive filtering desirable.

#### Random Search Algorithms

The random search algorithms perform a search through the weight vectors to reach the extremum of the desired performance measure (Refs.22:2-24,27). These algorithms are guided if information about past searches is retained and utilized, otherwise they are unguided. For practical PTFs with between 200 and 600 tap weights, random search techniques offer little application because of the increased convergence rate associated with many taps.

#### Sample Matrix Inversion Algorithms

Sample matrix inversion algorithms operate to choose the optimum tap weights by direct inversion of the sample input signal covariance matrix (Refs.22:2-24). These algorithms are useful when there is a small number of tap weights and when the channel bandwidth is narrow. Also, these techniques require samples of the signal at each tap creating the need for much additional hardware. Therefore, these algorithms are not suitable for implementation with the

PTF under study.

### Self-Orthogonalizing Algorithms

Self-orthogonalizing algorithms operate to overcome the sensitivity of the adapted response to the dynamic range of the input signal covariance matrix eigenvalues (Refs.7,22:2-25). These algorithms attempt to overcome this sensitivity by either deflecting the direction of the gradient vector toward the extremum of the desired performance measure or by orthogonalizing the input signal vector space. Since the frequency domain implementation of the steepest descent algorithms inherently provides a degree of orthogonalization, self-orthogonalization algorithms are considered less useful for implementation with the PTF under study.

## Appendix B

### Description of System Simulation Flowdiagrams

COMSIM (communications simulator) is a computer simulation of a direct sequence spread spectrum system with a pre-detection adaptive interference suppression (AIS) filter implemented in the receiver. The simulation includes modelling of the surface acoustic wave (SAW) AIS filter, its tap weights, the adaptive control algorithms, and filter fabrication and circuitry errors. Both the desired and interfering signals are generated in the simulator, passed through the AIS filter, and demodulated by a simulated correlation matched filter.

Flowdiagrams depicting the main program and the two subroutines necessary to describe system simulation are included in this Appendix. The flowdiagrams are for the most part self explanatory, however , further explanation is given here.

COMSIM is an interactive program intended to be run on a Tektronix graphics terminal. Therefore, in the beginning of the main program, several Tektronix subroutines are called to initialize the graphics terminal.

A brief description of the subroutines (and a few subroutines within subroutine SPS) called by the main program that are helpful in understanding system simulation is given in Table IV. A list of user entered input parameters and their nominal values is given in Table V.



Table IV  
Description of Primary COMSIM Subroutines

Subroutine	Description
PTF	Programmable transversal filter. Calculates the transfer characteristics of a PTF with complex weights introduced through I and Q channels. Fabrication and circuitry error are introduced in the calculation as normally distributed random variables.
SPS	Signal processing subroutine. Computes fast fourier transform of signals and filter response. Computes and plots the filtered signal and the correlation response. Provides a statistical analysis of the correlation response.
SJAM	Jammer and Gaussian noise generator. Generates the I and Q CW or pulsed jammer samples and the Gaussian noise samples.
SIGDS	Direct dequence signal generator. Generates the I and Q signal samples of a direct sequence SS signal.
STATS	Statistical subroutine. Computes the maximum, the average, and the RMS values of a user specified time interval of the correlation response.
PREPLT	Preplot. Prepares a complex array for plotting by returning magnitude and phase as real arrays.
TSOPLT	Tektronix terminal plotting routine. Plots the magnitude or phase passed by subroutine PREPLT on the graphics terminal.

Table V

User Entered Input Parameters and Their Nominal Values

Number of Filter Taps --- (16)  
Filter Intertap Spacing --- (5Nsec)  
Filter Quiescent Response Offset Frequency --- 50MHz  
Filter Tap Weight Word Length --- (8 bits)  
Filter Tap Weight Generation Error --- (5%)  
Filter Intertap Delay Error --- (0.017 Nsec)  
Filter Summing Delay Error --- (0.03 Nsec)  
Phase Error Between I and Q Channels --- ( $5^\circ$ )  
Quiescent Tap Weight Values for Applebaum Algorithm ---  
    (1,0,...,0,0)  
Signal Amplitude --- (0dB)  
Signal Bandwidth --- (1-50MHz)  
Time or Frequency Domain Implementation Choice  
Number of Frequency Bands for Frequency Domain --- (16)  
Number of Jammers --- (1-15)  
Jammer Amplitude --- (30dB)  
Jammer Frequency --- (200-300MHz)  
CW or Pulsed Jammer Choice  
Applebaum or Power Inversion Algorithm Choice  
Number of Iterations of Adaptive Algorithm --- (35)  
Algorithm Loop Gain Constant --- ( $10^{-6}$ )  
Lower and Upper Time Limits of Correlation Response for  
    Statistical Analysis --- (1-6  $\mu$ sec)

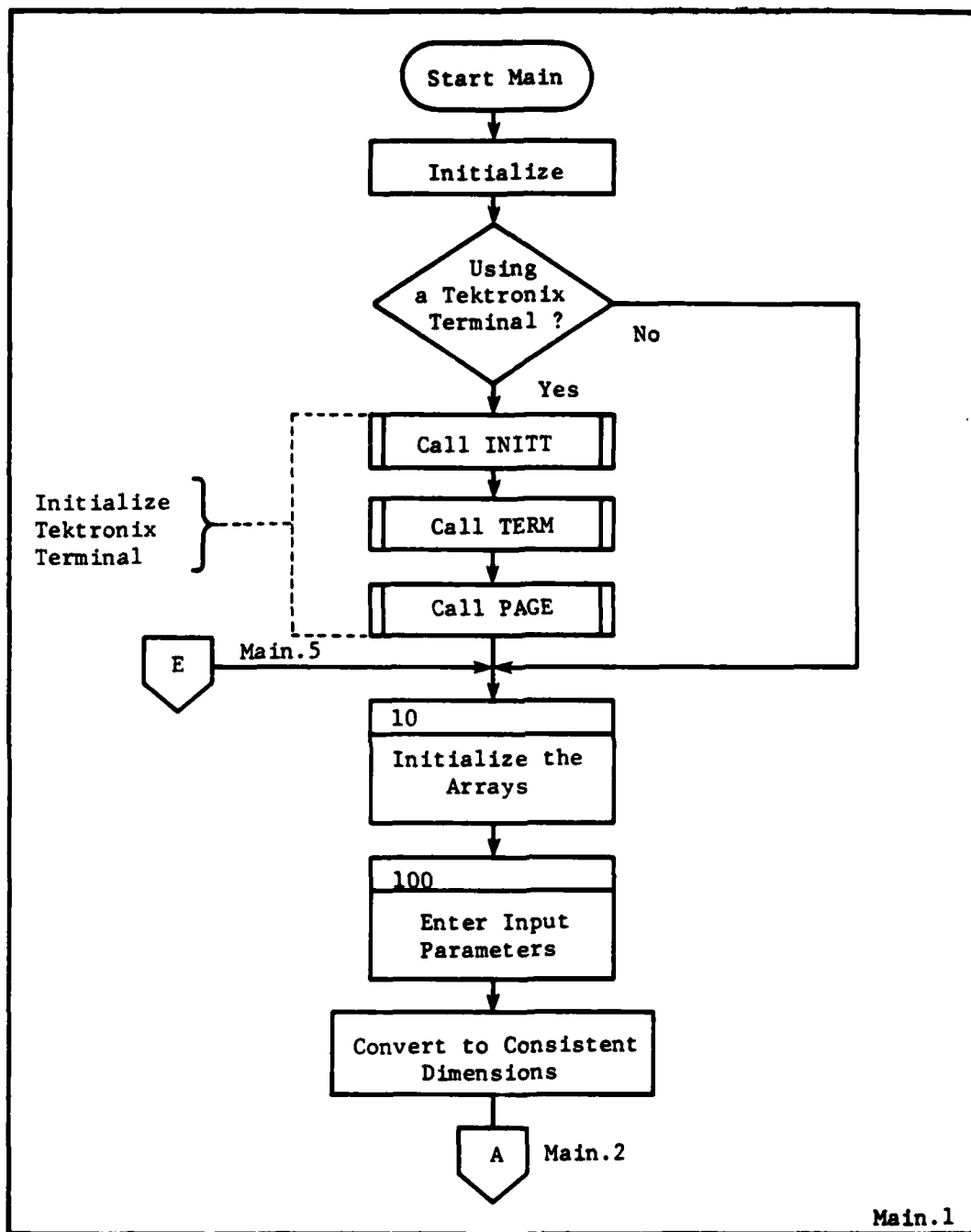


Figure 47. Flowchart for Module MAIN

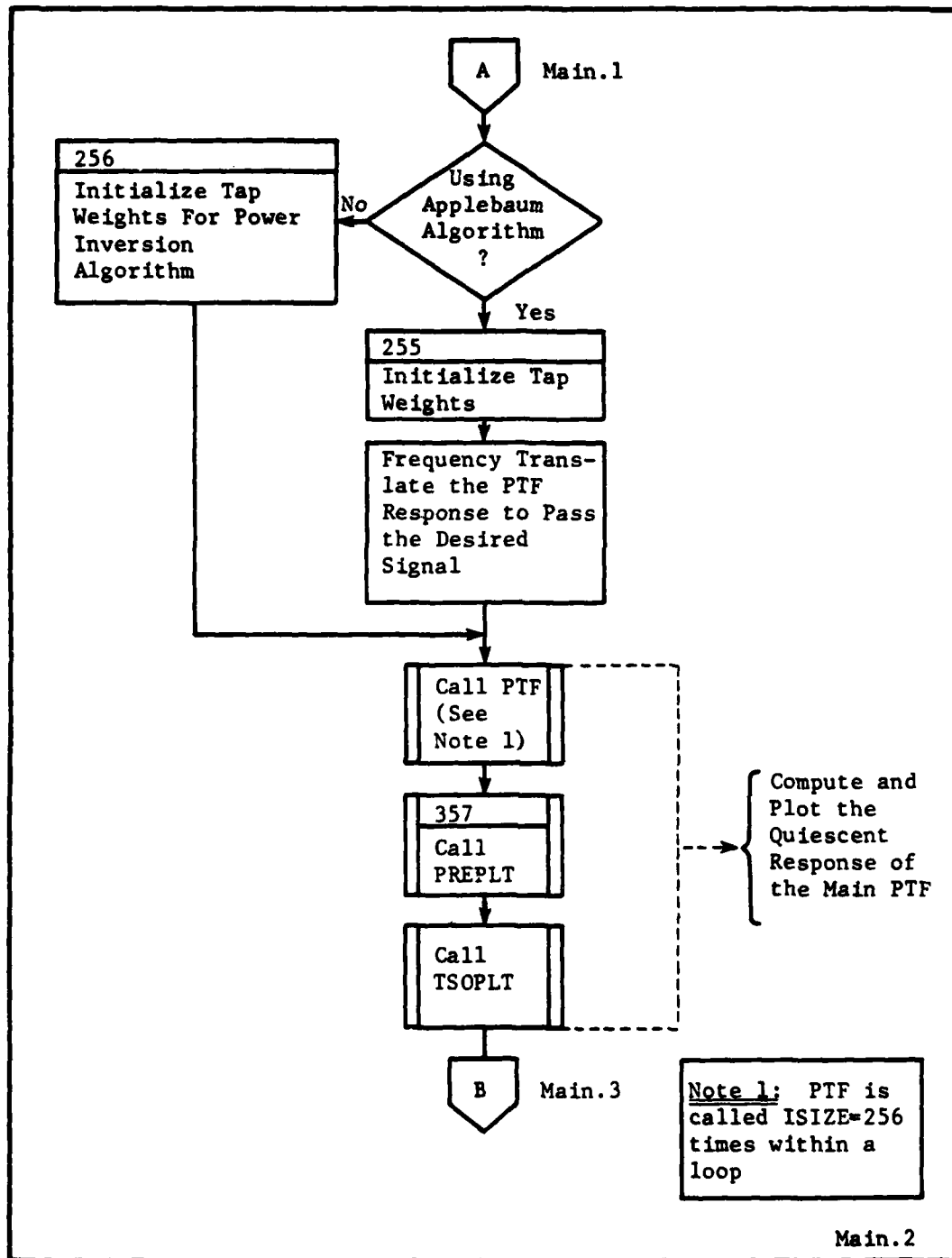


Figure 47. Flowchart for Module MAIN (cont.)

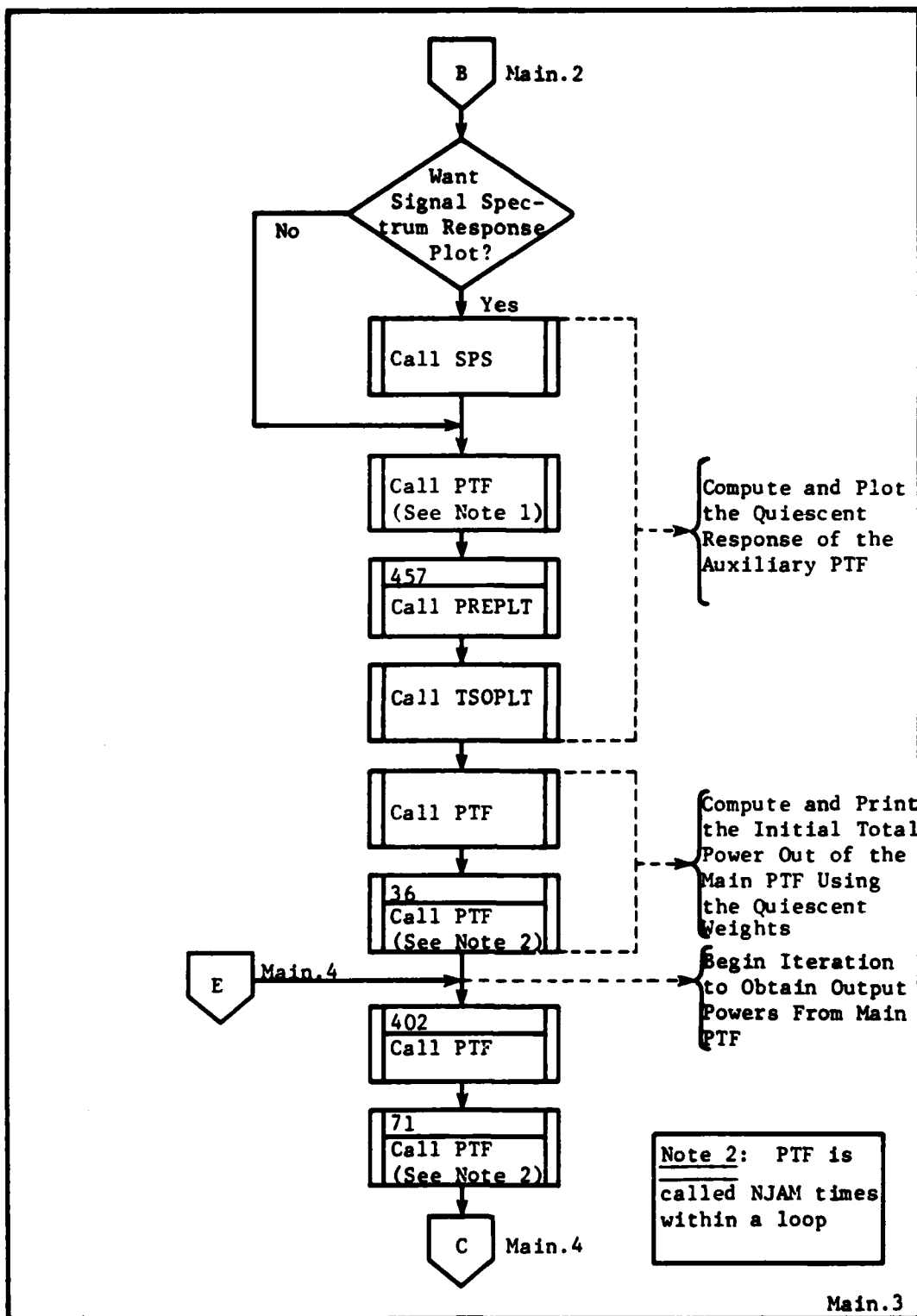


Figure 47. Flowchart for Module MAIN (cont.)

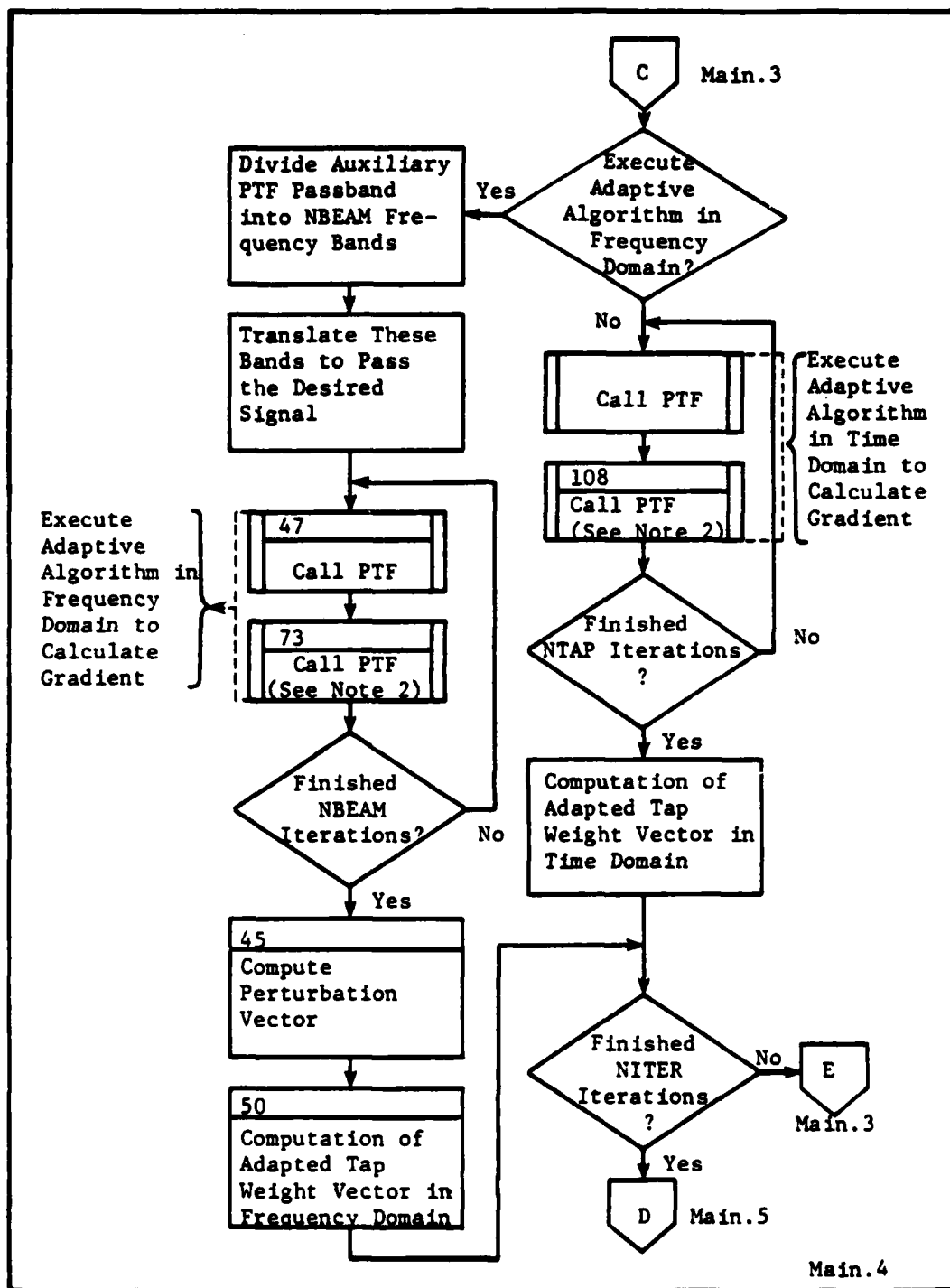


Figure 47. Flowchart for Module MAIN (cont.)

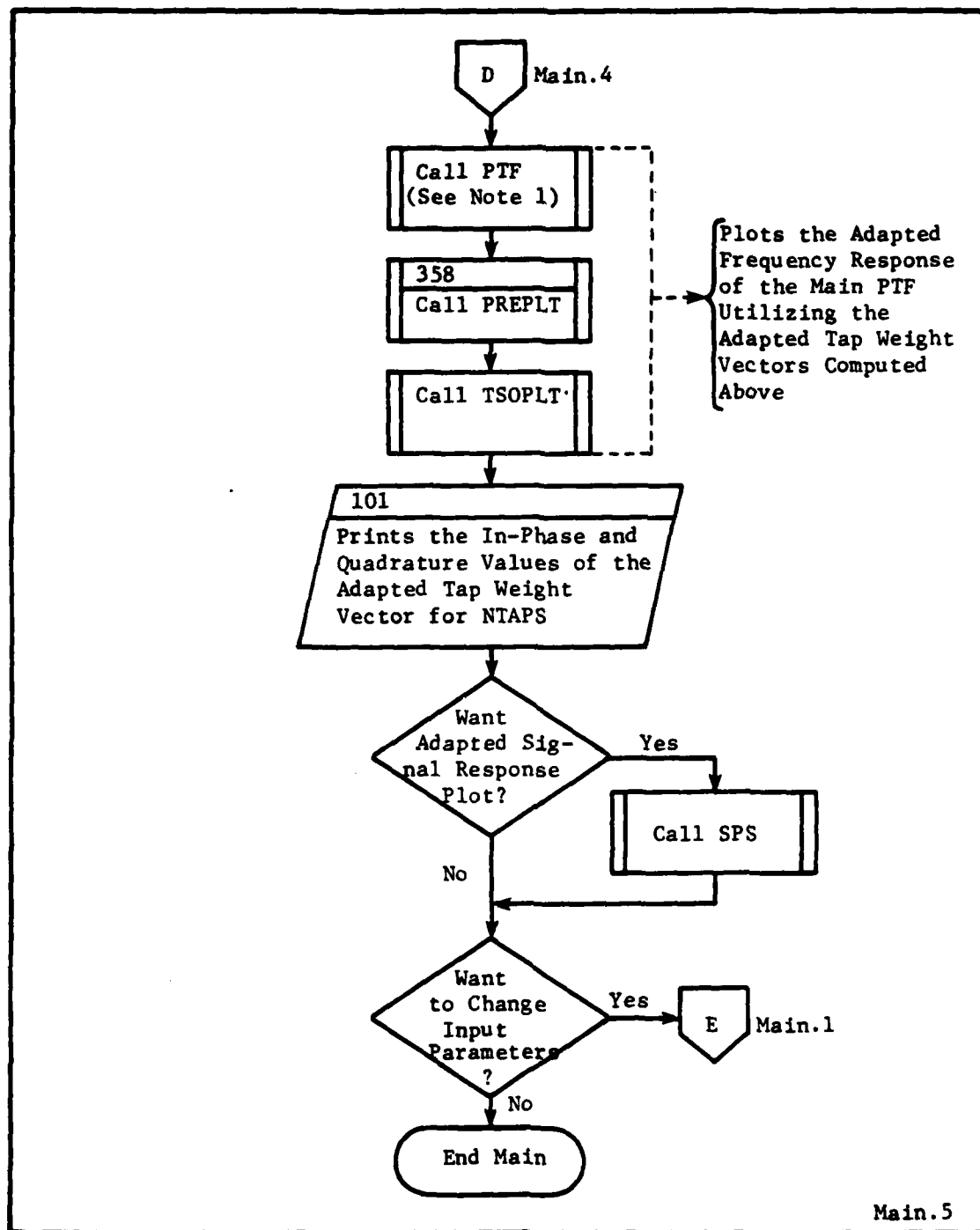


Figure 47. Flowchart for Module MAIN (cont.)

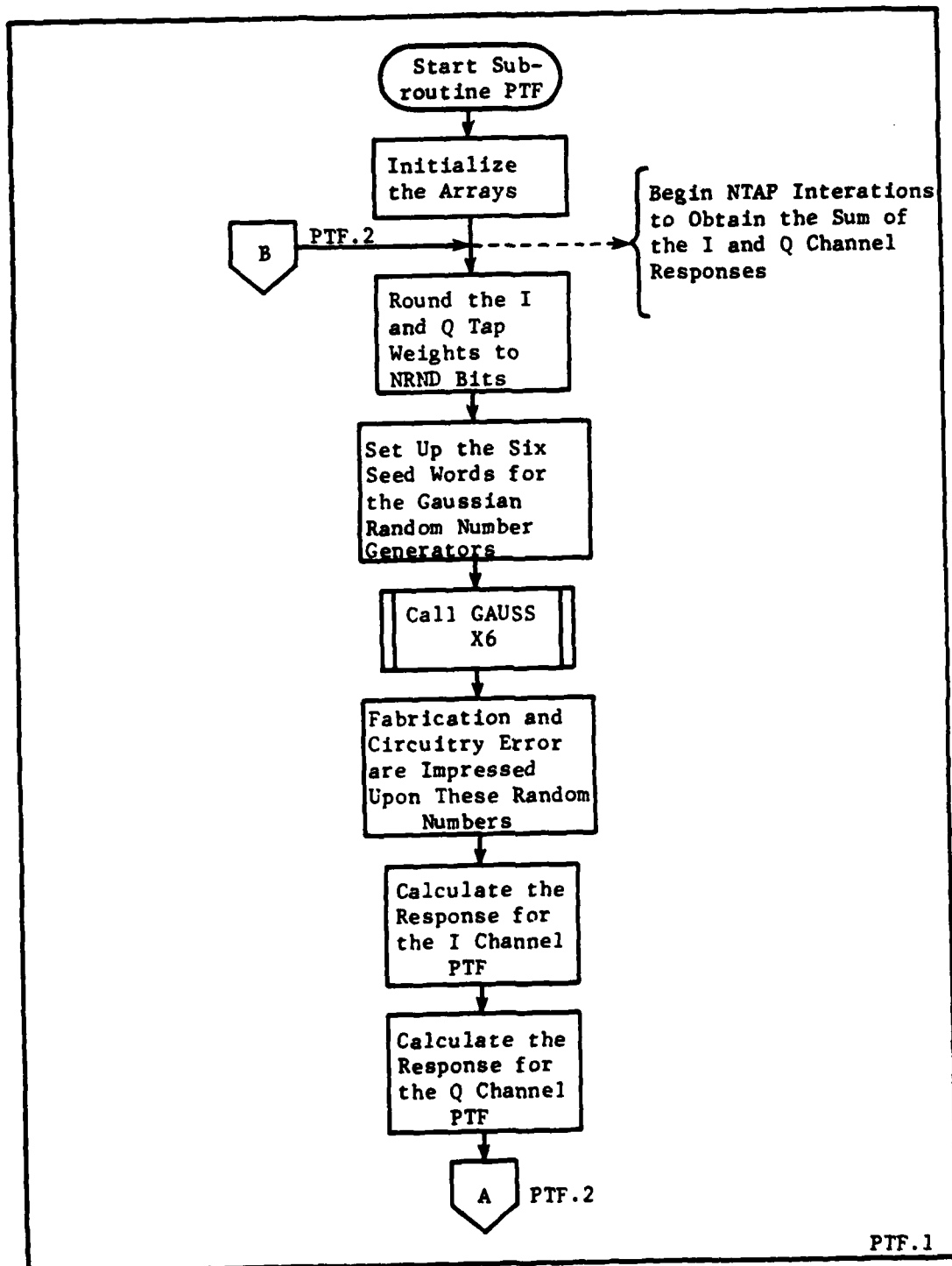


Figure 48. Flowchart for Subroutine PTF



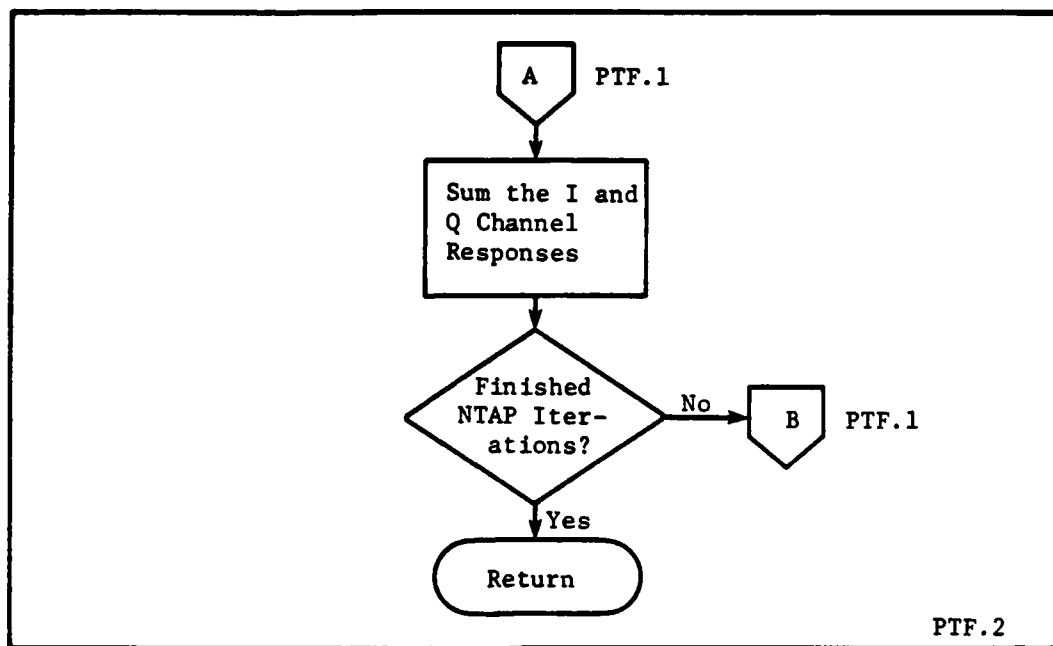


Figure 48. Flowchart for Subroutine PTF (cont.)

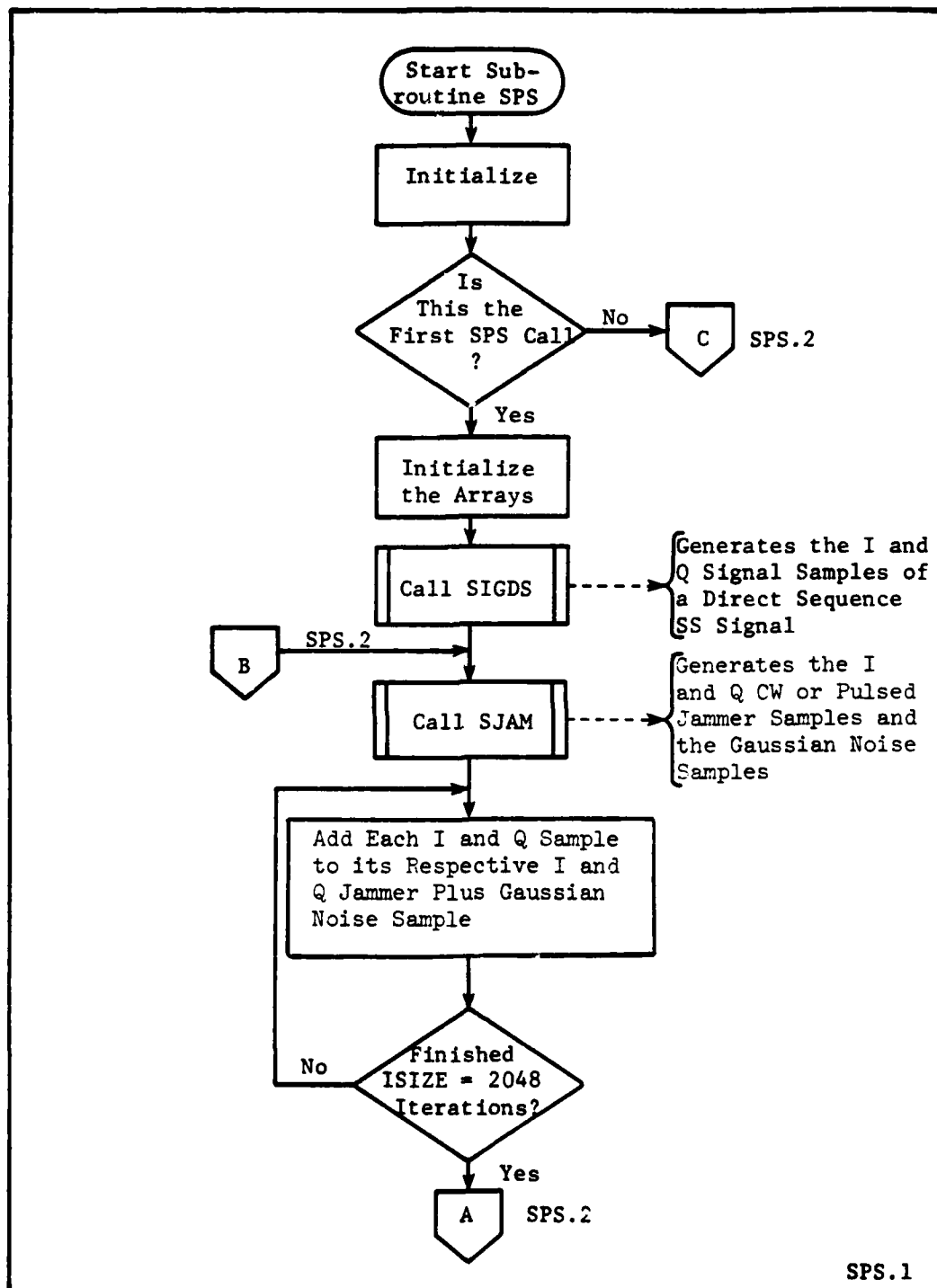


Figure 49. Flowchart for Subroutine SPS

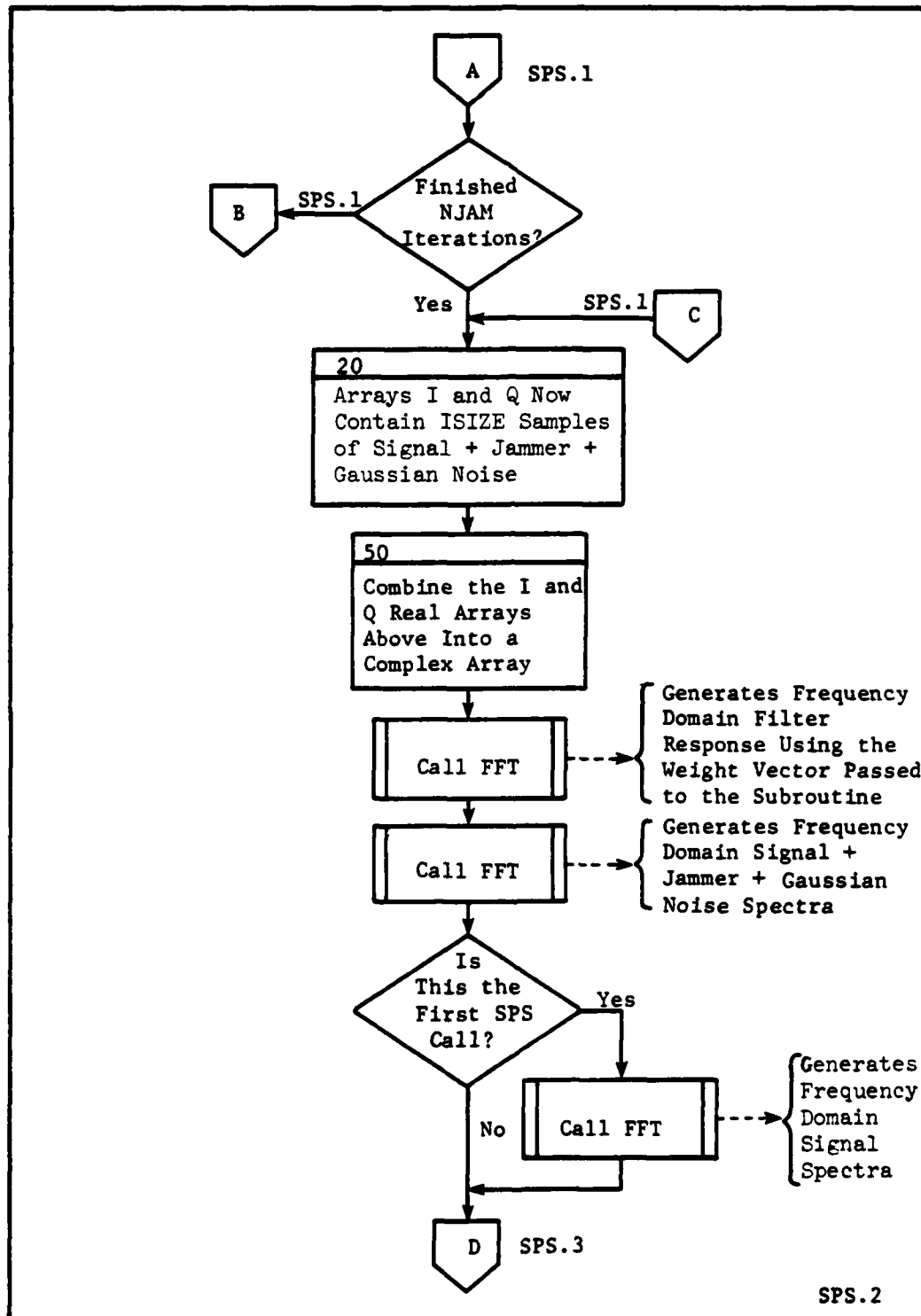


Figure 49. Flowchart for Subroutine SPS (cont.)

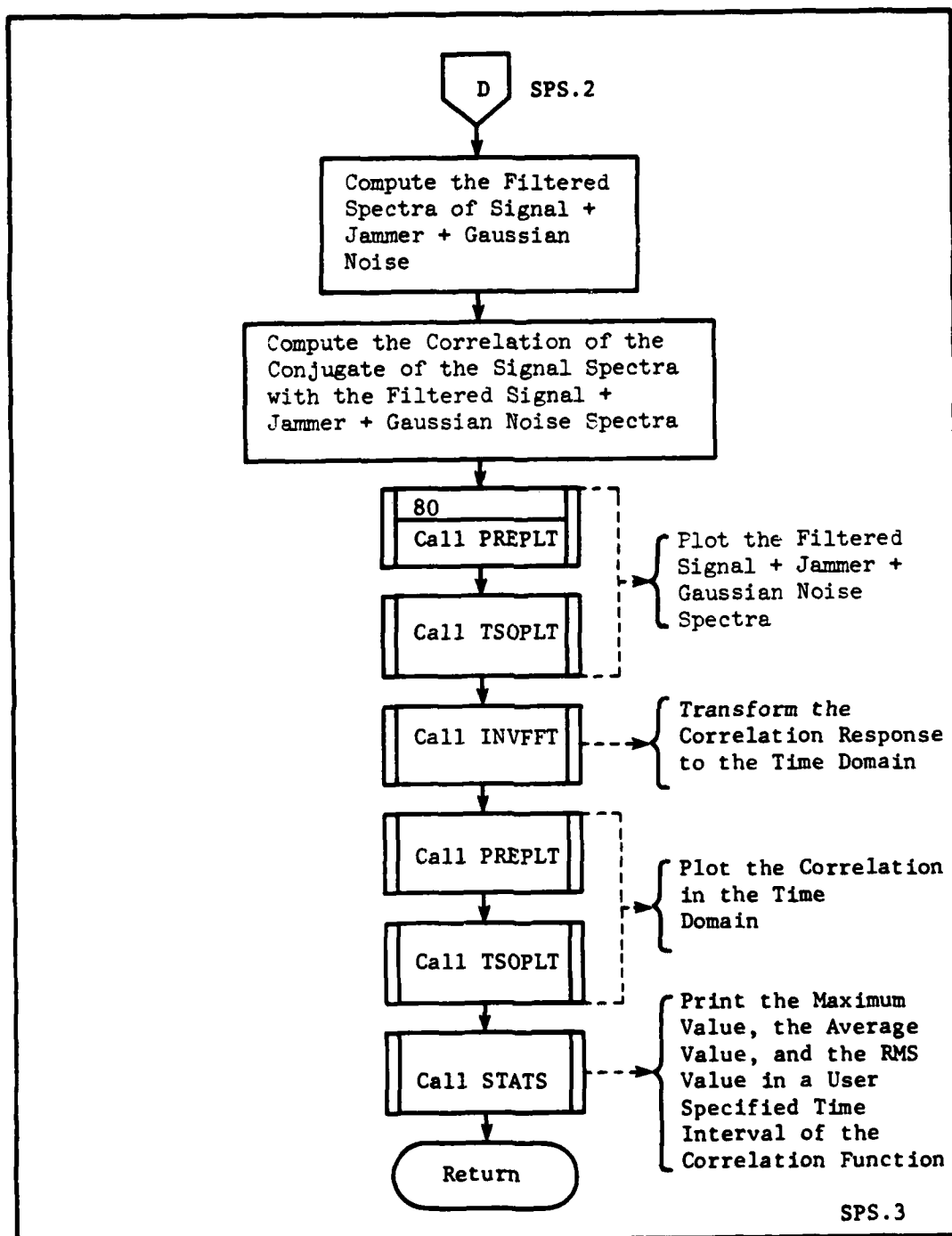


Figure 49. Flowchart for Subroutine SPS (cont.)

### Vita

Michael Martin Shepard was born on 26 May 1959 in Jacksonville, Florida. He graduated from Tucker High School in Tucker, Ga. in 1977. From August 1977 to May 1981 he attended The Citadel in Charleston, S.C. There he received, as a distinguished graduate, the degree of Bachelor of Science in Electrical Engineering and a commission into the United States Air Force in May 1981. Next, he entered the school of engineering at the Air Force Institute of Technology in Dayton, Ohio in June 1981. Upon graduation from the Air Force Institute of Technology in December 1982, he is scheduled for assignment to the Information Transmission Branch of the Air Force Avionics Laboratory at Wright-Patterson AFB in Dayton, Ohio.

Permanent Address: 900 Henderson Creek Drive #102  
Naples, Fla. 33942

UNCLASSIFIED

SECURITY CLASSIFICATION OF THIS PAGE (When Data Entered)

REPORT DOCUMENTATION PAGE		READ INSTRUCTIONS BEFORE COMPLETING FORM
1. REPORT NUMBER <b>AFIT/GE/EE/82-62</b>	2. GOVT ACCESSION NO. <b>AD-A124 903</b>	3. RECIPIENT'S CATALOG NUMBER
4. TITLE (and Subtitle) <b>THE PERFORMANCE OF A PN SPREAD SPECTRUM RECEIVER PRECEDED BY AN ADAPTIVE INTERFERENCE SUPPRESSION FILTER</b>		5. TYPE OF REPORT & PERIOD COVERED <b>MS Thesis</b>
7. AUTHOR(s) <b>Michael M. Shepard</b>		6. PERFORMING ORG. REPORT NUMBER
9. PERFORMING ORGANIZATION NAME AND ADDRESS <b>Air Force Institute of Technology (AFIT/EN) Wright-Patterson AFB, Ohio 45433</b>		8. CONTRACT OR GRANT NUMBER(s)
11. CONTROLLING OFFICE NAME AND ADDRESS <b>Information Transmission Branch (AFWAL/AAAI) Air Force Avionics Laboratory Wright-Patterson AFB, Ohio 45433</b>		10. PROGRAM ELEMENT, PROJECT, TASK AREA & WORK UNIT NUMBERS
14. MONITORING AGENCY NAME & ADDRESS (if different from Controlling Office)		12. REPORT DATE <b>December 1982</b>
		13. NUMBER OF PAGES <b>137</b>
		15. SECURITY CLASS. (of this report) <b>Unclassified</b>
		15a. DECLASSIFICATION/DOWNGRADING SCHEDULE
16. DISTRIBUTION STATEMENT (of this Report)  <b>Approved for public release; distribution unlimited</b>		
17. DISTRIBUTION STATEMENT (of the abstract entered in Block 20, if different from Report)		
18. SUPPLEMENTARY NOTES <b>Approved for public release: IAW AFR 198-17.</b> <b>LYNN E. WOLAVER</b> <b>Deputy for Research and Professional Development</b> <b>Air Force Institute of Technology (ATC)</b> <b>Wright-Patterson AFB OH 45433</b>  <b>4 JAN 1982</b>		
19. KEY WORDS (Continue on reverse side if necessary and identify by block number) <b>Interference Suppression                      Jammers</b> <b>Adaptive Filters                                  Tapped Delay Lines</b> <b>Spread Spectrum                                Transversal Filters</b> <b>Surface Acoustic Wave Filters</b>		
20. ABSTRACT (Continue on reverse side if necessary and identify by block number)  <b>The performance of a spread spectrum receiver preceded by an adaptive interference suppression (AIS) filter is determined for various CW jamming signals. An analysis and simulation of an AIS filter, covering the band from 200-300 MHz, implemented with a SAW device is presented. The simulation includes modeling of the SAW device, filter tap weights, Applebaum and power inversion adaptive control algorithms, and filter fabrication and circuitry errors. Both desired and interfering signals are generated in the simulator, (con't.)</b>		

DD FORM 1473

1 JAN 73

EDITION OF 1 NOV 65 IS OBSOLETE

UNCLASSIFIED

SECURITY CLASSIFICATION OF THIS PAGE (When Data Entered)

**Abstract (con't.)**

passed through the AIS filter, and demodulated by a simulated matched filter. System performance was determined by measuring the improvement in pre-detection signal-to-jammer ratio (SJR) and post-detection signal-to-jammer plus noise ratio (SJNR) provided by the AIS filter, and by computing the AIS filter convergence rate. To validate the AIS filter performance, the following additional simulation data was acquired both before and after filter adaption: The filter frequency response, the receiver correlation response, and the pre-detection signal plus jammer plus noise spectrum. In all 22 cases analyzed, the jammer power is 30 dB, the signal power is 0 dB, and the filter is allowed to adapt for 35 iterations. The AIS filter provided improvement in all cases analyzed except the case where the CW jammer is located at the center frequency of the signal. Typical improvement of pre-detection SJR ranged from 20-49 dB. The Applebaum algorithm provided greater improvement in SJR and in SJNR than the power inversion algorithm. Both the Applebaum and power inversion algorithms implemented in the frequency domain converged faster than their respective time domain implementations. However, the time domain implementation of the adaptive algorithms provided greater improvement in SJR and in SJNR than the frequency domain implementation. Filter fabrication and circuitry errors caused the null depths of the adapted filter responses to be degraded relative to their respective responses without errors.

DATE  
FILMED  
-8